Proceedings of the 113th Annual Meeting of

The American Association of Variable Star Observers

January 2025

ISBN 978-1-939538-72-7

The American Association of Variable Star Observers
185 Alewife Brook Parkway, Suite 410, Cambridge, MA 02138, USA

Proceedings of the AAVSO 113th Annual Meeting

Editor

Joyce A. Guzik

Los Alamos National Laboratory

Los Alamos, NM 87545, USA

The American Association of Variable Star Observers
185 Alewife Brook Parkway, Suite 410, Cambridge, MA 02138, USA

Proceedings of the AAVSO 113th Annual Meeting

Editor's Note

These articles were submitted as optional conference proceedings papers by participants of the 113th Annual Meeting of the AAVSO held November 8-10, 2024, at the U.S. Space & Rocket Center, Huntsville, Alabama.

Fourteen articles were received, representing contributed oral and poster presentations. These articles have been edited/curated, but not peer reviewed. In two cases, the authors' work has been published in the Journal of the AAVSO, and this volume contains the meeting abstract and link to the article. This proceedings volume also includes the abstracts for 18 additional invited and contributed talks and posters for which proceedings papers were not submitted.

Meeting abstracts were reviewed by a committee with members Joyce Guzik (chair), Tom Maccarone, Sebastián Otero, and Elizabeth Waagen before being accepted for presentation at the meeting.

The full meeting schedule with program and links to abstracts can be found at https://www.aavso.org/113.

We hope you enjoy reading this collection of articles and find inspiration for your own astronomy pursuits!

Meeting venue at U.S. Space & Rocket Center; Photo credit: Lauren Herrington.

Proceedings of the AAVSO 113th Annual Meeting

Reception and Keynote at U.S Space & Rocket Center; Photo credit: W. Armentor

Reception and Keynote at U.S. Space & Rocket Center
Photo credits: B. Kloppenborg (left) and L. Herrington (right)

The American Association of Variable Star Observers
185 Alewife Brook Parkway, Suite 410, Cambridge, MA 02138, USA

Proceedings of the AAVSO 113th Annual Meeting

Philip Kaaret presents at U.S. Space & Rocket Center; Photo credit: L. Herrington

U.S. Space & Rocket Center; Photo credit: L. Herrington

Proceedings of the AAVSO 113th Annual Meeting

Table of Contents: Proceedings Papers

The American Association of Variable Star Observers
185 Alewife Brook Parkway, Suite 410, Cambridge, MA 02138, USA

Proceedings of the AAVSO 113th Annual Meeting

The American Association of Variable Star Observers
185 Alewife Brook Parkway, Suite 410, Cambridge, MA 02138, USA

Proceedings of the AAVSO 113th Annual Meeting

Table of Contents: Abstracts Only

The American Association of Variable Star Observers
185 Alewife Brook Parkway, Suite 410, Cambridge, MA 02138, USA

Rapid and Periodic Spectroscopic Variation of the Hα Line of the Be Shell Star Omicron Andromedae

H. Rick Diz

Professor Emeritus, Department of Environmental Science and Engineering,
Gannon University, Erie, PA; hrickdiz@gmail.com

Abstract

The variable star omicron Andromedae (o And) is a Be shell star that has been reported to have rapid variations in its spectrum, including the Hα line at λ6562.85Å. This study provides quantitative documentation of that variation and identifies periodic behavior over short time frames. The 332 spectra used in this study, unless otherwise attributed, were obtained by the author, an amateur astronomer using a 203 mm SCT telescope equipped with a 3D-printed spectroscope during the period from August 2023, through January 2024. Analysis of a light curve for o And derived from TESS data yielded a period of 1.56 days in close agreement with that reported in the literature, and a previously unreported period of 0.695 days that fits the data well. Additionally, spectra obtained from the BeSS database established that o And has a recent history of forming circumstellar disks that last about seven years before they dissipate. The current disk began to form about one year prior to the beginning of this study. The spectra of o And revealed continuous rapid changes in the Hα line during the course of individual nights as well as over a longer time frame. Being a shell star, the Hα emission line is complex, consisting of a double peak separated by a central depression. The relationship of the two peaks (wings) is expressed by the V/R ratio. Analysis using CLEANest revealed multiple periods for the variation of the features of the Hα line. The following rapid periods (less than a day) were found: for the central depression a period of 0.683 days, for the V wing a period of 0.49 days, for the R wing a period of 0.66 days, and for the V/R ratio a period of 0.92 days. On a slightly longer timescale, the period for the V wing was found to be 11.92 days and for the V/R ratio it was 12.04 days. The R wing occasionally exhibited a 1.95-day period but often deviated from this. A discussion of possible explanations for this behavior is presented which may be helpful in understanding the variability observed.

This paper was published in 2024 in the Journal of the Association of the American Association of Variable Star Observers, https://apps.aavso.org/jaavso/article/3956/

References

Diz, H.R. 2024, JAAVSO, Vol. 52, No. 2.

Application of the O'Connell Effect to Detect BX Trianguli b: A Novel Approach to Exclude the Applegate Mechanism

Mark Eaton[1,2] and Seif Atwa[1]

[1]Waterloo Collegiate Institute Astronomy Club, Waterloo, Ontario, Canada;
mark_eaton@wrdsb.ca
[2]Royal Astronomical Society of Canada, Kitchener-Waterloo Chapter

Abstract

We present a novel approach to detect circumbinary planets using the O'Connell effect to exclude stellar magnetic activity as a driver of eclipse timing variations (ETVs). Applied to the M-dwarf binary system BX Trianguli, this methodology enabled the discovery of a circumbinary planet with an orbital period of 10.74 years, mass of 7.5 Jupiter masses, and eccentricity of 0.4. By systematically eliminating alternative mechanisms—mass transfer, orbital precession, and the Applegate mechanism—we confirmed the gravitational influence of a planet. Our findings underscore the potential of integrating O'Connell effect analysis into ETV studies, paving the way for further exploration of circumbinary planets in low-mass stellar environments.

1. Context and Motivation

Eclipse timing variations (ETVs) have emerged as a powerful indirect method for detecting circumbinary planets (Borkovits et al. 2016). These subtle shifts in eclipse minima timings arise from the gravitational influence of a third body, often leading to sinusoidal periodicities in timing data (Deeg et al. 2008). However, distinguishing planetary signals from intrinsic stellar phenomena such as mass transfer or magnetic energy redistribution (Applegate mechanism) (Applegate 1992; Lanza 2006) is crucial to ensure reliable planetary detections.

BX Trianguli, an ultra-short period M-dwarf contact binary system, provides an excellent testbed for such methodologies. Its 0.192634-day orbital period and availability of nearly 24 years of historical timing data (Kloppenborg 2023) make it a promising candidate for ETV studies (Borkovits et al. 2016).

Our primary objective was to determine the source of ETV signals observed in BX Trianguli. A key innovation in our approach was leveraging the O'Connell effect (Wilsey & Beaky 2009)—a photometric asymmetry linked to stellar activity—to exclude the Applegate mechanism and confirm the presence of a planet.

2. Observations and Methods

2.1 Observations

Observations of BX Trianguli were conducted on January 25, 2023, using the RASC Sierra Remote Observatories telescope (MacDonald 2018), and on September 14 to 15, 2023, with the Insight Observatory ATEO-1 telescope (Petrasko 2023). The January 25th observation captured nearly one complete orbital cycle capturing 254 minutes of continuous data. The September 14th to 15th observation captured the entire orbital cycle recording 358 minutes in total. Both observations were sufficient to allow for the precise measurement of the primary and secondary eclipse minima timings. These observations were supplemented with historical data from the AAVSO (Kloppenborg 2023) and O-C Gateway (Paschke & Brat 2006) databases spanning 24 years.

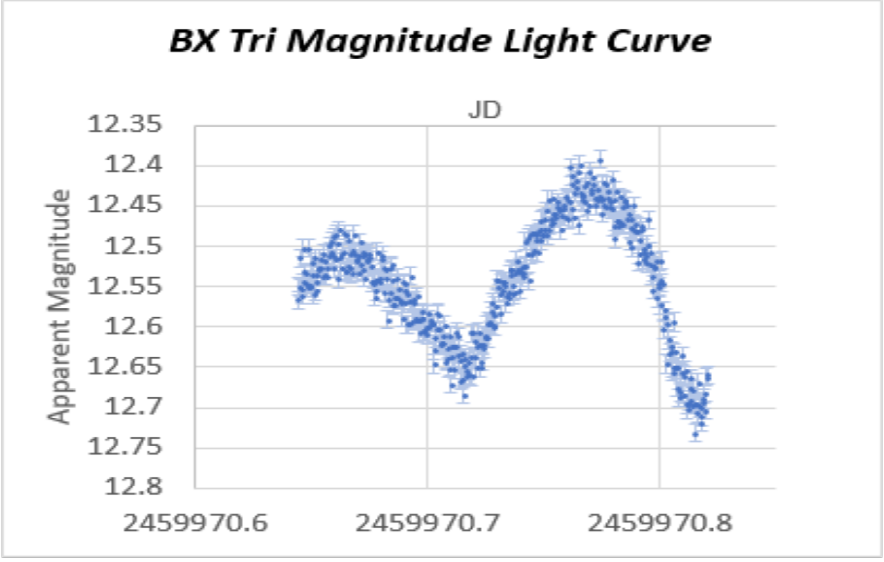

Figure 1. Light curve of the January 25th Observation.

2.2 Data Analysis

Eclipse timing residuals (O-C values) were computed by comparing observed minima timings to those predicted by a linear ephemeris. MATLAB (MathWorks, 2022) was used for sinusoidal regression, revealing a periodic signal with a 10.74-year period and 7-minute amplitude.

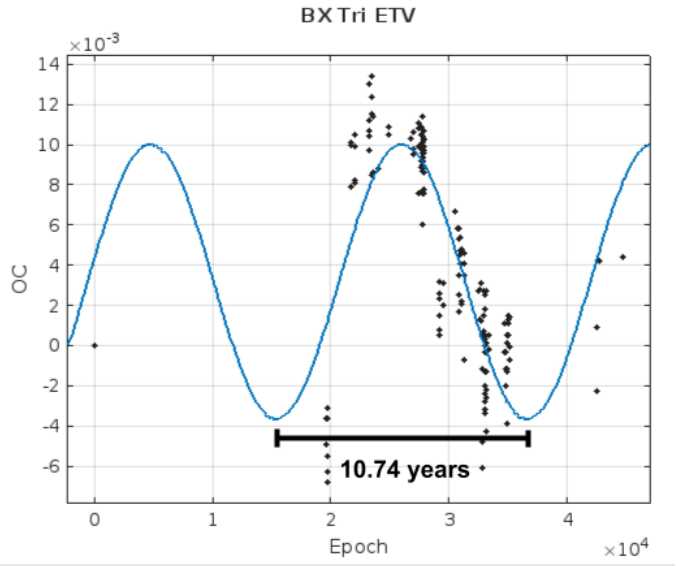

Figure 2. Eclipse timing residuals (O-C values) versus time and corresponding sinusoidal model.

2.3 Hypothesis Testing

To identify the source of ETV signals, we systematically tested four hypotheses:

a) Mass Transfer

Mass transfer in close binary systems results in a parabolic trend in ETVs, with periods much longer than the observed 10.74 years. Additionally, periodic mass transfer effects are rare and typically occur in binaries with high eccentricity. In the contact configuration of BX Trianguli, the stars have reached Roche lobe equilibrium, making significant mass exchange unlikely (Eggleton 1983). The absence of a parabolic signature in the ETV data allowed us to confidently eliminate this hypothesis.

b) Orbital Precession

Orbital precession, caused by gravitational perturbations within the system, is negligible in contact binaries with low eccentricity (Zahn 1977). BX Trianguli's orbit is nearly circular, precluding significant precessional effects. Furthermore, the amplitude of the observed ETV signal is too large to be explained by precession alone. Based on these constraints, we excluded this mechanism as a potential cause.

c) Applegate Mechanism

The Applegate mechanism redistributes angular momentum within stars through magnetic energy transfer, producing periodic orbital variations. Energy calculations by the Applegate Mechanism Calculator (Zamponi, accessed 25 Aug 2023) using models by Voelschow et al. (2016) showed that two of the three theoretical models yielded energy requirements exceeding the available stellar energy by factors of 100 or more. However, the third model by Tian et al. (2009)

produced a marginally viable energy ratio of 1.08, introducing uncertainty. To resolve this, we analyzed the O'Connell effect for periodic signals matching the ETV period. No such periodicity was detected, ruling out the Applegate mechanism.

d) Gravitational Influence of a Third Body

The remaining hypothesis involved the gravitational pull of a third body, such as a planet. A sinusoidal ETV pattern, with a well-defined period and amplitude, strongly supports this explanation. Deriving planetary parameters based on ETV modeling confirmed that the inferred body possessed planet-like properties.

3. O'Connell Effect Analysis

3.1 Background

The O'Connell effect, characterized by an asymmetry between the primary and secondary maxima in the light curves of eclipsing binaries, is typically attributed to stellar activity. This phenomenon is often associated with star spots or localized temperature variations caused by magnetic activity (Wilsey & Beaky 2009; Berdyugina 2005). In systems like BX Trianguli, such asymmetries can indicate significant magnetic interactions, which are also implicated in the Applegate mechanism (Applegate 1992). If this mechanism were responsible for the observed ETVs, a periodic signal in the O'Connell effect, corresponding to the 10.74-year ETV cycle, would be expected.

BX Trianguli displays a pronounced O'Connell effect, with measurable differences in the luminosities of its primary and secondary maxima. While such asymmetries are common in M-dwarf contact binaries (Knote et al. 2022), their periodic analysis offers a diagnostic tool for identifying stellar magnetic cycles. This study marks the first application of the O'Connell effect to exclude the Applegate mechanism in the context of ETV analysis.

3.2 Methodology

To assess the role of magnetic activity, we analyzed the O'Connell effect using historical (Kloppenborg 2023; Paschke & Brat 2006) and original observational data. The relative magnitudes of the primary and secondary maxima were measured for each available observation. These differences were plotted as a function of time to evaluate potential periodic trends. MATLAB was used to fit sinusoidal regression curves to the data, and the period of the regression was compared to the period of the original ETV signal. Additionally, noise analysis was conducted to quantify the residuals of the sinusoidal fits. This step was essential for determining whether the observed variations in the O'Connell effect were statistically significant or dominated by measurement uncertainties and noise.

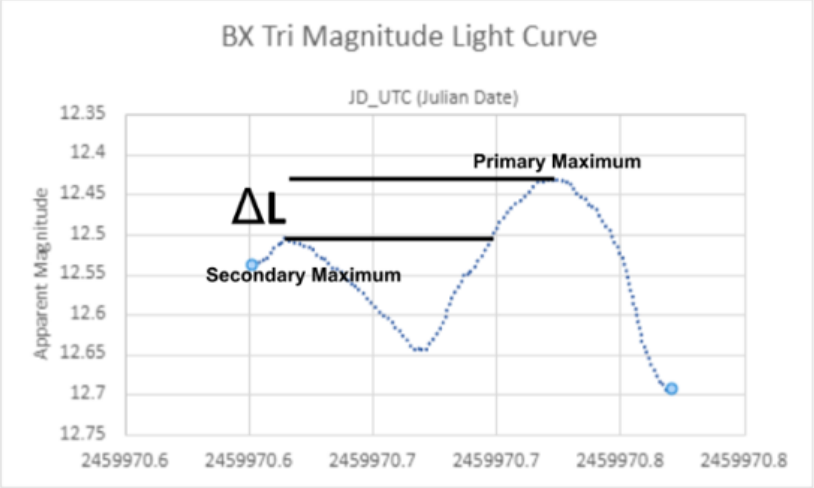

Figure 3. BX Trianguli light curve showing how the relative magnitudes (ΔL) were measured.

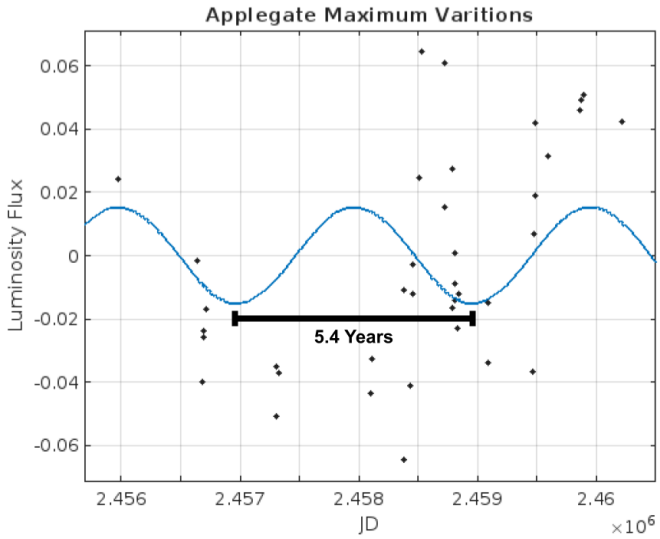

Figure 4. A plot of the O'Connell effect over time, showing the lack of correlation with the ETV periodicity.

3.3 Results

The analysis revealed a lack of meaningful periodic trends in the O'Connell effect. While the dataset included variations in primary and secondary maxima luminosities, these fluctuations exhibited no correlation with the 10.74-year ETV period. Residual analysis further demonstrated that the noise levels in the data exceeded the amplitude of any potential periodic signal by a factor of several times, rendering the fits unreliable for inferring magnetic cycles.

The absence of a periodic signal in the O'Connell effect strongly suggests that stellar activity, and by extension the Applegate mechanism, is not responsible for the observed ETVs in BX Trianguli. This finding is corroborated by earlier energy calculations, which showed that the system's

secondary star lacked sufficient energy to drive the Applegate mechanism under most theoretical models (Voelschow et al. 2016; Wilsey & Beaky 2009).

3.4 Significance of Findings

By integrating O'Connell effect analysis into ETV studies, we provide a robust framework for differentiating between planetary influences and stellar magnetic interactions. The novelty of this approach lies in its ability to use readily available photometric data to probe stellar activity cycles, circumventing the need for extended, high-precision monitoring. In the case of BX Trianguli, this analysis conclusively ruled out the Applegate mechanism, leaving the planetary hypothesis as the sole viable explanation for the observed ETVs (Doyle et al. 2011; Orosz et al. 2012).

4. Results

4.1 Planetary Parameters

The planetary parameters of BX Trianguli b were derived using a combination of ETV analysis and theoretical modeling. The mass of the planet was estimated from the amplitude of the observed ETV signal, which directly relates to the gravitational perturbation caused by the third body (Borkovits et al.,2016). By applying Kepler's third law and incorporating the known masses of the BX Trianguli binary stars, we calculated the planetary mass to be approximately 7.5 Jupiter masses. This mass was determined using the relationship between Mass and the Semi-Amplitude (K) described by Voelschow et al. (2016).

$$K = \frac{M_{Plan} G^{\frac{1}{3}}}{c} \left[\frac{P_{Plan}}{2\pi (M_{Pri} + M_{Sec})} \right]^{\frac{2}{3}}$$

This value is consistent with the classification of the third body as a planet rather than a brown dwarf or stellar companion (Sahlmann et al. 2010).

The orbital radius of BX Trianguli b was inferred from the period of the ETV signal. The 10.74-year periodicity, combined with the masses of the binary stars, provided a mean orbital radius of 4.5 astronomical units. This distance places the planet well within the dynamically stable region for circumbinary planets, as predicted by theoretical models of binary star systems (Holman & Wiegert 1999).

Finally, the orbital eccentricity of the planet was determined using a Monte Carlo simulation approach (Ford 2005). In this analysis, a range of eccentricity values was tested against the timing data to identify the configuration that best matched the observed ETV pattern. The optimal fit yielded an eccentricity of 0.4, indicating a moderately elliptical orbit. This value aligns with

expectations for giant planets in binary systems, which often exhibit higher eccentricities due to complex gravitational interactions during their formation and evolution (Sotiriadis 2018).

Together, these parameters—mass, orbital radius, and eccentricity—confirm the planetary nature of the third body responsible for the ETVs in BX Trianguli. The derived values are well within the range observed for other circumbinary planets (Doyle et al. 2011; Orosz et al. 2012), reinforcing the robustness of the ETV method and the credibility of our findings.

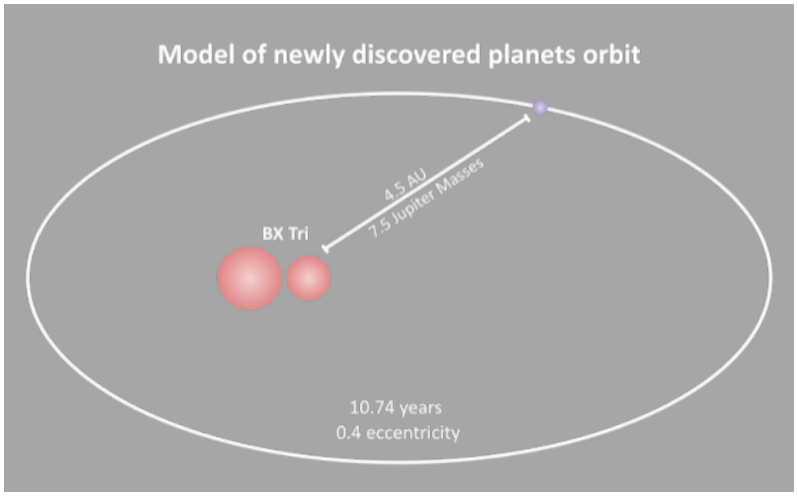

Figure 5. A diagram of the inferred orbit of BX Trianguli b (The sizes of the stars and planet have been exaggerated approximately 10 thousand times to make them visible).

4.2 Methodological Implications

By employing the O'Connell effect analysis, we introduced a novel diagnostic tool to differentiate between stellar activity and planetary influences in ETV studies. This approach enhances the reliability of circumbinary planet detections, especially in systems where traditional methods struggle to eliminate confounding factors like the Applegate mechanism (Applegate 1992; Voelschow et al. 2016).

5. Conclusion

The application of the O'Connell effect to BX Trianguli represents a significant advancement in the study of circumbinary planets. By conclusively ruling out the Applegate mechanism, we confirmed the existence of a planet in this dynamically complex system. Future research should extend this methodology to other contact binaries, potentially uncovering additional planets and broadening our understanding of planet formation in low-mass stellar environments.

Acknowledgments

We thank the Royal Astronomical Society of Canada and Insight Observatory for their support and resources. Historical timing data from AAVSO and O-C Gateway contributors worldwide were invaluable to this study. I respectfully acknowledge the Haudenosaunee, Anishinabewaki, and

Attiwonderonk peoples of Waterloo, Ontario; the Nyyhmy (Western Mono/Manache) peoples of Auberry, California; and the Nuwuvi (Southern Paiute) peoples of Beryl, Utah as the traditional stewards of the lands on which this research was conducted, recognizing that explicit permission to live and work on these lands has not necessarily been granted.

References

Applegate, J. H. (1992). A mechanism for orbital period modulation in close binaries. *Astrophysical Journal, 385*, 621–629.

Berdyugina, S. V. (2005). Starspots: A key to the stellar dynamo. *Living Reviews in Solar Physics, 2*(1), 8.

Borkovits, T., Hajdu, T., Sztakovics, J., et al. (2016). A comprehensive study of Kepler triples: Their properties and the outer third bodies' effects on binary stars. *Monthly Notices of the Royal Astronomical Society*, 455(4), 4136–4155.

Deeg, H. J., et al. (2008). Extrasolar planet detection by binary stellar eclipse timing: evidence for a third body around CM Draconis. *Astronomy & Astrophysics, 480*, 563–571.

Doyle, L. R., et al. (2011). Kepler-16: A transiting circumbinary planet. *Science, 333*(6049), 1602–1606.

Eggleton, P. P. (1983). Approximations to the radii of Roche lobes. *The Astrophysical Journal, 268*, 368–369.

Ford, E. B. (2005). Quantifying uncertainty in orbital parameters. *Astronomical Journal, 129*, 1706–1717.

Holman, M. J., & Wiegert, P. A. (1999). Long-term stability of planets in binary systems. *The Astronomical Journal, 117*(1), 621–628.

MacDonald, W. (2018). *The RASC Robotic Telescope*. Royal Astronomical Society of Canada. Retrieved [1 June 2023], from https://www.rasc.ca/telescope

Holman, M. J., & Wiegert, P. A. (1999). Long-term stability of planets in binary systems. *Astronomical Journal, 117*, 621–628.

Kloppenborg, B. K. (2023), Observations from the AAVSO International Database, https://www.aavso.org

Knote, M., Caballero-Nieves, S. M., Gokhale, V., Johnston, K. B., & Perlman, E. S. (2022). Characteristics of Kepler eclipsing binaries displaying a significant O'Connell effect. *Astrophysical Journal Supplement Series*.

Koen, C. (2014). An O-C (and light travel time) method suitable for application to large photometric databases. *Monthly Notices of the Royal Astronomical Society, 444*(3), 1514–1523.

Orosz, J. A., et al. (2012). Kepler-47: A transiting circumbinary multiplanet system. *Science, 337*(6101), 1511–1514.

Paschke, A. & Brat, L. (2006). O-C Gateway, a Collection of Minima Timings. *Open European Journal on Variable Stars, 23, p13.*

Petrasko, M. (2023). *ATEO-1: Astronomical Telescope for Educational Outreach*. Insight Observatory, Retrieved [16 Dec. 2024] from https://www.insightobservatory.com/p/ateo-1.html

Sahlmann, J., Ségransan, D., Queloz, D., & Udry, S. (2010). A possible dividing line between massive planets and brown-dwarf companions. *arXiv: Earth and Planetary Astrophysics*.

Sotiriadis, S., Libert, A.-S., & Raymond, S. N. (2018). Formation of terrestrial planets in eccentric and inclined giant planet systems. *Astronomy & Astrophysics, 614*, A39.

Voelschow, M., et al. (2016). Applegate's mechanism for orbital period variations revisited. *Astronomy & Astrophysics, 587*, A34.

Wilsey, N. J., & Beaky, M. M. (2009). The O'Connell effect in eclipsing binary stars. *Society for Astronomical Sciences Annual Symposium, 28*, 107–114.

Zahn, J.-P. (1977). Tidal friction in close binary stars. *Astronomy & Astrophysics, 57*, 383–394.

Zamponi, J. F. (n.d.). *Applegate Mechanism Calculator*. Theory of Star Formation Group, Universidad de Concepcion. Retrieved [25 Aug. 2023], from http://theory-starformation-group.cl/applegate/

Period Analysis of Eclipsing Cataclysmic Variable Stars

Mennatalla Mahmoud Ellaqany, Valeria Garcia-Lopez, Emily S. Hatten, Mridul Agarwal, and David A. Moffett

Department of Physics, Furman University, Greenville, South Carolina 29613, USA;
david.moffett@furman.edu

Subject Keywords

Eclipsing Binary Stars; Cataclysmic Variable Stars; Period Determination; Orbital Evolution

Abstract

We have performed a study of the orbital properties of seven eclipsing cataclysmic variable (CV) binary systems by analyzing photometric time series from the Transiting Exoplanet Survey Satellite (TESS). We employed Python code to determine the eclipse epochs and orbital periods for each system and constructed O-C diagrams from observed and predicted eclipse epochs. By analyzing the O-C diagrams of our target CVs, we have constrained values for changes in orbital period with time. Our targets include a sample of sources from each class of non-magnetic, eclipsing CVs: dwarf novae variables, Z Cam type, and U Gem subclasses. We include in our study classical novae variables, nova-like variables (including the VY Scl and UX UMa subclasses), and recurrent novae variable stars. We approached this project with goals of developing time series analysis techniques for future undergraduate-level studies of eclipsing CVs, and how they may contribute to the understanding of their orbital evolution.

1. Introduction

Eclipsing Cataclysmic Variables (ECVs) are a subset of cataclysmic variable (CV) systems whose high inclination angles give us an unambiguous measurement of orbital period and eclipse phase of the white dwarf and companion star. Observations of ECV light curves allow observers to study the orbital dynamics of the binary system and the accretion disk. Eclipsing CVs sample several classes of cataclysmic variables and can be divided into even more subclasses which have their own distinct accretion mechanisms and outburst behaviors, although we will only be focusing on dwarf novae (DN) and classical novae (CN). Dwarf Novae systems exhibit periodic outbursts, driven by the gravitational energy released from an instability in the binary's accretion disk or from a sudden variation in the mass-transfer process. The outburst intervals range from days to decades, and the outburst period can last from two to 20 days. Dwarf nova systems are divided further into three subclasses: U Gem, Z Cam and SU UMa. Classical Novae are a subclass of variable novae systems, which have a high and steady accretion rate but do not exhibit large-scale outbursts like Dwarf Novae. The typical brightness range for CN range from magnitude 6 to greater than 19. Brighter novae have shorter durations than fainter novae. CN outbursts are

usually modeled as thermonuclear runaways originating in accreted hydrogen-rich material on the surface of the primary star.

Studying different types and subtypes of eclipsing cataclysmic variable systems allows us to break down the accretion properties while under different conditions. Understanding the accretion process and properties contribute to understanding the long-term evolution process of ECVs. We hope to observe these systems using TESS archival data to model the orbital period and period derivative (if present) of CV systems, with the intent to search for other periodic and aperiodic behavior associated with the accretion disk, hotspots, and any other unknown mechanisms that might impact the light curve.

2. Observational Data

Our small survey consists of the light curves of eclipsing cataclysmic variable (CV) stars observed by TESS, initially processed at NASA's Science Processing Operations Center (SPOC). TESS was designed to discover exoplanets that transit stars bright enough to enable follow-up spectroscopic observations for determining planet masses and atmospheric compositions. Since its launch in 2018, TESS has observed over 200,000 main-sequence dwarf stars using four wide-field optical cameras, detecting periodic brightness variations caused by planets passing in front of their host stars. The satellite's unique elliptical high Earth orbit provides a stable platform for continuous photometric measurements, surveying over 85% of the sky and focusing on stars brighter and closer than those observed by the Kepler mission (Barclay 2024). The SPOC pipeline identifies potential planetary transits, corrects systematic errors, and conducts diagnostic tests, distinguishing TESS's data processing from that of Kepler (Barclay 2024). In this study, we are evaluating the target light curve files, which include photometric analysis and systematically corrected time series data, to investigate the period behavior of eclipsing CVs.

We acquired 2-minute cadence photometric data of normalized flux versus BTJD (Barycentric TESS Julian Date) of seven CVs: QZ Aur, EX Dra, EX Hya, AY Psc, DO Leo, GY Cnc, and HBHA 4204--09. The data comprises of multiple segments extending over BTJD ranges that together span about 3 to 4 years, providing a long dataset suitable for our study. This duration is sufficient for observing many eclipses, as most CVs have an orbital period of a few hours. We retrieved the data using a Python code that accesses MAST via the unique TIC (TESS Input Catalog) ID number assigned to each object. Our objective is to construct an O-C diagram and forecast their rate of period change, denoted as $\dot{P}$. The observational details of CVs we chose in our study can be found in Table 1.

3. Data Processing Methods

3.1 Data smoothing and interpolation

After importing the data from MAST, the light curves then undergo a few data processing steps. First, we remove any *NaN* values, and remove any bright, long-term features in the photometric flux data (i.e., outbursts) using a Savitzky-Golay filter. The way the Savitzky-Golay filter smooths

light curves is through convolution. We used a sliding window (a number of consecutive data points) and then fitted a second-degree polynomial to the flux values to get a smoothed value for each data point. The coefficients of the polynomial are obtained using least squares regression. After computing a smoothed flux value, it is subtracted from the original flux value to get a 'detrended' residual light curve. Large-scale flux variations are removed, leaving smaller variations like the eclipses unchanged. The Savitzky-Golay filter method is also used in the same way to smooth the eclipses in the light curves by fitting a Gaussian to a smaller sliding window instead. We apply a spline to the residual data to create a 12-second cadence light curve while skipping over observing gaps to avoid introducing unwanted artifacts. We use cubic splines to fill in the gaps between 2-minute cadence data points while skipping over gaps of 20 minutes or longer. An example of a detrended light curve for EX Dra can be found in Figure 1 below.

Table 1. TIC identification, source name, CV type, and observed time range of our CV sample.

TIC	CV	Class	ΔY (Years)
3034524	QZ Aur	C Nova	2019-2023
219107776	EX Dra	D Nova	2019-2024
9560142	EX Hya	D Nova	2019-2023
346897118	AY Psc	D Nova	2021-2023
61285257	DO Leo	D Nova	2020-2023
238609772	GY Cnc	D Nova	2021-2023
304628774	HBHA 4204-09	D Nova	2019-2024

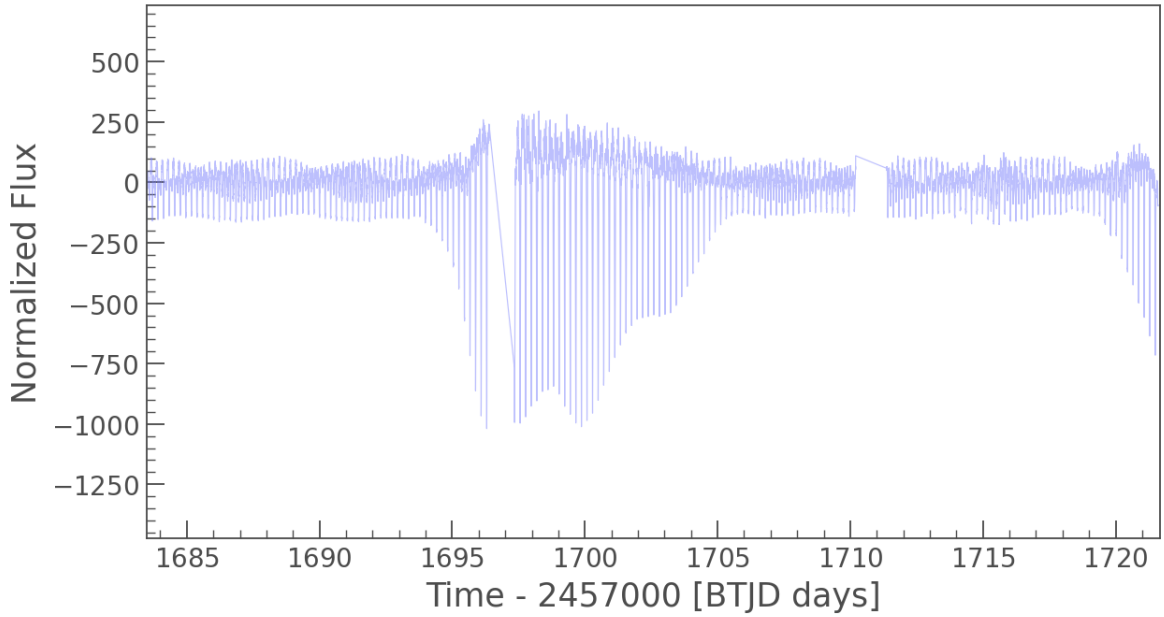

Figure 1. Detrended TESS light curve of Ex Dra. Time is in units of Barycentric Julian Day (BTJD), and amplitude is in units of normalized flux.

3.2 Periodogram analysis

To find the orbital period of the binary star we applied a Lomb-Scargle periodogram to the residual light curve. Once a periodogram is obtained, we further processed it by applying cubic spline interpolation to smooth the power spectrum, making it easier to identify the desired peaks. Then, we used the smoothed periodogram to detect significant peaks, defined as those exceeding 10% of the maximum power. Once we manually identified the highest peak corresponding to the best-fit period, an initial Gaussian is fitted to the aforementioned peak based on the peak's height, center, and the estimated width. This initial guess for the Gaussian fit is used to find a best-fit Gaussian function allowing for a more accurate peak characterization, including the time of eclipse. We present an example periodogram fit in Figure 2 for Ex Dra.

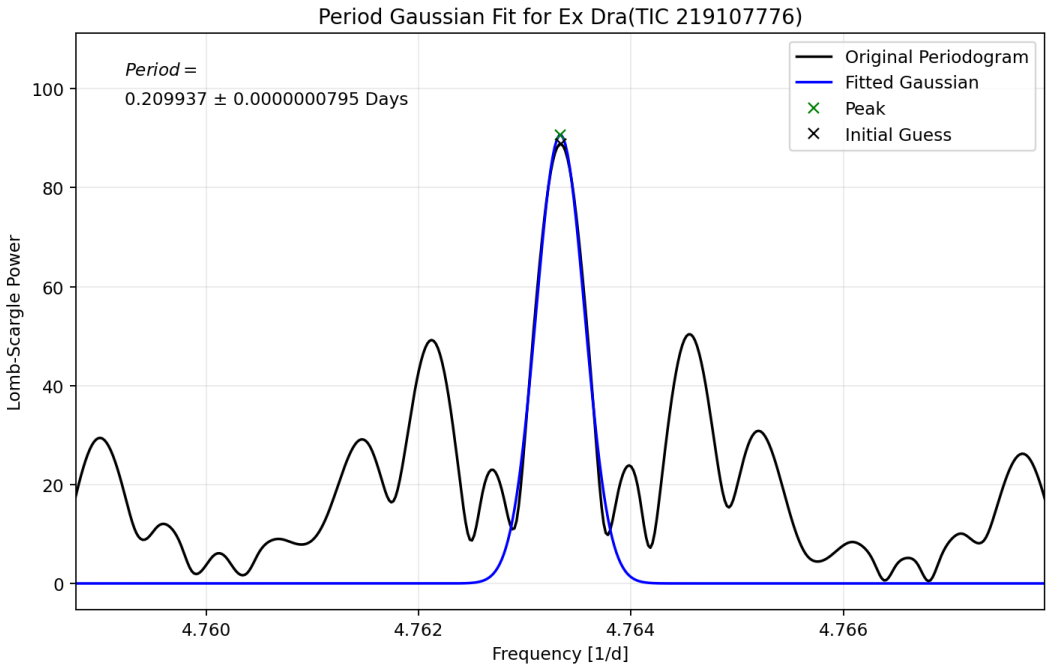

Figure 2. Lomb-Scargle periodogram for EX Dra. The highest peak was fitted by a Gaussian function for the orbital period.

3.3 Eclipse time fitting

Once we determined the orbital period, we used it to divide the light curve data into one period wide chunks containing the primary and secondary eclipses. We modeled the primary eclipse with an inverted Gaussian. From a sample chunk, we manually select two points in the eclipse portion of the light curve for which an initial guess of the full width at half maximum (FWHM) and the center of the eclipse are derived. Once the initial guess for both parameters are determined, we use them to generate a best-fit Gaussian for all eclipses in the light curve. An inverted Gaussian appears to work well for sources like EX Dra (Figure 3); however, we note here that low signal-to-noise, and contamination from features associated with outbursts and the accretion disk, can make fitting difficult. As we progress toward surveying additional sources in the future, we may utilize a phase-folded light curve as a template for fitting eclipse times. This

processing step allows us to extract the observed (*O*) eclipse times necessary for creating an O-C diagram.

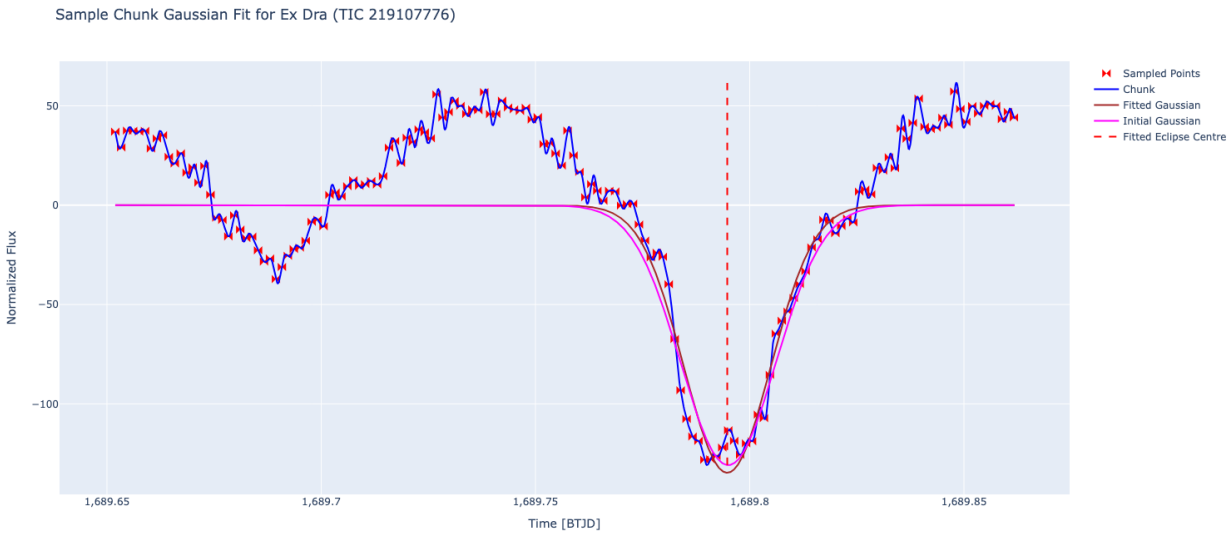

Figure 3. Sample chunk from EX Dra with inverse Gaussian fit. Time is measured in Barycentric Julian Day (BTJD), and amplitude is expressed in normalized flux.

3.4 $O-C$ diagrams and $\dot{P}$

After extracting the observed eclipse times O we then calculated the predicted C eclipse times from the following equation:

$$C = T_0 + EP$$

Where T_0 is the initial time value in the light curve, E is the epoch or cycle number of the eclipse, and P is the orbital period we determined from the Lomb-Scargle periodogram. Once we have both O and C values, we plot $O-C$ versus eclipse cycle number E and fit a quadratic curve to the data. If there is a non-zero period derivative we expect the $O-C$ diagram to exhibit a quadratic curvature according to the following relationship:

$$O - C = \frac{1}{2} P \dot{P} E^2$$

The $O-C$ diagram for EX Dra (Fig. 4) exhibits a positive quadratic curve, indicating a positive value of $\dot{P}$. The $O-C$ diagrams of the other six sources (Fig. 5) exhibit positive and negative quadratic trends.

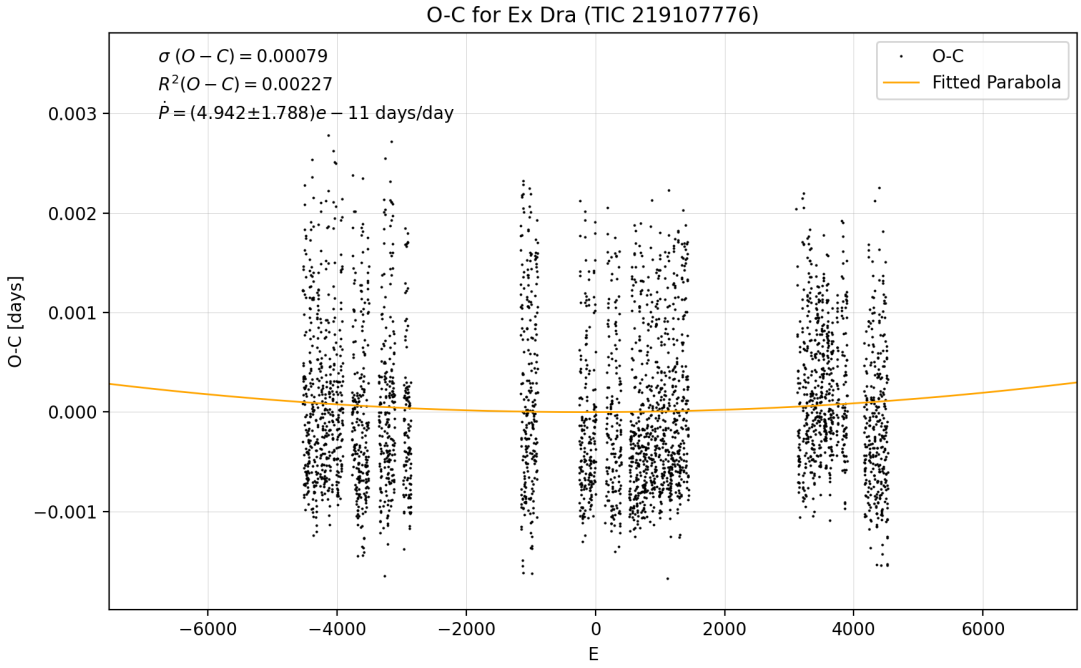

Figure 4. $O-C$ diagram for EX Dra with time measured in epochs.

4. Results and Discussion

We summarize the results of our time series analysis of the target sources in Table 2 and briefly discuss our findings for each source. The periods are listed in units of days, and the period derivative $\dot{P}$ is in units of days/day.

Table 2. Period (P) and period change ($\dot{P}$) values for our sources.

CV	P (days)	P-dot (10^{-9} days/day)
QZ Aur	0.35750347 ± 0.0000001	1.563 ± 0.198
EX Dra	0.209937 ± 0.00000000795	4.942 ± 1.788 x 10^{-2}
EX Hya	0.068228 ± 0.000000021	9.1322 ± 4.142 x 10^{-1}
AY Psc	0.217323 ± 0.0000008643	2.189 ± 1.388
DO Leo	0.234516 ± 0.0000000555	-5.901 ± 0.875 x 10^{-1}
GY Cnc	0.175441 ± 0.0000005915	-1.912 ± 3.930 x 10^{-1}
HBHA 4204-09	0.141295 ± 0.0000001229	-7.279 ± 5.059 x 10^{-2}

4.1 QZ Aur

QZ Aur is classified as a classical nova, last seen to go nova in 1964 (Sanduleak 1975). In its quiescent state, QZ Aur has a typical V magnitude of ~17 (Shi and Qian 2014). The orbital period of QZ Aur is 0.3575 days, or about 8.58 hours, in agreement with previous measurement (Campbell and Shafter 1995). Using only TESS data, our O-C diagram yielded a positive $\dot{P}$ of 1.563 (± 0.198) x 10^{-9}. However, after including additional eclipse times over a span of several decades, Schaefer (2004) found that the O-C is inverted, with a $\dot{P}$ of -3.9(± 1.4) x 10^{-11}. While the cadence and repetition of TESS data can provide us with highly precise orbital information on short time

scales of a few years, we cannot discount the power of time domain astronomy to reflect the true nature of the orbital dynamics of complex systems like cataclysmic variables.

4.2 EX Dra

EX Dra was discovered as a variable star in the Hamburg Quasar Survey (Bade et al. 1989). It was identified as an eclipsing dwarf nova due to its periodic outbursts and the accumulation and release of material from the donor star onto the white dwarf (Barwig et al. 1993). During outbursts, EX Dra's brightness can rise from its quiescent state of magnitude of 15 to as high as 13.5. Outbursts occur every 10 to 30 days and last about 10 days (Voloshina et al. 2021). The orbital period of EX Dra is 0.21 days, or about 5 hours, in agreement with previous observations (Voloshina et al. 2021). Using only TESS data, a fit of our O-C diagram (Fig. 4) shows a $\dot{P}$ of 4.942 (± 1.788) x 10^{-11}, almost one standard deviation from the value determined by Schaefer (2024) of 3.05 (± 0.32) x 10^{-11}, who used data from TESS and eclipse epochs from as early as 1991.

4.3 EX Hya

EX Hya was discovered as a variable star by Brun and Petit (1957) and classified as a dwarf nova in 1980 (Andronov and Breus 2013). It is an eclipsing intermediate polar-type cataclysmic variable with ultrashort periods. EX Hya shows dwarf nova oscillations with highly erratic outbursts, where the magnitude can vary from about 14.1 to 9.2 (AAVSO 2024). This eclipsing binary has a very short orbital period of 0.068234 days, or about 1.6 hours, in agreement with the optical and X-ray observations of Mukai (2024). The $\dot{P}$ derived from our O-C diagram is 9.132 (± 4.142) x 10^{-10}. However, over a longer time period, Schaefer (2024) found a $\dot{P}$ of - 7.2 (± 0.5) x 10^{-12} from records dating back to 1962. This CV is certainly more of a challenge to characterize, as the O-C timing jitter require longer term time domain observations to characterize its orbital dynamics.

4.4 AY Psc

AY Piscium is classified as a Z Camelopardalis (Z Cam) type dwarf nova, identified by Green et al. (1982). This subtype of cataclysmic variable stars exhibits both normal outbursts and standstills, where the brightness remains nearly constant for extended periods (Kára et al. 2023). AY Psc experiences quasi-periodic outbursts with an amplitude of about 2.5 magnitudes during which the system reaches the maximal brightness of 14.6 mag (Han et al. 2017). For AY Psc, we measured an orbital period of 0.2173 days, or about 5.2 hours, in agreement with the period found by Kára et al. (2023). The $\dot{P}$ we measured from a quadratic fit of the O-C diagram is 2.189 (± 1.388) x 10^{-9}; however, we note that Kára et al. (2023) found a value about 100 times lower (2.08 x 10^{-11}) from recorded eclipse times spanning almost thirty years.

4.5 DO Leo

DO Leo was found by Green et al. (1986) while searching for faint blue stars at high galactic latitudes. This binary system is a dwarf nova of the SU Ursae Majoris (SU UMa) subtype with a magnitude of 16 (Abbott et al. 1990). DO Leo undergoes frequent outbursts, with super outbursts occurring irregularly during its orbital period of 0.2345 days, or about 5.63 hours, as found by Abbott et al. (1990) and Bruch (2024). The $\dot{P}$ derived from our O-C diagram is -5.90(± 0.88)x10^{-10}.

4.6 GY Cnc

GY Cnc is an eclipsing cataclysmic variable star with an M-dwarf donor of spectral type M3 (Bours 2015). The system experiences frequent dwarf nova outbursts and eclipse timings with significant variability in brightness between 11.4 and 17.94 magnitudes (British Astronomical Association 2024). The orbital period we obtained for this object is 0.1754, or about 4.2 hours, in agreement with studies by Littlefair et al. 2023) and Cañizares et al. (2018). The $\dot{P}$ derived from our O-C diagram is -1.912(± 3.930) x 10^{-10}. Using Kepler observations, Cañizares et al. (2018). were unable to measure a $\dot{P}$. Our value has a high error, likely because there were only two TESS segments used in the quadratic fit. Future TESS (or other) observations can more precisely constrain the period derivative for this system.

4.7 HBHA 420-09

HBHA 4204-09 is an eclipsing binary system with negative superhumps (nSHs) detected in its light curve. It was discovered by ASAS-SN and classified as a CV by Jayasinghe et al. (2018) with a mean magnitude of 16.9. This system has been studied more extensively in recent years, particularly with data from the TESS. The orbital period of HBHA 4204-09 is approximately 0.1413 days, or about 3.4 hours, which is the same found by Stefanov and Stefanov (2023). The $\dot{P}$ derived from our O-C diagram is -7.279(± 5.059) x 10^{-11}. While the error is high compared to our $\dot{P}$ value, it is almost a factor of 10 lower than the error for GY Cnc because there are more segments to constrain the quadratic fit.

5. Conclusions

We have analyzed the TESS light curves of seven CV systems by creating Python code to download two-minute cadence photometric flux data, process them to find the orbital periods of these binary systems, and compared the observed to predicted O-C eclipse times to search for positive or negative changes of period with time. O-C diagrams are a versatile tool in astrophysics, particularly beneficial for studying binary star systems, including eclipsing cataclysmic variable stars, which system we can observe edge-on. Continued studies of these high-inclination systems could aid us in understanding the complex dynamics and evolutionary processes of these systems.

The fitted orbital periods of all our eclipsing CVs are in agreement with previous measurements found in literature. However, our success with determining the period derivative varied. By using only TESS data, our O-C diagrams had a three- to four-year time range from which we could make quadratic fits for $\dot{P}$. Our measured values of P and $\dot{P}$ for EX Dra were within one sigma of previous measurements, confirming the veracity of the processing applications we developed. However, our $\dot{P}$ values for QZ Aur, EX Hya, and AY Piscium did not agree with those determined from O-C studies that included data over longer time intervals. Our results can be improved with the inclusion of additional eclipse epochs for our sample CVs along with other systems we choose to study in the near future.

Our most promising results were those for DO Leo, GY Cnc, and HBHA 4204-09. Our measured periods are in agreement with those found in literature, and there appears to be no recent determination of $\dot{P}$ in literature for comparison. All three sources have negative period derivatives, indicating that their orbital periods are decreasing over time. A commonly cited explanation for period decrease over time is the action of magnetic braking in the binary system.

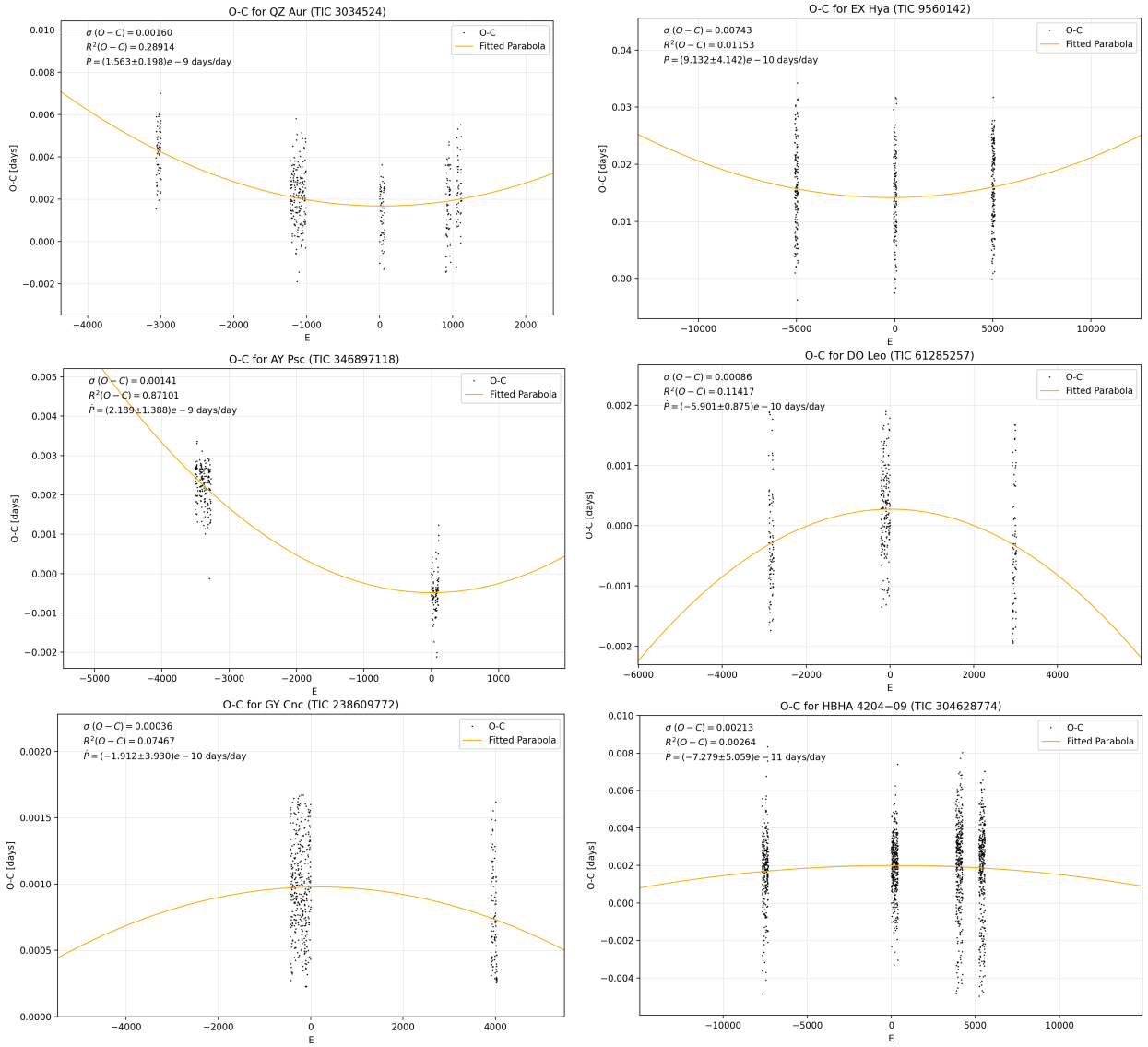

Figure 5. O-C diagrams with time measured in epochs.

Acknowledgements

The authors acknowledge support from the Furman University Summer Research Fellowship program. This paper includes data collected by the TESS mission. Funding for the TESS mission is provided by NASA's Science Mission Directorate. This research has used the SIMBAD database, operated at CDS, Strasbourg, France. We acknowledge with thanks the variable star observations from the AAVSO International Database contributed by observers worldwide and used in this research.

References

Abbott, T. M. C., Shafter, A. W., Wood, J. H., Tomaney, A. B., & Haswell, C. A. 1990, Publications of the Astronomical Society of the Pacific, 102, 558, doi: 10.1086/132669

American Association of Variable Star Observers (AAVSO). 2024, Ex Hydrae: Variable Star of the Season, https://www.aavso.org/vsots exhya

Andronov, I. L., & Breus, V. V. 2013, Astrophysics, 56, 518–530, doi: 10.1007/s10511-013-9304-7

Bade, N., Hagen, H.-J., & Reimers, D. 1989, in Two Topics in X-Ray Astronomy, ed. J. Hunt & B. Battrick, ESA SP-296 (Noordwijk: ESA), 883

Barclay, T. 2024, NASA - TESS Science Support Center

Barwig, H., Fiedler, H., Reimers, D., & Bade, N. 1993, in Compact Stars in Binary Systems, ed. H. van Woerden (Dordrecht: Kluwer), 89

Bours, M. C. P. 2015. http://webcat.warwick.ac.uk/record=b2844675~S1

British Astronomical Association. 2024, Observation Summary for Variable Star GY CNC, https://britastro.org/vssdb/objectsummary.php?object id=GY%20CNC

Bruch, A. 2024, ApJS, 273, 6, doi: 10.3847/1538-4365/ad43ec

Brun, A., & Petit, M. 1957, Peremennye Zvezdy, 12

Cañizares, L. A., Garnavich, P., Littlefield, C., et al. 2018, Research Notes of the American Astronomical Society, 2, 184, doi: 10.3847/2515-5172/aae48d

Campbell, R., & Shafter, A. 1995, ApJ, 440, 336, doi: 10.1086/175275

Green, R. F., Ferguson, D. H., Liebert, J., & Schmidt, M. 1982, PASP, 94, 560, doi: 10.1086/131022

Green, R. F., Schmidt, M., & Liebert, J. 1986, ApJS, 61, 305, doi: 10.1086/191115

Han, Z.-T., Qian, S.-B., Voloshina, I., & Zhu, L.-Y. 2017, Research in Astronomy and Astrophysics, 17, 056, doi: 10.1088/1674-4527/17/6/56

Jayasinghe, T., Kochanek, C. S., Stanek, K. Z., et al. 2018, MNRAS, 477, 3145, doi: 10.1093/mnras/sty838

Kára, J., Zharikov, S., Wolf, M., et al. 2023, The Astrophysical Journal, 950, 47, doi: 10.3847/1538-4357/accd63

Littlefair, S. P., Rodríguez-Gil, P., Marsh, T. R., Parsons, S. G., & Dhillon, V. S. 2023, Monthly Notices of the Royal Astronomical Society, 527, 4353, doi: 10.1093/mnras/stad3500

Mukai, K. 2024, EX Hydrae, https://asd.gsfc.nasa.gov/Koji.Mukai/iphome/systems/exhya.html

Sanduleak, N. 1975, Information Bulletin on Variable Stars, 1011, 1

Schaefer, B. E. 2024, Evolutionary Period Changes For 52 Cataclysmic Variables, and the Failure For the Most Fundamental Prediction of the Magnetic Braking Model. https://arxiv.org/abs/2404.12525

Shi, G., & Qian, S.-B. 2014, Publications of the Astronomical Society of Japan, 66, 41, doi: 10.1093/pasj/psu004

Stefanov, S. Y., & Stefanov, A. K. 2023, Monthly Notices of the Royal Astronomical Society, 520, 3355–3367, doi: 10.1093/mnras/stad259

Voloshina, I., Khruzina, T., & Metlov, V. 2021, in Photometric study of eclipsing dwarf nova EX Dra, 010, doi: 10.22323/1.368.0010

Engaging Amateur Astronomers with Dark Skies

Vayujeet Gokhale[1], John Barentine[2], Jessica Heim[3], and James Lowenthal[4]

[1]Truman State University, 100 E. Normal Street, Kirksville, MO, 63501, USA; gokhale@truman.edu; [2]Dark Sky Consulting, PMB 237, 9420 E. Golf Links Rd., Ste 108, Tucson, AZ, 85730, USA; john@darkskyconsulting.com; [2]DarkSky Southern Arizona, 5049 East Broadway Blvd #105, Tucson, AZ, 85711, USA; [3]University of Southern Queensland, Centre for Astrophysics West Street, Toowoomba Qld 4350, Australia; Jessica.Heim@usq.edu.au; [4]Dept. of Astronomy, Smith College, Northampton, MA, 01060, USA; jlowenth@smith.edu

Subject Keywords

AAVSO keywords = Light Pollution; Satellites; Professional-Amateur Collaboration

Abstract

We present an overview of the American Astronomical Society's Committee for the Protection of Astronomy and the Space Environment (COMPASSE). Light pollution has always presented a challenge to both amateur and professional astronomers, but this problem has become increasingly acute with the advent of unshielded outdoor LED lights and the launching of massive groups of satellites by private commercial space companies. In this talk, we outline the efforts currently underway to (re-)engage professional and amateur astronomers in quantifying the effects due to both these causes, as well as in outreach efforts made recently towards engaging the media and policy-makers. Finally, we describe the resources available for amateur astronomers and casual stargazers to contribute towards protecting the night sky, starting with collecting and analyzing original measurements.

1. Introduction

Ground-based astronomy is facing several challenges, both from the exponentially growing use of artificial light at night (ALAN) and increasingly from the proliferation of commercial activity and large satellite swarms in low Earth orbit (LEO). Amateur astronomers and casual stargazers have long been aware of ground-based light pollution, usually manifesting itself as either skyglow or direct glare, but the increasing use of LED lighting has made the problem much more acute. In fact, some estimates show that skyglow is increasing at an average annual rate of about 10% in North America (Kyba et al., 2023). Similarly, amateur astronomers, and especially astrophotographers, have long treated the occasional satellite streak in their images as a relatively minor nuisance. However, in just the last decade the number of satellites in LEO has increased from about 2,000 to close to 10,000 (McDowell, 2025). Within the next few years and decades, this number is expected to rise at least by one order of magnitude (Falle et al., 2023), which means that at any moment, several dozen satellites will be above the horizon from any location of our planet throughout the night, not just around twilight. Without appropriate

mitigations, this is likely to have a significant and detrimental effect on casual stargazing, astrophotography, radio-astronomy, and optical astronomical observations (Walker et al., 2021).

In view of these potentially existential threats, the *Committee on Light Pollution, Radio Interference, and Space Debris* (LPRISD) of the American Astronomical Society (AAS), was handed an expanded charge and renamed in April 2023 as the AAS *Committee for the Protection of AStronomy and the Space Environment* (COMPASSE)[1]. COMPASSE represents the interests of AAS relating to the protection of dark and radio-quiet skies, the safe and sustainable use of outer space, and related issues, and empowers AAS members to be effective advocates for the protection of US astronomy.

In this paper, we outline the ways in which the amateur astronomy community can contribute towards mitigating some of these threats. Amateur astronomers are well versed in various technical aspects of these issues: properties associated with light such as brightness, magnitude, color spectrum; as well as the basic Earth-Sun-satellites geometry. We begin in Section 2 with an overview of COMPASSE: its structure, composition, and activities. In Section 3.1, we outline how amateurs can help quantify ground-based ALAN, and help advocate for the relatively simple solutions to this problem. In Section 3.2, we provide suggestions and resources for amateurs to contribute towards addressing the problems posed by satellite streaks on CCD and digital camera images. We also list other ways in which amateur astronomers can leverage their access and natural talent for public outreach, to help raise awareness about this issue with members of the general public, government officials, and satellite operators. We conclude with a discussion on some of the successes and challenges astronomers face and how astronomers of all stripes need to work together to preserve the night sky for future generations.

2. An Overview of COMPASSE

COMPASSE is a committee of the AAS Board of Trustees tasked with building up expertise and engaging in advocacy around a series of issues affecting astronomy and the ability of AAS to achieve its mission[2], which goes beyond just representing a society of professional astronomers. These range from more familiar topics like terrestrial light pollution to emergent concerns such as the use of the Earth's Moon and the space surrounding it. In addition to its advisory role, COMPASSE educates and informs the AAS membership, the media, public officials, and the public. Based on the backgrounds, interests, and expertise, COMPASSE members are focussing their efforts on the following broad topics:

a) **Light Pollution**: Educate AAS members and the public about terrestrial light pollution problems and solutions, and collaborate with DarkSky International and other organizations (such as AAVSO) with a shared interest in preserving dark skies and naturally dark night-time environments.

[1] https://compasse.aas.org/

[2] "*The mission of the American Astronomical Society is to enhance and share humanity's scientific understanding of the universe as a diverse and inclusive astronomical community.*"

b) **Satellite Constellations**: Provide briefings for various agencies of the U.S. federal government, engage in research relating to satellite constellations and astronomy, and offer interviews to interested media.
c) **Community Engagement (CE)**: Engage with the AAS membership specifically on all aspects of the COMPASSE remit. Be the conduit for communicating COMPASSE activities and related information to the broader AAS membership.
d) **Space Debris**: Monitor developments in the orbital debris population, technologies to reduce debris proliferation, and explore opportunities to strengthen regulation of space activities that contribute to debris generation.
e) **Electromagnetic Interference**: Advocate for radio astronomy protections at fora such as the World Radiocommunication Conferences and other meetings of the International Telecommunications Union.
f) **Public Policy**: Examine opportunities across all COMPASSE subjects to formulate and analyze U.S. federal policy, propose new policy agenda for AAS to consider, and help articulate AAS positions on various policy issues. Work closely with the AAS Committee on Astronomy and Public Policy as well as the AAS Public Policy office, which tracks related federal legislation and agency rulemaking relating to satellite constellations and radio spectrum allocation.

COMPASSE members are appointed by approval of the AAS Board of Trustees and serve three-year terms. COMPASSE currently has nearly 30 members, spanning faculty and staff from research as well as teaching-focused universities, members of advocacy groups or small private firms, planetaria staff, individuals/retirees with no working affiliation, policy experts, and graduate and undergraduate students. Committee members are engaged in a broad range of advocacy areas, ranging from professional astronomy to dark-sky advocacy, space law, environmental concerns and sustainability, amateur astronomy, planetaria communities and development of exhibits/shows, and broader community concerns.

A growing realization within the astronomy community is that professional astronomers alone often do not have the wherewithal, capacity, and influence to make a consequential impact on mitigating or reversing the current trend in the worsening situation in our night sky. Amateur astronomers possess many of the technical skills required to contribute to the science necessary to define the problems posed by light pollution and also have an interest in advocating for some of the mitigation strategies proposed by COMPASSE. Also, they often have more of a prominent public platform than most professional astronomers by virtue of extensive outreach work in their communities. Consequently, it makes sense for professional and amateur astronomers to work together, and this presentation is a modest attempt to re-engage. In the following sections, we list how amateur astronomers can contribute towards COMPASSE efforts to address ground-based ALAN, satellite swarms, and public outreach and policy solutions.

3. Amateur Astronomers, COMPASSE and Dark & Quiet Skies

3.1 ALAN: Ground-based light pollution

Amateur astronomers are well aware of the effects of the use of ALAN, and how the resulting skyglow affects stargazing and astronomical observations (Barentine, 2022; Green et al., 2022; Varela Perez, 2023). With the advent of LED lights, an increasing concern is direct glare and the presence of short-wavelength radiation in the outdoor environment (Barentine, 2024 and references therein). This is not just detrimental to astronomy, but also has a negative impact on human health, safety, and wildlife. Given that astronomers have a vested interest in keeping the skies dark from the impacts of ground-based lighting, we suggest the following ways in which amateurs can contribute towards COMPASSE's goal of protecting our night sky:

1) Help communities create lighting inventories of outdoor luminaires that catalog lumen levels, spectral information, and the CCT temperature of lights,
2) Conduct sky brightness measurements using Sky Quality Meters (SQMs) and participating in the Globe at Night program[3],
3) Coordinate and conduct star parties that include demonstrations and discussions on light pollution in local parks and downtown areas,
4) Partner with, and provide technical support (inventories, lighting specs, SQM measurements, etc.) to other dark sky advocates and local, regional, and statewide ecological conservation and human health organizations (e.g. statewide chapters of Sierra Club, Audubon, medical associations, etc.) that have an interest in protecting human health and safety, migratory birds, pollinators, and wildlife in general. This will help significantly broaden the reach and impact of the "protect the night" message and,
5) Talk to local city administrators, homeowners, and businesses about the benefits of using fully shielded, low-color temperature lights of appropriate brightness that are consistent with the Five Principles for Responsible Outdoor Lighting (see Figure 1).

Along with the materials available via DarkSky International[4], COMPASSE has put together a slew of materials that includes 2-page "Leave-behinds" for lawmakers, a slide-deck for outreach and 101-level classes, and a "Campus SHINE" package for school campuses. The Campus SHINE package contains, among other things, how-to guides for doing inventories, measuring color temperatures and light intensities, as well as taking SQM readings[5]. These materials can be readily modified or used as-is by amateur astronomers for personal use and for training other interested individuals.

[3] https://globeatnight.org/
[4] https://darksky.org/resources/
[5] https://www.campusshine.org/aas245.html

Figure 1. The five principles for responsible outdoor lighting, as articulated by DarkSky International and the Illuminating Engineering Society.

3.2 Satellite swarms

As mentioned above, the growth of LEO satellites is likely to have a significant and detrimental effect on amateur and professional astronomy. COMPASSE is working on several fronts to address this issue, including helping the AAS frame policy position statements, provide briefings for various US federal agencies and raising this topic during AAS Congressional Visit Days[6]. The International Astronomical Union (IAU) has organized the world's professional astronomical community to address the problem and propose solutions (Józsa et al., 2024). Several COMPASSE members are working with the IAU, in particular with its Centre for the Protection of the Dark and Quiet Sky from Satellite Constellation Interference (IAU-CPS[7]) and IAU Commission C.B7[8], which is concerned with protecting current and potential astronomical observatory sites from light pollution.

An increasingly crowded LEO space will not just interfere with astronomical observations; it will affect astrophotography and casual stargazing (Venkatesan et al., 2021). Radio transmissions from satellites can also overload the sensitive detectors of radio telescopes (Walker and Benvenuti, 2022). Again, amateur astronomers have a vested interest in protecting the night sky by working with other interested parties in mitigating the impact of this new trend. We suggest the following ways in which amateur astronomers can do this:

[6] https://aas.org/advocacy/how-aas-advocates/congressional-visits-days
[7] https://cps.iau.org/
[8] https://www.iau.org/science/scientific_bodies/commissions/B7/

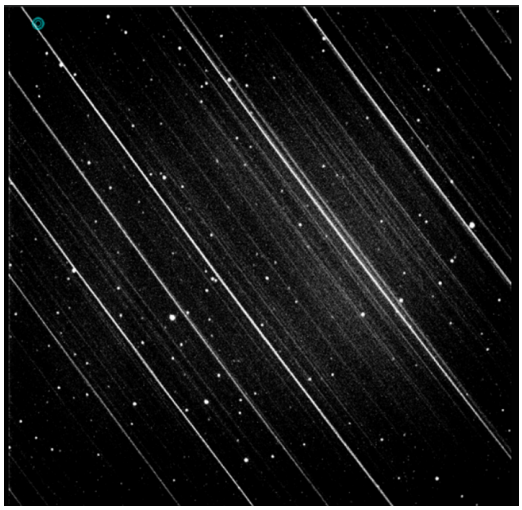

Figure 2. Optical interference of a science image from satellite swarm trails.

1) Submit visual magnitudes of satellites: Satellite brightness measurements can be made in different ways, even without recourse to expensive optical set-ups. For example, visual observations of satellites have already contributed towards quantifying satellite brightness (Mallama et al., 2024). Images from digital cameras used in video mode and wide-field CMOS sensors, as well as from CCD cameras (Figure 2) can be submitted for further analyses[9]. IAU-CPS has developed the Satellite Constellation Observation Repository (SCORE[10]), where anyone can submit their observations into a data repository and use other tools, depending on their interests and capabilities. A training curriculum is also available, for those who might be interested in pursuing satellite observations.
2) Create awareness: The general public is largely unaware of the potential problems associated with having close to 400,000 satellites in LEO. More than 1 million debris fragments larger than 1-cm may already be in orbit around the Earth. Apart from the threat of collisions that could trigger the Kessler syndrome (Kessler and Cour-Palais, 1978), the limited lifecycle of satellites poses both security and environmental threats[11]. Pollution from launches, deposition of rare Earths and other metals in the upper atmosphere has consequences on the Earth system and on the wellbeing of life on our planet (Boley and Byers, 2021). Amateur astronomers and astrophotographers, who have their vigilant eyes on the night sky, are ideal ambassadors to highlight these issues and drive public opinion towards reaching a sustainable and responsible LEO environment. The IAU CPS offers materials to help the public understand the issues, including its "SatCons 101" curriculum[12].

[9] https://trailblazer.dirac.dev/
[10] https://score.cps.iau.org/
[11] https://www.kesslerrebellion.com/
[12] https://cps.iau.org/community-engagement-hub/satcons-101/

4. Discussion

The increased use of outdoor LED lights and the proliferation of satellite swarms represent a paradigm shift in our relationship with natural darkness in the nighttime environment, and by extension, to the night sky. These are no longer minor nuisances that can be ignored or dealt with by "moving a few more miles away from town": Ground-based astronomy worldwide is now facing an existential threat. Consequently, it is in the interests of *all* astronomers — professionals, amateurs, astrophotographers, nightscapers, and casual stargazers — to work together to mitigate the detrimental effects of these developments, and preserve the night sky for ourselves and for future generations.

COMPASSE members are working with various partners at the national and international level to help quantify these problems, brief public officials to help them formulate dark-sky-friendly policies, and inform the public about light pollution and the myriad of issues that go with the exponential crowding of LEO. However, professional astronomers cannot do this alone. They need help from amateur astronomers, who bring with them a much broader range of experiences, expertise, and skills necessary to address these challenges. In fact, many of the issues that these developments will create go way beyond astronomy: human health (Cao, Xu and Yin, 2023), the effect on migratory birds and pollinators and other ecological issues associated with ALAN (Rich & Longcore, 2005), the loss of night as a cultural and inspirational resource (Dunn and Edensor, 2024); environmental concerns associated with launches and deposition of metals into the upper atmosphere (Schulz and Glassmeier, 2021), and security concerns such as the Kessler syndrome are all real and consequential matters that are of greater relevance to the general public.

To conclude, we, as representatives of COMPASSE, invite the amateur astronomy community to collaborate with us as we seek to address these questions and more in coming years:

1. *What does the amateur community need?*
    a. *Develop a CHOICE Course[13]?*
    b. *Or a special web-seminar or web-series?*
2. *How can AAVSO members (and others) contribute?*
3. *What role do we play in this as individual astronomers?*
4. *What role do we play in this as a community?*
5. *Beyond astronomy, what are the environmental and ethical questions that need to be highlighted and addressed?*
6. *What are the best communication strategies based on experience and research? (towards the general public, policy makers, etc.)*
7. *How to develop synergy between COMPASSE, DarkSky International, AAVSO, and the Astronomical League, as well as environmental organizations such as National Audubon Society and the Sierra Club?*

[13] https://www.aavso.org/tags/choice-courses

If you would like to engage with us on one or more of these questions, explore collaborations, or have other general comments and suggestions, please do not hesitate to contact us.

Acknowledgements

VG would like to thank the Missouri Space Grant Consortium for travel support. VG also would like to thank Michelle Wooten (University of Alabama-Birmingham) for her help during the AAVSO meeting.

References

Barentine, J. 2022, *Nat. Astron.*, 6, 1120

Barentine, J. 2024, *Artificial Light at Night: State of the Science 2024*. Zenodo. https://doi.org/10.5281/zenodo.11431447

Boley, A. C., & Byers, M. 2021, *Sci. Rep.*, 11, 10642

Cao, M., Xu, T., & Yin, D. 2023, *J. of Env. Sci.*, **127**, 589

Dunn, N., & Edensor, T. 2024. *Dark skies: places, practices, communities*, London: Taylor & Francis

Falle, A., Wright, E., Boley, A. C., & Byers, M. 2023, *Science*, **382**, 150

Green, R.F., Luginbuhl, C.B., Wainscoat, R.J. et al. 2022, Astron. Astrophys. Rev. **30**, 1.

Józsa, G., et al. 2024, *Call to Protect the Dark and Quiet Sky from Harmful Interference by Satellite Constellations*. arXiv. https://doi.org/10.48550/ARXIV.2412.08244

Kessler, D. J., & Cour-Palais, B. G. 1978, *J. Geophys. Res.: Space Phys.*, **83**, 2637

Kyba, C. C. M., Altıntaş, Y. Ö., Walker, C. E., & Newhouse, M. 2023, *Science*, **379**, 265

Mallama, A., Cole, R. E., Harrington, S., & Respler, J. 2024, arXiv, arXiv:2407.03092

Rich, C., & Longcore, T. (Eds.) 2005, *Ecological Consequences of Artificial Night Lighting*, Washington D.C.: Island Press

Schulz, L., & Glassmeier, K.-H. 2021, *Adv. in Space Res.*, **67**, 1002

Varela Perez, A. M. 2023, Science, **380**, 1136

Venkatesan, A., et al. 2021, *SATCON2 Community Engagement Working Group Report*. Zenodo. https://doi.org/10.5281/ZENODO.5608920

Walker, C., et al. 2021, *Dark and Quiet Skies for Science and Society: Report and recommendations*. Zenodo. https://doi.org/10.5281/ZENODO.5898785

Walker, C., & Benvenuti, P. (Eds). 2022, *Dark and Quiet Skies II Working Group Reports*. Zenodo. https://doi.org/10.5281/ZENODO.5874724

Time Series Analysis of Mira SED Fits

Zachariah Goodrich, Atticus Stewart,
Dana K. Baylis-Aguirre, Michelle J. Creech-Eakman

New Mexico Institute of Mining and Technology, 801 Leroy Place, Socorro, New Mexico, USA;
zachary.goodrich@student.nmt.edu

Gerard van Belle
Lowell Observatory, 1400 West Mars Hill Road, Flagstaff, Arizona, USA; gerard@lowell.edu

Subject Keywords

Mira variables, stars: individual (S Lac), Mira Reference Dataset, AAVSO

Abstract

The conditions in Mira variable atmospheres make them wonderful laboratories to study a variety of stellar physics such as molecule plus grain formation, dust production, shock chemistry, stellar winds, mass-loss, opacity driven pulsation, and shocks. Mira stars are asymptotic giant branch (AGB) stars that regularly pulsate and release copious dust from their atmospheres that chemically enrich their surrounding environments. Mira progenitors are low-to-intermediate mass stars (0.8-8 solar masses) while on the main sequence and can be found all over the galaxy. The goal of this project is to develop spectral energy distribution (SED) models as part of the *Mira Reference Dataset*. This dataset will provide information on 106 Mira variables and be readily accessible, serving as a reference tool for both professional astronomers and citizen scientists studying these stars. We show preliminary time-series analysis of the SED fits for S Lac. Photometric data for these SED fits were taken with the fully automated Titan Monitor (TiMo) telescope at Lowell Observatory. The SED fits allow us to study how much energy is coming out of the atmosphere through the pulsation cycle and make basic predictions on flux, temperature and angular diameter with phase.

1. Introduction

Mira variables are regularly pulsating Asymptotic Giant Branch (AGB) stars with periods ranging from 100 to 500 days. We track pulsation with phase, φ, which allows us to study and compare time-dependent behavior from different pulsation cycles. Phase values range from 0 to 1, with φ = 0 (or 1) corresponding to maximum optical brightness and φ ~ 0.4-0.6 corresponding to minimum optical brightness. Maxima are expected to occur when the Mira is smallest, hottest, and optically brightest, while minima occur when the Mira is most expanded, coolest, and optically dimmest.

The regular pulsations of these stars help drive significant mass loss and release substantial

amounts of dust and molecules from their atmospheres, which chemically enriches the surrounding environment (Nakagawa et al. 2012). The pulsations create highly dynamic local environments, and significant fluctuations in their visual brightness. During their pulsation cycle, the star's atmospheric opacity increases, leading to energy retention, which lifts the atmosphere, causing it to expand until it cools enough that the energy escapes, at which point the atmosphere contracts again (Templeton et al. 2005).

In their envelopes, convective cells can reach the carbon-oxygen degenerate core, dredging up material from deeper layers to the stellar surface. This material is eventually expelled, enriching the dusty circumstellar envelope around the star. The effective temperature of the photosphere ranges from 2000 to 3500 K, allowing for the formation of more complex molecules and molecular condensates (i.e. dust). M-type stars, which are oxygen-rich, and C-type stars, which are carbon-rich, differ based on the elements present in their respective circumstellar environments (CSEs) (Nakagawa et al. 2012). These unique conditions in the atmospheres of Mira variables make them excellent laboratories for studying a variety of stellar phenomena, including molecular and grain formation, dust production, shock chemistry, stellar winds, mass loss, opacity-driven pulsations, and shock dynamics. By analyzing the spectral energy distribution (SED) of the star, we can fit synthetic spectra to the CSE to obtain valuable information, such as effective temperature and bolometric flux. Given the star's pulsation period, a time-series SED can be created to examine how the CSE responds to stellar pulsation.

2. Mira Reference Dataset

The *Mira Reference Dataset* contains 106 Miras that were monitored for a decade with the Palomar Testbed Interferometer (PTI), which was a single-baseline near-IR long-baseline astronomical interferometer. PTI monitored the angular diameters of the Miras across their pulsation cycles. Directly measuring their sizes in this manner allows us to directly determine fundamental parameters such as the stellar radius, effective temperature, and bolometric flux, with a minimum of assumptions. The *Mira Reference Dataset* will provide these fundamental parameters as well as ancillary data such as spectroscopy and will be made publicly available online. Full details can be found in Baylis-Aguirre et al. (2024) and Creech-Eakman et al. (2022). We are presently developing detailed time-series spectral energy (SED) fits for target stars in the set to see what can be predicted from photometry alone.

3. Case Study: Time Series SED Fit of S Lac

3.1 Photometric Data Collection

The Titan Monitor (TiMo) is a robotic 0.5 m PlaneWave CDK20 operated out of Lowell Observatory (Figure 1). TiMo is equipped with a CCD-based photometer with a Sloan *u'g'r'i'z'* filter set, as well as 13 narrow-band (10nm wide) filters from 430 to 940nm. TiMo operates robotically on clear nights and can provide time-series absolute photometry by obtaining calibration objects at a range of zenith angles and performing nightly calibrated fits. Backend post-processing is then

used to fit spectral energy distributions, providing fits for spectral type, bolometric flux, angular diameter and interstellar reddening.

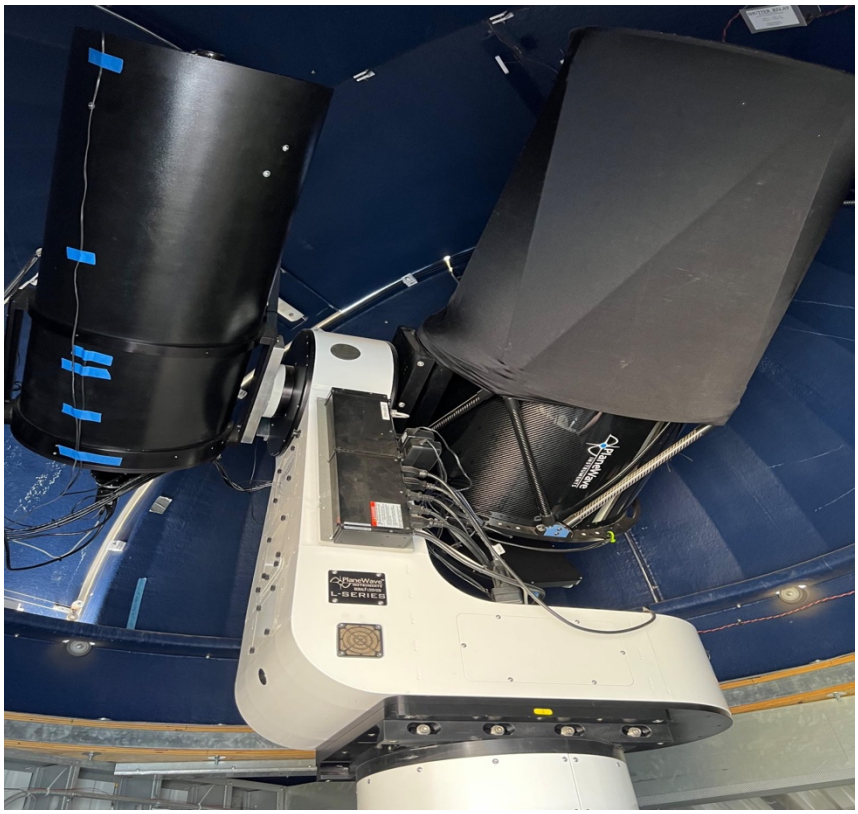

Figure 1. Photometry data presented in this work were collected using the Lowell Observatory's Titan Monitor (TiMo), a robotic 0.5 m PlaneWave CDK20. TiMo is equipped with a CCD-based photometer with a Sloan u'g'r'i'z' filter set, as well as 13 narrowband (10nm) filters from 430 to 940nm.

3.2 SED Fit and PHOENIX Grids

SED fits were created by fitting the TiMo photometry data with the *sedFit* code. sedFit works by performing a best fit to the photometry data with a synthetic stellar atmosphere calculation or grid. We chose to use the PHOENIX grid (Husser 2011) of synthetic stellar atmospheres because of its extensive spectral line list and match to the appropriate temperatures (at 100K spacings). sedFit calculates the star's effective temperature, bolometric flux, and estimated angular diameter. Creating time-series of these fits will allow us to track how a particular Mira changes with the pulsation period. A preliminary time series for the oxygen-rich Mira S Lac is presented in Figure 2. An accompanying light-curve, generated from AAVSO data is presented in Figure 3 for comparison of these fundamental parameters to S Lac's visual period.

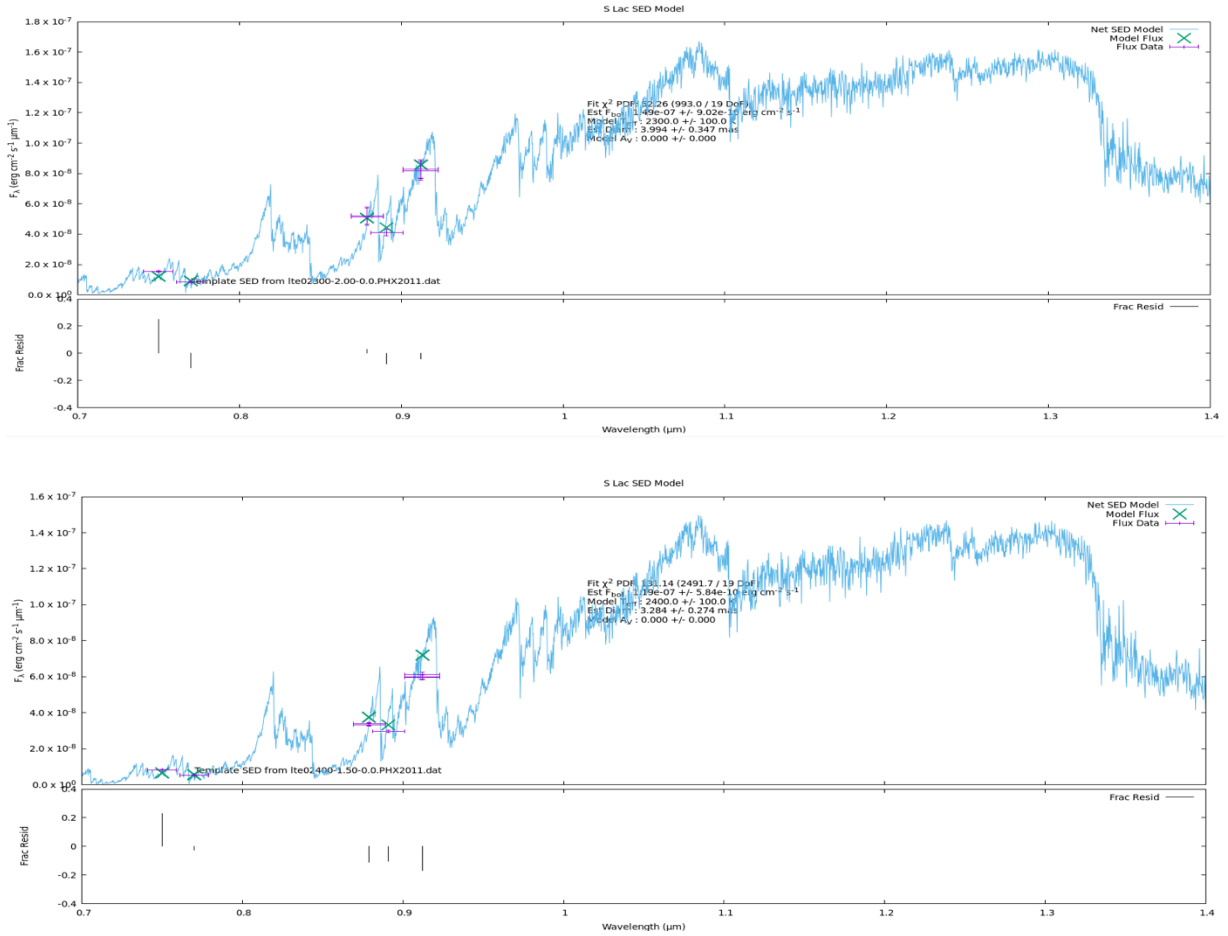

Figure 2. Preliminary time-series of SED fits for M-type Mira S Lac between June-July 2024. SED fits were done using sedFit and best fits were determined using minimization of the residuals. Top: sedFit model fit to the TiMo photometry (purple) and associated residuals (bottom) for S Lac on 2024-06-15 at φ = 0.32. The model indicates an effective temperature of 2300 K, a bolometric flux of 1.49E-7 erg cm^{-2} s^{-1} and an approximate angular diameter of 4 milliarcseconds. *Bottom: sedFit model fit to the TiMo photometry (purple) and residuals (bottom) for S Lac on 2024-07-06 at ϕ = 0.42. The model indicates an effective temperature of 2400 K, a bolometric flux of 1.19E-7 erg cm^{-2} s^{-1} and an approximate angular diameter of 3.3 milliarcseconds.*

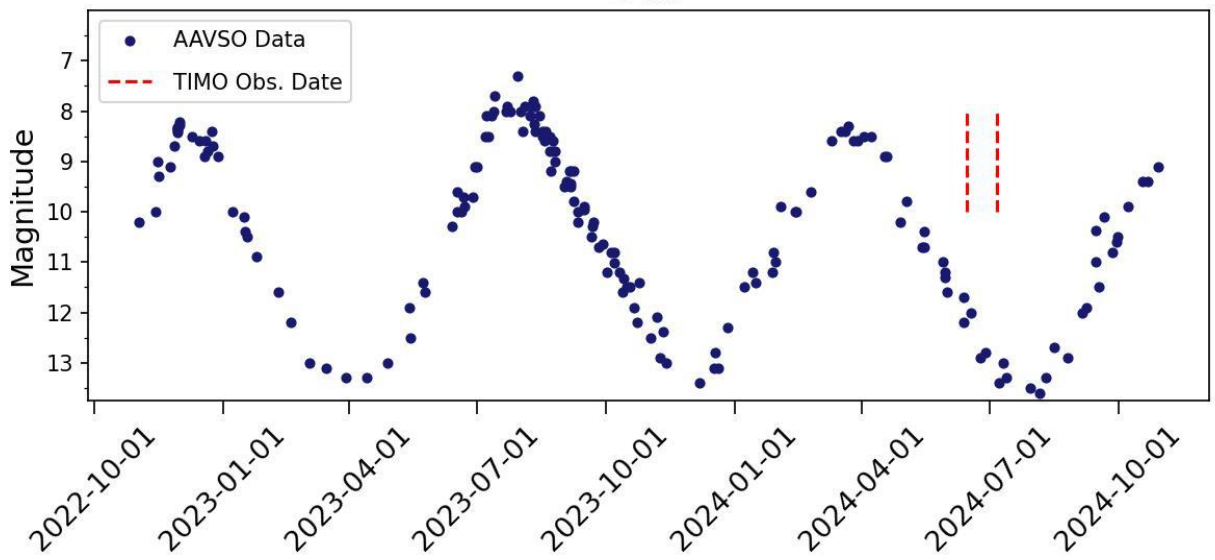

Figure 3. Visual light-curve for S Lac from October 2022 to present day (blue) plotted using AAVSO data. The dashed lines indicate corresponding TiMo observation dates (red) for the SED models presented in Figure 2.

4. Discussion and Initial Conclusions

The SED fits to the TiMo photometry are relatively straightforward to perform and quickly derive fundamental parameters about the stars from the optical photometry. It is easy to see in the atmospheric fits that there is more variation in the SEDs at optical wavelengths (500 to 900 nm) than in the infrared (~1-2 microns), which presents challenges when trying to find best fits. A few dozen Miras are presently being monitored during any given month using TiMo.

Initial analysis suggests that the effective temperature of S Lac is lower when the visual brightness is decreasing. Because the luminosity scales as R^2 and T^4, a lower effective temperature at approximately the same physical size means the star will appear optically dimmer. The bolometric flux decreases during the two phase points, as expected for a system that is getting dimmer in the optical as well. We have not yet fit for the extinction, which is problematic to disentangle for red stars.

Finally, angular diameter of these stars can be estimated from the sedFit plots. Counterintuitively the angular diameter is larger at the 0.32 than at the 0.42 phase point. We believe this is an artifact of the fitting residuals and the binning of the temperatures used in the PHOENIX grids and likely not real. We are continuing to analyze these results as they are likely inaccurate based on the PTI data which made angular diameter measurements in the near-infrared at K-band. Further investigations are ongoing using a more sophisticated wrapper to quickly explore the full fitting space available using the PHOENIX grids, or potentially other synthetic spectral models if we are dissatisfied with the SEDfit residuals upon performing more fits.

Future work will include building time-series SED fits for the targets in the *Mira Reference Dataset* and continued robotic monitoring of these targets with narrow-band photometry. This will

provide more detailed information about the CSE and the changes in the Mira atmospheres. When combined with measurements from PTI or other interferometers this could lead to a clearer understanding of these stars and potentially allow for the use of a Mira distance ladder to supplement the Cepheid distance ladder, helping to address the Hubble tension.

Acknowledgements

We acknowledge with thanks the variable star observations from the AAVSO International Database contributed by observers worldwide and used in this research. This work is currently supported through the National Science Foundation under grant number 2206803. The TiMo facility was established by a generous grant from the Mount Cuba Astronomical Foundation, and by support from Robert Martin Ayers. This research has made use of NASA's Astrophysics Data System. This work utilized the SIMBAD database, operated by the CDS in Strasbourg, France (Wenger et al. 2000).

References

Kloppenborg, B. K. (2023). Observations from the AAVSO International Database.

Baylis-Aguirre, D. K., Creech-Eakman, M. J., & van Belle, G. T. (2024). A "Wonderful" Reference Dataset of Mira Variables. *Galaxies*, *12*(6), 72. https://doi.org/10.3390/galaxies12060072

Creech-Eakman, M. J., van Belle, G. T., Baylis-Aguirre, D. K. (2022). A Reference Set of Mira Variables for the World to Share and Explore *Proceedings of the 111th Annual Meeting of The American Association of Variable Star Observers,* p.31.https://www.aavso.org/sites/default/files/publications/Proceedings%20of%20Annual%20Meetings/AAVSO111thMeetingProceedingsopt.pdf

Hill, S. J., & Willson, L. A. (1979). Theoretical velocity structure of long-period Variable Star photospheres. *The Astrophysical Journal*, *229*, 1029. https://doi.org/10.1086/157038

Huang, C. D. (2024). The Mira Distance Ladder. *Springer Series in Astrophysics and Cosmology*, 191–218. https://doi.org/10.1007/978-981-99-0177-7_11

Husser, T.-O., Wende-von Berg, S., Dreizler, S., Homeier, D., Reiners, A., Barman, T., & Hauschildt, P. H. (2013). A new extensive library of Phoenix stellar atmospheres and Synthetic Spectra. *Astronomy & Astrophysics*, *553*. https://doi.org/10.1051/0004-6361/201219058

Nakagawa, A., Kurayama, T., Omodaka, T., Kamezaki, T., Nishida, Y., & Matsui, M. (2012). The period–luminosity relation of Mira variable stars. *Proceedings of the International Astronomical Union*, *8*(S289), 217–217. https://doi.org/10.1017/s1743921312021412

Templeton, M. R., Mattei, J. A., & Willson, L. A. (2005). Secular evolution in Mira Variable Pulsations. *The Astronomical Journal*, *130*(2), 776–788. https://doi.org/10.1086/431740

Wenger, M., Ochsenbein, F., Egret, D., Dubois, P. Bonnarel, F., Borde, S., Genova, F., Jasniewicz, G., Laloë, S., Lesteven, S., & R. Monier, R. (2000) SIMBAD astronomical database--The CDS reference database for astronomical objects. *Astron. Astrophys. Suppl. Ser.*, 143 1 (2000) 9-22.DOI: https://doi.org/10.1051/aas:2000332

Abrupt Pulsation Resumptions in Deneb: An Update

Joyce A. Guzik[1], Brian Kloppenborg[2], Noel Richardson[3], Jason Jackiewicz[4], Nancy Morrison[2,5], Tom Calderwood[2], and Andrzej Pigulski[6]

[1]Los Alamos National Laboratory, Los Alamos, NM (joy@lanl.gov); [2]American Association of Variable Star Observers; [2]Embry Riddle Aeronautical University, Prescott, AZ; [4]New Mexico State University; Las Cruces, NM, [5]University of Toledo, Toledo, OH; [6]University of Wroclaw, Poland

Subject Keywords

Alpha Cygni Variables; stars: individual (α Cyg); AAVSO International Database; NASA TESS Spacecraft; BRITE Constellation Satellites

Abstract

Deneb, the prototype α Cygni variable, is a bright A2 Ia supergiant which shows irregular variability with a 12-day quasi-period, presumed to be caused by pulsations. At the 2023 AAVSO Annual Meeting we discussed radial velocity and photometry data from several sources showing that the 12-day variations begin abruptly at an arbitrary phase, damp out after several cycles, and resume at intervals of around 75 days. Additional data with more frequent time sampling and longer time series were needed to verify the existence and precision of the 75-day interval.

We have identified additional data sets and have intensified ground-based observing programs. Here we present analysis of 1) an 8.6-year photometric data set from the Solar Mass Ejection Imager; 2) BRITE Constellation light curves from six observing seasons of 60 to 180 days each, 2014-2021; 3) 4.6 years of radial velocity data from Morrison; 4) 1.4 years of radial velocity data from Eaton; and 5) additional V-band photometry from the AAVSO Photoelectric Photometry (PEP) section. Examining the SMEI data set, we find a most common 100 to 125 day interval between 'pulsation' resumptions. These resumptions sometimes skip intervals. We also find sudden large excursions in brightness and radial velocity which are distinct from the 'pulsation' resumptions and may or may not be data artifacts. We point out changes in the average level of Deneb's radial velocity which appear to be real given the accuracy of the measurements but are not explained.

1. Introduction

Despite being one of the brightest stars, Deneb (spectral type A2 Ia) holds many mysteries. Deneb is the prototype of the α Cyg variables, which are characterized by small-amplitude (0.1 mag) variations. Deneb varies in both brightness and radial velocity with a quasi-period around 12 days. These variations have been attributed to pulsations (see, e.g., Abt 1957; Lucy 1976), but, unlike typical pulsational variability, these variations do not have a regular period or amplitude[1]. Abt et

[1] Further references to pulsation will be in quotation marks.

al. (2023) found evidence in radial velocity data that these variations start abruptly at an arbitrary phase, damp out over a few cycles, and then resume at intervals of around 75 days. Sometimes there are also sudden excursions in brightness or radial velocity, which are distinct from resumption of the 12-day quasi-periodic variations.

These analyses raise many questions, such as: How precise and regular is the time interval of around 75 days between resumption of the variations with quasi-period 12 days? Do these resumptions in fact occur abruptly and at an arbitrary phase? What is the cause of these variations? Why do they damp out and resume? Do other α Cygni variables show similar behavior? What is the evolutionary state of Deneb and the α Cygni variables?

At the 2023 AAVSO 112th Annual Meeting we discussed radial velocity data from Paddock (1935) and Abt (1957), photometry and radial velocity data from Richardson et al. (2011), photometry from the American Association of Variable Star Observers database (Kloppenborg 2023), and photometry by the NASA TESS spacecraft (Ricker et al. 2015) presented by Abt et al. (2023). (See also Guzik et al. 2023 AAVSO proceedings.). For the above-mentioned data sets, either the sampling was too sparse or the time series were too short to confirm the precision and repeatability of the suggested 75 day interval between 'pulsation' resumptions.

We have identified additional data and have begun new observing programs. Here we present analysis of an 8.6-year photometric data set from the Solar Mass Ejection Imager (Kloppenborg 2023), BRITE Constellation (Weiss et al. 2014) light curves, radial velocity measurements from Morrison extending the time series of Richardson et al. (2011), radial velocity measurements from Eaton (2020), and new photometry by the AAVSO Photoelectric Photometry (PEP) section.

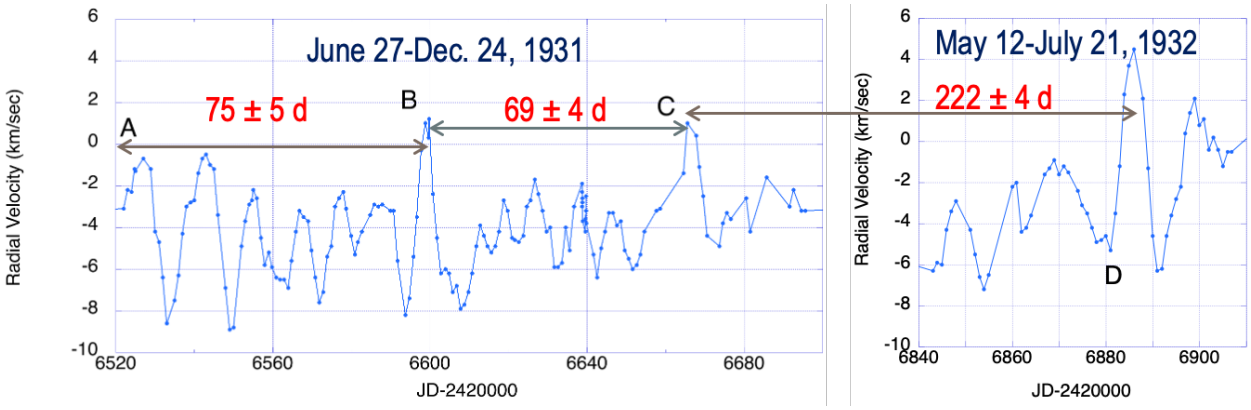

Figure 1. Radial velocity measurements from Paddock (1935) as presented by Abt et al. (2023). The interval between events C and D could correspond to 3 x 73-75 days.

2. Deneb Data Presented by Abt et al. (2023)

We first review observations from Abt et al. (2023) providing evidence for the 'pulsation' resumptions and large excursions in photometry and in radial velocity. Figure 1 shows radial velocity measurements by Paddock (1935). Intervals between points labeled A, B, and C are multiples of 69-75 days. The 'pulsation' resumption at A probably occurred a short time before

the beginning of this time series. Also, there seem to be larger excursions without resumption of 'pulsations' at points B and C.

Figure 2 shows ground-based Deneb photometry and radial velocity measurements of Richardson et al. (2011) from April 1997 to December 2001. Several points are identified where large excursions are evident in one data set (E, F, H) and possibly in both data sets (G). There are three nearly equal intervals between events of 447-448 days, which could be a could be a multiple of a smaller interval, e.g., 6 x 74-75 days. Some events may have been missed because of data gaps; alternatively, perhaps the events are not regular and the star sometimes skips events.

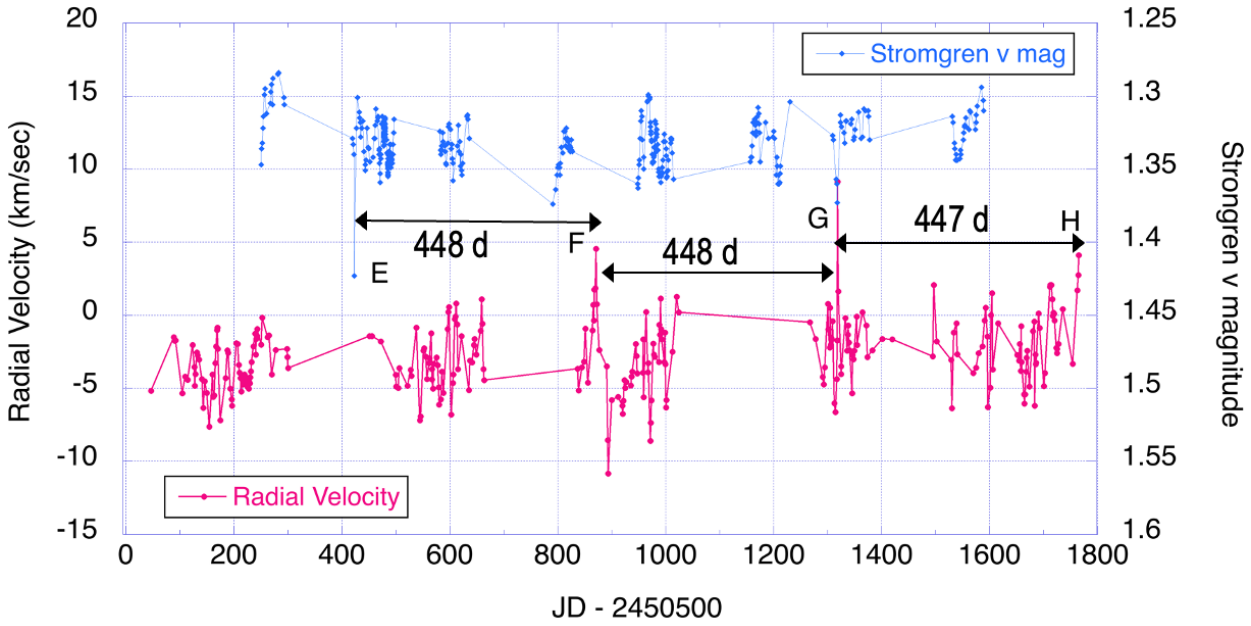

Figure 2. Deneb photometry and radial velocity measurements from Richardson et al. (2011) as presented in Abt et al. (2023). Abrupt excursions in radial velocity and/or photometry occur at intervals of about 448 days.

Deneb was in the field of view of the Transiting Exoplanet Survey Satellite (TESS, Ricker et al. 2015) during three 27-day observing 'Sectors' in 2021 and 2022. The 2-minute cadence high-level science product (HLSP) light curves are available at the Mikulski Archive for Space Telescopes (MAST, https://archive.stsci.edu). These light curves (Figure 3) show mostly irregular variations in Sector 41 and resumption of the quasi-periodic 12-day variations during Sector 55, continuing into Sector 56.

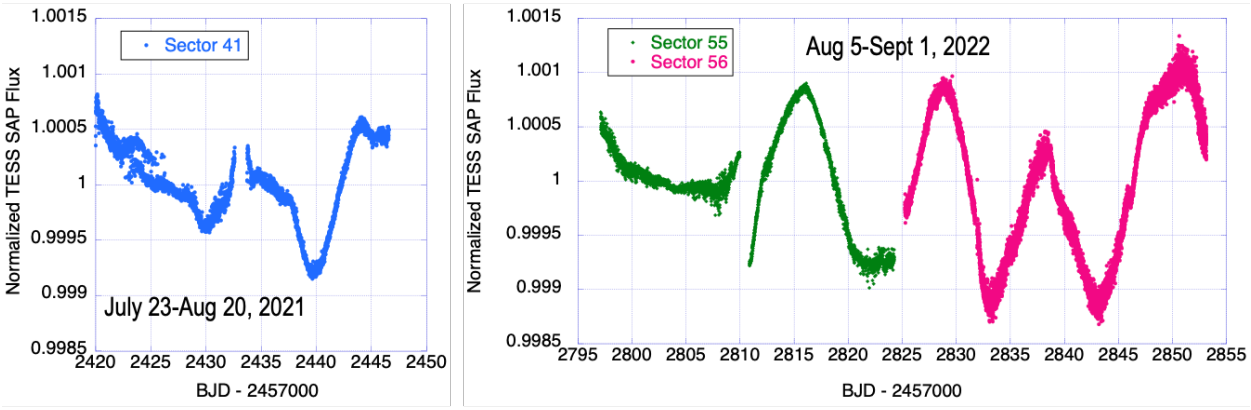

Figure 3. Deneb photometry from TESS spacecraft as presented by Abt et al. (2023). Variations with quasi-period around 12 days resume around day 2810 in Sector 55 data.

Abt et al. (2023) also examined Deneb V-magnitude photoelectric photometry (PEP) from the AAVSO International Database (AID) taken June 16, 2021–June 15, 2023 (128 data points). The PEP team has intensified its observing campaign for Deneb in 2024; the results are discussed in Section 3d.

3. Additional Deneb Data

After the AAVSO 112th Annual Meeting we identified and analyzed data from several sources: The Solar Mass Ejection Imager photometry, spanning 8.6 years; BRITE Constellation satellite photometry (2 to 6 month time series, 2014-2021); Morrison radial velocity data (4.3 years, 2002-2007); Eaton (2020) radial velocity data (1.4 years, 2008-2009); and AAVSO photoelectric photometry (PEP) data (118 new observations, June-October 2024).

3.1 Solar Mass Ejection Imager Light Curves

At the 112th AAVSO meeting, B. Kloppenborg informed us about Deneb photometric data taken by the Solar Mass Ejection Imager satellite (Jackson et al. 2004, Clover et al. 2011). This satellite was in a Sun-synchronous polar orbit from 2003-2011. Although the satellite was designed to study solar coronal mass ejections (CMEs), it also observed almost every bright (V < 6) star at a cadence of one data point per 102-minute (1.7-hour) Earth orbit. Kloppenborg processed these data to remove zero-point offsets and angle-dependent flux loss causing a 100-day curvature in the light curve.

We presented initial analysis of these data for the Society at Astronomical Sciences June 2024 meeting (see Guzik et al. 2024 SAS proceedings). Figure 4 shows the 8.6-year Deneb SMEI light curve. It is evident that additional processing is needed to remove remaining trends and offsets. Figure 5 zooms in on a few segments of the light curve. Sometimes the 12-day quasi-periodicity is evident, sometimes this variability almost disappears, and sometimes abrupt large discontinuities or excursions occur.

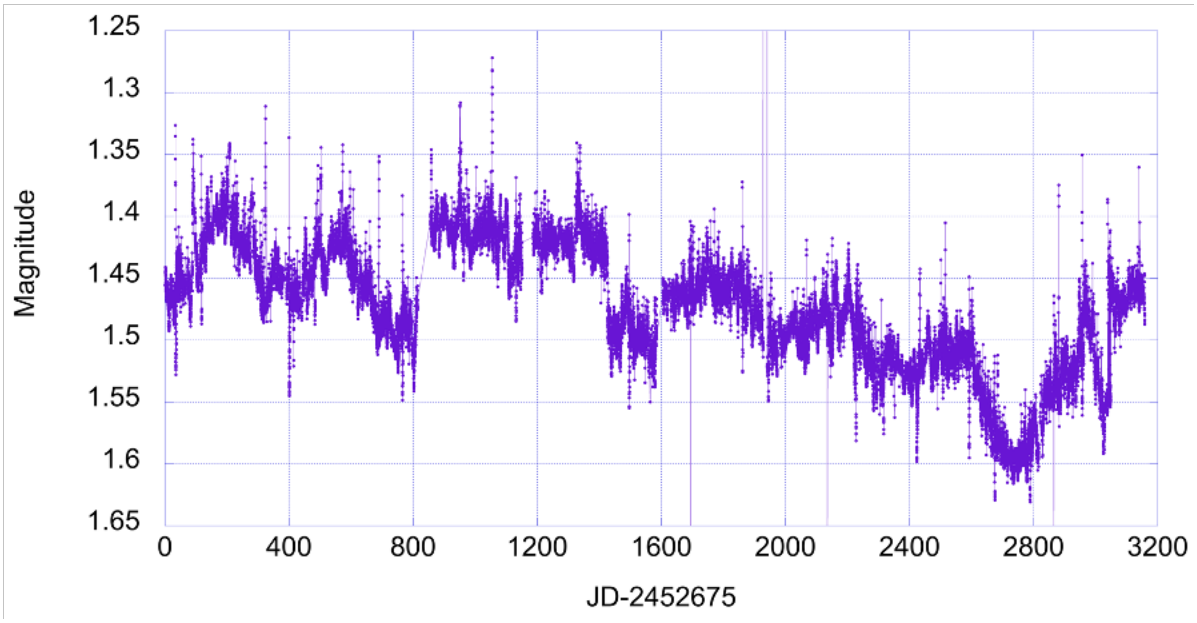

Figure 4. Deneb light curve from Solar Mass Ejection Imager. The data require further processing to remove offsets and trends.

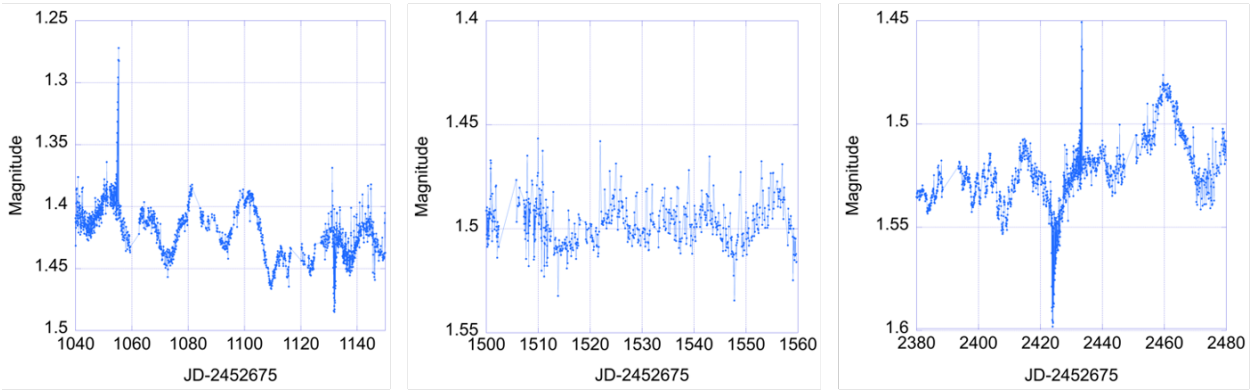

Figure 5. Zoom-in on portions of Deneb SMEI light curve. Left: 12-day variations plus a couple of abrupt excursions. Center: Smaller amplitude variability, with 12-day variations less evident; Right: Larger amplitude variations and a large excursion.

We reviewed the entire data set and measured the time intervals between resumptions of larger amplitude 12-day 'pulsation' variations, as well as the intervals between the abrupt excursions. Figure 6 (left) shows a histogram counting the number of events per time interval between resumptions of larger amplitude variations. The bin size is 50/4 = 12.5 days per bin. The resumptions occur most often at intervals of 100-125 days. These intervals are longer than the 75-day intervals hypothesized by Abt et al. (2023). The resumptions are not regular and appear to skip intervals. These resumptions also don't seem to occur abruptly at an arbitrary phase in the 'pulsation' cycle, as was suggested by Abt et al. (2023). Abrupt excursions/discontinuities in the Deneb SMEI data occur most often at intervals of 75-90 days (Figure 6, right). These events seem to be unrelated to the larger amplitude 'pulsation' resumptions. They may be caused by

geomagnetic storm interference during the SMEI 102-minute polar orbit, and unrelated to Deneb. We discuss our initial attempts to confirm this hypothesis in Section 3c.

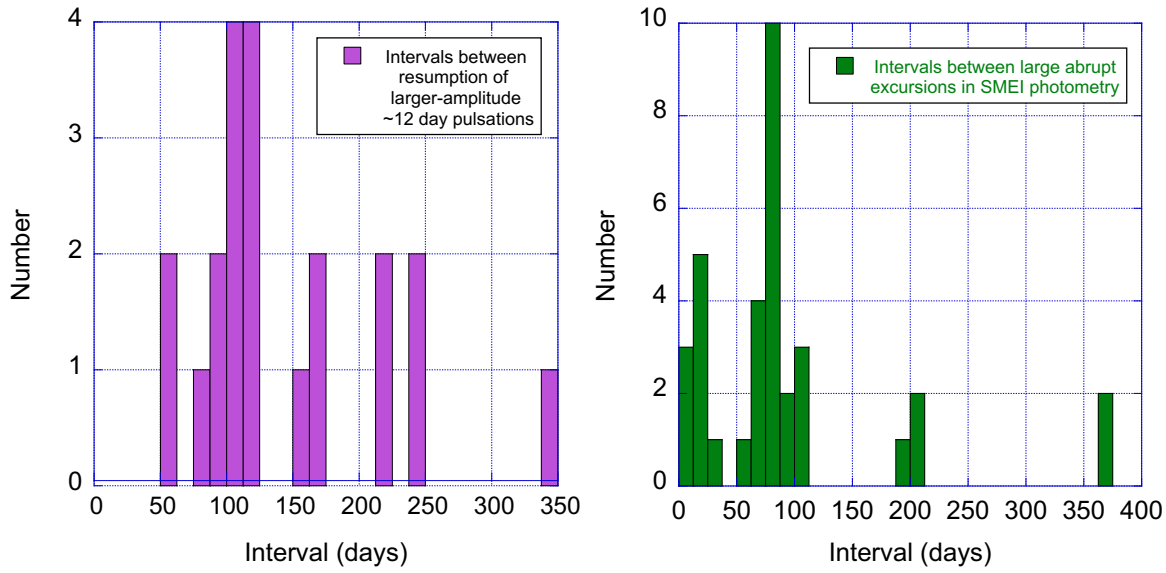

Figure 6. Time intervals between resumption of larger-amplitude quasi-periodic 'pulsations' (left), and between abrupt excursions (right) in Deneb SMEI photometry.

3.2 BRITE Constellation Light Curves

We also examined BRITE Constellation (Weiss et al. 2014) satellite data acquired during six observing seasons from 2014 through 2021. The BRITE Constellation consists of five nanosatellites in low Earth orbit, three observing in red and two in blue passbands. The satellites observe the target for 15-35 minutes per orbit, acquiring a photometric data point every 21 seconds, with 1 to 5-second exposures per observation. The BRITE data were decorrelated by A. Pigulski and some remaining trends/slopes were removed by J. Guzik.

The results of our analyses were first reported at the 2024 BRITE conference (Guzik et al. 2024; https://zenodo.org/records/14236753). Here we show a few BRITE light curves from 2015 and 2016 (Fig. 7). We found that 'pulsation' resumptions with amplitude around 20 millimag occur around days 1210, 1310 and 1600 after Barycentric Julian Date 2456000. The approximate 100-day interval between 'pulsation' resumptions at day 1210 and 1310 is consistent with the most common interval found in the SMEI photometric data. When Deneb was observed simultaneously by two BRITE satellites, one in red and the other in blue passband, the light curves show good correlation.

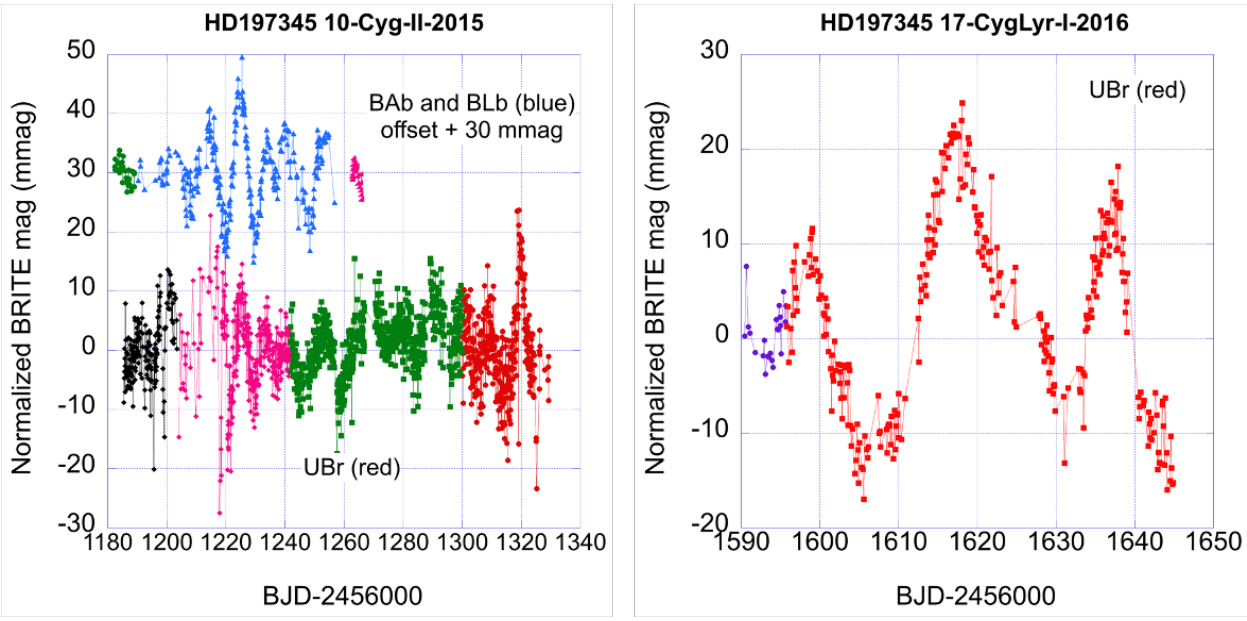

Figure 7. Deneb BRITE Constellation photometry from 2015, showing 12-day variations in blue and red passbands (left), and large amplitude variations in 2016 in red passband (right)[2]. Larger amplitude (± 20 millimag) variations resume around days 1210, 1310, and 1600 after BJD 2456000.

3.3 Radial Velocity Measurements

After the Richardson et al. (2011) project on Deneb photometry and radial velocity measurements concluded, high-resolution time-series spectra continued to be taken for several years at the Ritter Observatory 1-meter telescope of the University of Toledo. From these spectra, N. Morrison extracted 208 radial velocities covering the time period October 31, 2002 to January 16, 2007 (Fig. 8, left). A single spectral line, Si II λ6371, was used. The estimated uncertainty in a single measurement (mainly caused by the breadth of the line and by slight, time-variable profile asymmetries) is in the range 0.2 to 0.3 km/s.

While these data show variations consistent with the 12-day quasi-period, we also noticed average radial velocity level changes. For example, the average radial velocity is around -4 km/sec from day 600-800 after Heliocentric Julian Date 2452500, then increases to +1 km/sec around day 1000, and then decreases to -2 km/sec around days 1100-1200. We also notice smaller average radial velocity offsets in earlier radial velocity data sets; see, e.g., the data of Paddock (1935) and Richardson et al. (2011) of Figures 1 and 2. Morrison analyzed Ritter Observatory spectra for the radial velocity standard star β Oph, and found it to be constant in radial velocity to ± 0.13 km/sec standard deviation during the same time frame. This result rules

[2] The colors represent different segments or 'setups' of observation in a given field and are processed separately (Popowicz et al. 2017). The reason for splitting the data into setups is usually a change in observing conditions, and sometimes a change in exposure time.

out an instrumental cause for the change in average velocity. There is no obvious periodicity to the level changes as would be expected if Deneb had a binary companion.

Morrison also pointed out the availability of Deneb (HD 197345) radial velocity data from Eaton (2020), which we downloaded and plotted (Fig. 8, right). This data set included 134 observations from June 5, 2008 to November 3, 2009. The quoted uncertainty in radial velocity is 0.1 km/s. There is a possible large excursion event around day 1075 after HJD 2454000.

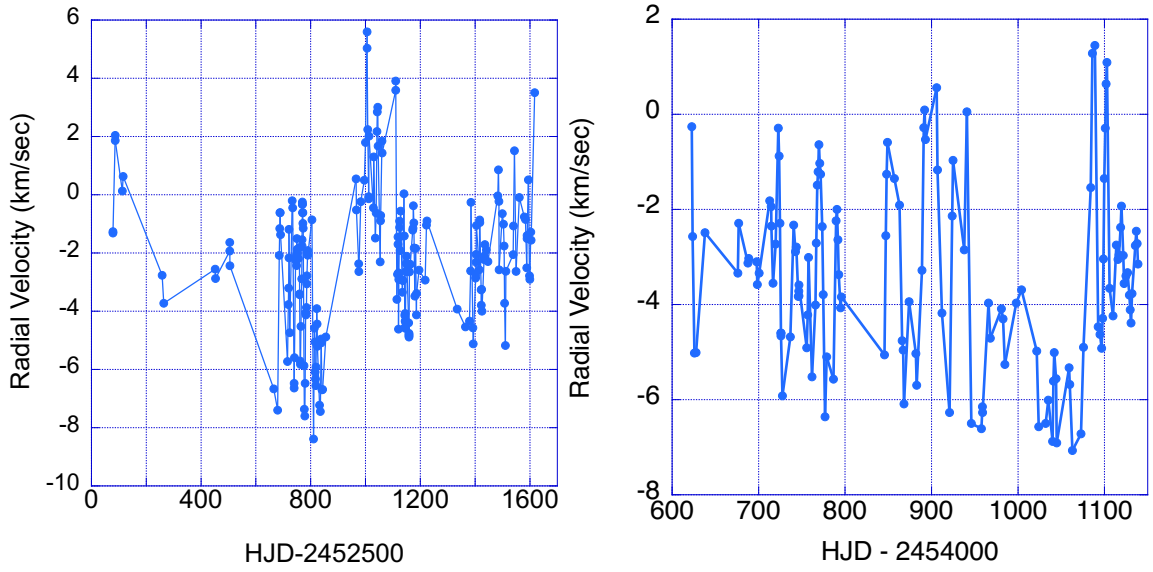

Figure 8. Deneb radial velocity data from Morrison (left) and Eaton (2020, right). The average radial velocity appears to change in the Morrison data. A possible large excursion is seen in the Eaton data around HJD 2455075.

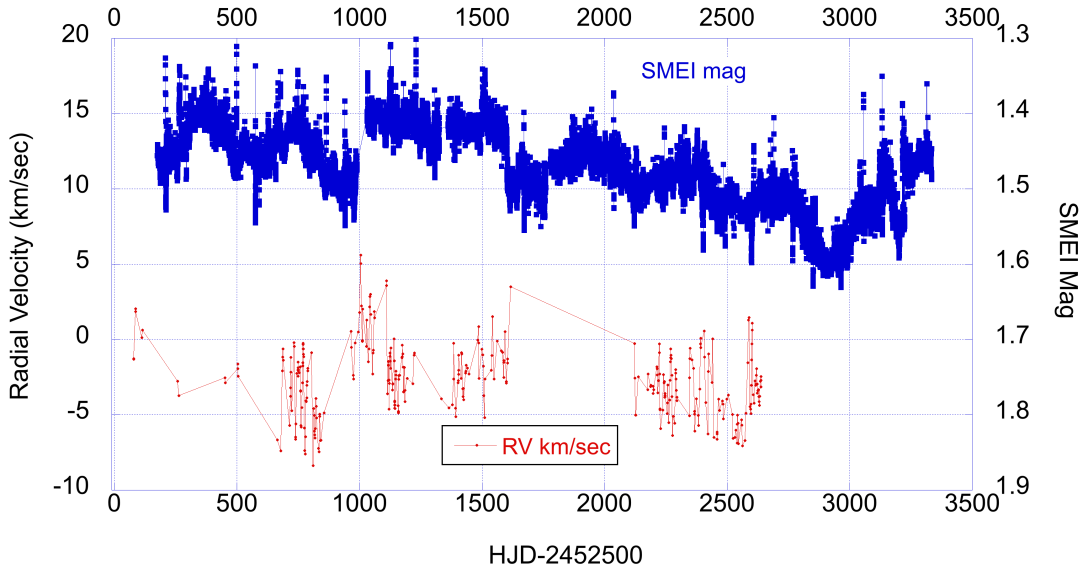

Figure 9. Deneb Solar Mass Ejection Imager photometric data (blue) and Morrison/Eaton radial velocity data (red).

The SMEI photometric data and Morrison/Eaton radial velocity data overlap in time. Figure 9 shows both data sets on the same plot. While more work will be required to identify a correlation between these data sets, we see that the large excursion in the Eaton radial velocity data is near in time to SMEI excursion of Figure 5 (right). Figure 10 zooms in on both data sets near this time.

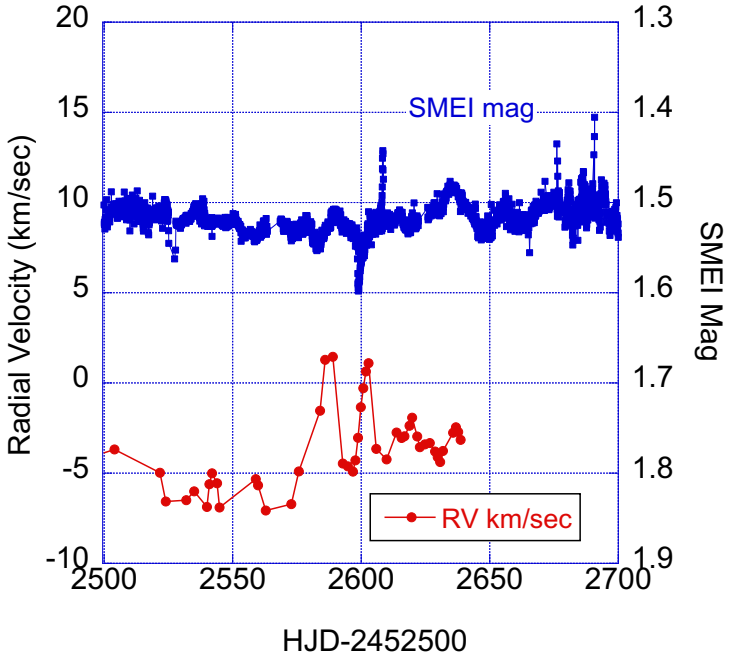

Figure 10. Zoom-in on the large excursion event in SMEI data (Fig. 5, right) which is close in time to the large excursion in the Eaton (2020) radial velocity data (Fig. 8, right).

We are working to determine the reality of the sudden excursions in the SMEI data, which were hypothesized to be caused by geomagnetic storms when the spacecraft passes through the Earth's magnetic field. We examined one variable and one 'constant' star very near to Deneb's coordinates: 55 Cyg = V1661 Cyg, with apparent magnitude 4.86, which is a blue supergiant also classified as an α Cyg variable; and 56 Cyg, a nearby main-sequence A-type star with apparent magnitude 5.06 believed to be a Hyades member. The light from these two stars would fall near to the same location on the SMEI cameras as Deneb's. If the excursions are caused by geomagnetic storms, the light curves of all three stars should show anomalies at the same time. Although we found that similar abrupt events are present in all three light curves, they do not correlate in time.

We also zoomed in further on a few of the abrupt excursions in the Deneb SMEI data and sometimes find oscillations every other data point (taken 1.7 hours apart) between values that are consistent with the light curve trends and points that deviate considerably. Such behavior, even if unexplained, seems even more likely to be artificial and should be cleaned from the light curves. However, we are reluctant to dismiss all of these events in the Deneb SMEI data as artifacts since large excursions are sometimes seen in other photometry and radial velocity data sets.

3.4 AAVSO V-Band Photoelectric Photometry

Since the 2023 AAVSO meeting, the AAVSO Photoelectric Photometry section has intensified its efforts to observe Deneb. At the 2024 AAVSO meeting, we presented PEP data from the AAVSO International Database (Kloppenborg 2023) from June 16, 2021 to October 16, 2024 (Fig. 11, 246 data points). Eleven observers with observing codes CTOA, FBA, FXJ, MPFA, BVE, DFR, BWU, GMV, GTIA, WIG, and DJAD contributed V magnitude observations. The median uncertainty of the data points is 0.003 mag. At the 2023 meeting, we noted that a large excursion may have been caught around day 200 after JD 2459300 (Fig. 11, left). There may be another event just before day 1200, but the coverage is a little too sparse to confirm. After day 1200 there are irregular variations with periods mostly longer than 12 days (Fig. 11, right).

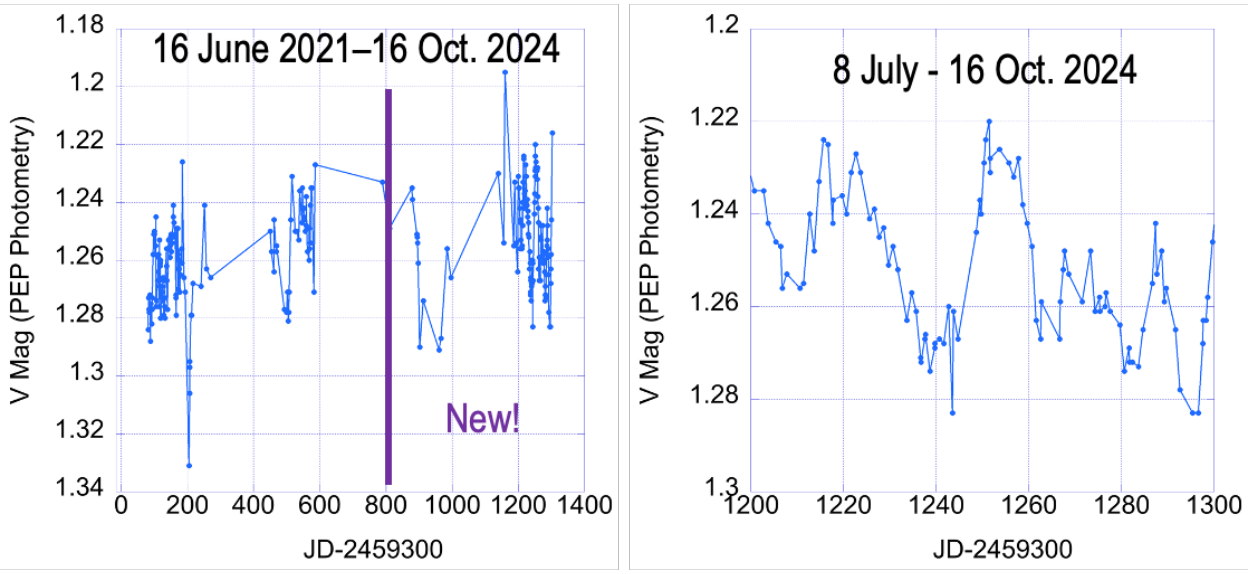

Figure 11. Left: Deneb V magnitude photometric data from AAVSO International database (AID, Kloppenborg 2023). Data examined after the 2023 AAVSO meeting begin at day 800 after JD 2459300. Right: Zoom-in on new data, where at least one data point was acquired nearly every night. The median uncertainty in the data points over the time span of each figure is 0.003 magnitudes.

4. Summary and Future Work

To summarize highlights from new data examined:

SMEI Photometry: Large-amplitude 'pulsation' resumptions occur most commonly every 100-125 days, longer than the 75-day intervals hypothesized by Abt et al. (2023). Sometimes intervals are shorter or are skipped entirely. Abrupt excursion events occur most commonly every 75 to 90 days. Most of these are likely to be data artifacts, but we haven't been able to prove that geomagnetic storms are responsible for these events, as hypothesized.

BRITE Photometry: We find one 100-day interval between large-amplitude 'pulsation' resumption, consistent with the most common SMEI interval.

Radial Velocity: Average radial velocity changes were noticed in recently reduced data from Morrison. One possible large excursion is found in data from Eaton (2020). These data sets overlap in time with SMEI photometry, so correlations can be studied. One of the SMEI large excursion events seems to correlate with the Eaton radial velocity event.

AAVSO Photometry: High-quality, high-cadence data are being acquired by the AAVSO Photoelectric Photometry section.

For the future, we will clean up the data for Deneb and other bright stars observed by SMEI, attempting to understanding and remove artifacts. Cotton et al. (2024) find that Deneb is a polarimetric variable, with an event occurring just after 'pulsations' resumed in TESS data**.** We are looking into whether amateurs can carry out polarimetry observations of Deneb and other α Cyg variables. We will look for additional TESS data for Deneb. TESS observed Deneb during Sector 76 in 2024, but a HLSP light curve was not yet available at MAST. In addition to continuing to observe Deneb, the AAVSO PEP section is also intensifying its observations for other α Cyg variables, such as Rigel.

In answer to a question at the 113th AAVSO meeting, Morrison noted that slight line-profile variations are evident in the Deneb spectra. These may provide important clues to the nature of Deneb's variability.

We are also beginning to use stellar modeling to investigate the evolution and pulsational stability of massive stars near the location of Deneb in the Hertzsprung-Russell diagram. A poster on this work was presented by A. Moore at the 2024 AAVSO meeting (see proceedings paper).

We hope that these studies will lead to a better understanding of the origin of the variability and the evolutionary state of Deneb and the α Cygni variables.

Acknowledgements

We acknowledge with thanks the variable star observations from the AAVSO International Database contributed by observers worldwide and used in this research. We also acknowledge the students and staff of Ritter Observatory (The University of Toledo), who acquired the spectra that we measured for radial velocity but who are too numerous to list here. This collaboration was facilitated by a Los Alamos National Laboratory Center for Space and Earth Sciences grant XX8P SF2. J.G. acknowledges support from Los Alamos National Laboratory, managed by Triad National Security, LLC for the U.S. DOE's NNSA, Contract #89233218CNA000001. Based on data collected by the BRITE Constellation satellite mission, designed, built, launched, operated and supported by the Austrian Research Promotion Agency (FFG), the University of Vienna, the Technical University of Graz, the Canadian Space Agency (CSA), the University of Toronto Institute for Aerospace Studies (UTIAS), the Foundation for Polish Science & Technology (FNiTP MNiSW),

and National Science Centre (NCN). This research made use of data from the Mikulski Archive for Space Telescopes (MAST).

References

Abt, H.A. 1957, The Variability of Supergiants, ApJ 126, 138

Abt, H.A., Guzik, J.A., and Jackiewicz, J. 2023, The Abrupt Resumptions of Pulsations in α Cygni (Deneb), PASP 135, 1054, 124201

Clover, J.M., et al. 2011, Epsilon Aurigae light curve from the Solar Mass Ejection Imager, AAS Meeting Abstracts 217, 257.02

Cotton, D. V., et al., 2024, Deneb is a large-amplitude polarimetric variable, ApJ Letters 967, L43

Eaton, J.A., 2020, 35,000 Radial Velocities for 348 Stars from the Tennessee State University Automatic Spectroscopic Telescope, JAAVSO 48, 91

Guzik, J.A., Abt, H., Jackiewicz, J., and Kloppenborg, B.K. 2023, Abrupt Periodic Pulsation Resumptions in Deneb, Proceedings of the 112th Annual Meeting of the AAVSO, https://www.aavso.org/112, doi: 10.48550/arXiv.2410.23936

Guzik, J.A., Kloppenborg, B., and Jackiewicz, J. 2024, Deneb and the alpha Cygni Variables, Society for Astronomical Sciences Symposium on Telescope Sciences 2024 proceedings, eds. J.C. Martin, R.K. Buchheim, R.M. Gill, W. Green, and J. Menke, https://socastrosci.org/wp-content/uploads/2024/08/2024-Proceedings_Ver1.3d.pdf, doi: 10.48550/arXiv.2410.23985

Guzik, J.A., Richardson, N.D., Kloppenborg, B., Jackiewicz, J., and Pigulski, A. 2024, Deneb's Variability as Viewed by BRITE Constellation and the Solar Mass Ejection Imager, The BRITE Side of Stars Electronic Proceedings, University of Vienna, August 20-23, 2024, Online at https://britestars.univie.ac.at/home/, id.68, doi: 10.5281/zenodo.13858241

Jackson, B.V., et al. 2004, The Solar Mass Ejection Imager (SMEI) Mission, Sol. Phys. 225, 177

Kloppenborg, B.K. 2023, Observations from the AAVSO International Database, https://www.aavso.org

Lucy, L.B. 1976, An analysis of the variable radial velocity of alpha Cygni, ApJ 206, 499

Paddock, G.F. 1935, Spectrographic Observations of Alpha Cygni, Lick Obs. Bull. 17, No. 472, 99

Popowicz, A., et al. 2017, BRITE Constellation: data processing and photometry, A&A 605, A26

Richardson, N.D., Morrison, N.D., Kryukova, E.E., and Adelman, S.J. 2011, A five-year spectroscopic and photometric campaign on the prototypical alpha Cygni variable and A-type supergiant star Deneb, AJ 141, 17

Ricker, G.R., et al. 2015, Transiting Exoplanet Survey Satellite, Journal of Astronomical Telescopes, Instruments, and Systems, Volume 1, id. 014003

Weiss, W., et al. 2014, BRITE-Constellation: Nanosatellites for Precision Photometry of Bright Stars, PASP 126, 573

Sources of Error in the Times of Maximum Light for Pulsating Variable Stars

Michael D. Joner, Oliver Hancock, Michael W. Holland, Peter Jensen, Tyler Jensen, and Denzil E. Watts

Brigham Young University, Department of Physics and Astronomy, Provo, UT 84602; xxcygni@byu.edu

Subject Keywords

Variable Stars, Period Changes; Photometry, CCD; Undergraduate Education

Abstract

In this presentation we examine various possible sources of error for determinations of times of maximum light for pulsating variable stars. The O – C results presented in Yang et al. (2012) for the SX Phoenicis star XX Cygni show large scatter during single observing seasons (see especially data from 2009). This is especially noteworthy since the largest scatter appears in some of the most recent data sets used in this study. We examine several possible reasons why time periods of just a few months exhibit excessive scatter in the maximum light timings. None of the ideas we tested produced timing errors large enough to account for scatter greater than 10 minutes for a monoperiodic variable star with a pulsation period of just over three hours. Based on a careful examination of the individual data sets used by Yang et al. (2012), we conclude that the regions of large scatter in the O – C diagram for XX Cygni are likely the result of significant analysis errors.

1. Introduction

The analysis of O – C diagrams often includes a mix of data from many sources with observations secured using a wide variety of different filters and instrumental systems. While observations are commonly made using a standard V filter, it is not unusual to see these results mixed with observations obtained through other Johnson/Cousins, Sloan, Strömgren, and in some cases simply a blocking filter, clear filter, or no filter at all. Many observations before 1950 were made with photographic plates and the magnitudes reported are dependent on responses of various photographic emulsions. Recent space-based missions often utilize an instrumental system that is designed for a specific survey. Data from these missions often requires a complicated transformation to compare the space-based observations to one of the standard photometric systems. The original goal of this study was to see if the choice of filter could be used to explain the seasonal scatter in observed times of maximum light within O – C diagrams for pulsating variable stars.

Initially this project was designed to investigate a possible wavelength dependence on determined times of maximum light correlated with filter choice. We planned to base the analysis on new observations of three pulsating variable stars. The original plan was to compare times of

maximum light from different filters that were rigorously determined from BVRI observations secured using a single instrumental system. The original submitted abstract stated our intention to analyze results from observations of V2455 Cygni, DY Pegasi, and XX Cygni. It was decided that undergraduate student observers would make all observations during 2024 using the 0.32-m reflecting telescope at the Brigham Young University (BYU) West Mountain Observatory (WMO). Not long after submitting our abstract, it became clear from the first analysis of XX Cyg data that any timing differences (even if they had been statistically significant) from filter to filter were not nearly large enough to explain the observed scatter in published O – C diagrams. It was also realized that we would be short on the time needed to complete this analysis for all three stars and that there would not be enough time in the oral presentation to include all these results. Thus, the oral presentation that was given at the 113th AAVSO Annual Meeting addressed possible sources of error in maximum light timings based on observations of the SX Phoenicis (SX Phe) variable star XX Cyg.

1.1 O – *C Diagrams and Seasonal Scatter*

The O – C diagram is a valuable tool used to look for period changes in pulsating variable stars that may be related to evolutionary effects. The presence of periodic changes in O – C diagrams can be analyzed to detect possible stellar companions of the observed variable star. In both applications, it is important that the individual data sets that make up the O – C diagram are as accurate as possible so that the derived period change or orbital parameters have predictive power at future epochs.

The variable star XX Cyg is an SX Phe star (Population II high-amplitude δ Scuti star (HADS)) which is known to exhibit single-mode pulsation. An analysis of data from the Transiting Exoplanet Survey Satellite (TESS) by Niu et al. (2023) concluded that the periodogram of XX Cyg is dominated by the fundamental frequency (f_0 = 7.4148 c day^{-1}, P = 0.134865 day or approximately 3 hours and 14 minutes) and an accompanying 19 harmonics. This well-defined monoperiodic pulsation cycle makes XX Cyg an ideal candidate for long-term study of period changes, detecting stellar companions, and possibly finding timing irregularities in observational data.

Figure 1 shows data drawn from the period analysis section of Yang et al. (2012) in an annotated O – C diagram. Much of the data contributing to Figure 1 up through the group of points marked 1980 fall into tightly clumped bins. Points prior to 1955 are from photographic photometry. The data reported by Detre (1936) are marked 1935 in Figure 1. They form a particularly tight group for the era with a top to bottom scatter for the seven times of maximum light reported being just 0.0021 days (approximately 3.0 minutes). The nine data points marked 1957 are unpublished maxima derived from photoelectric photometry obtained by Detre and reported in Szeidl and Mahdy (1981). These data show a top to bottom scatter of 0.0017 days (approximately 2.5 minutes). The six points marked 1980 are Strömgren photoelectric photometry from Joner (1982) with times of maximum light determined by Yang et al. (2012) showing a top to bottom scatter of 0.0029 days (approximately 4.2 minutes). The thesis by Joner (1981; see Table 8) gives times of maximum light for the same six Strömgren *y* maxima and an additional four Johnson V maxima. The times given there have a total top to bottom scatter of 0.0014 days (approximately 2.0

minutes). Data after 1990 are almost exclusively the result of work done using CCD detectors. We noted that the greatest scatter in the O – C diagram for XX Cyg is for the points marked 2009. The top to bottom scatter in the 2009 data from Yang et al. (2012) is 0.0079 day (approximately 11.4 minutes).

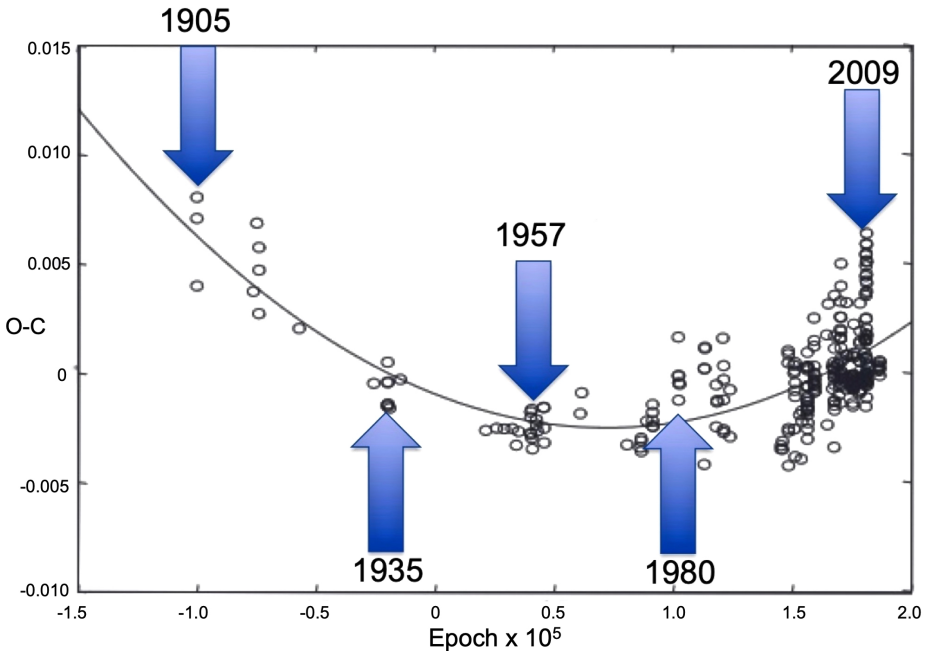

Figure 1. Annotated O – C diagram for XX Cyg with data and the parabolic fit from Yang et al. (2012).

The scatter in the 2009 data is almost four times larger than the scatter in the photographic maxima from 1935 and more than four and a half times the scatter noted in the photoelectric maxima from 1957. It appears that either XX Cyg was having a prolonged period of atypical activity that altered the regular pulsation cycle or that there is another explanation for the observed scatter in the observed times of maximum light from 2000 onward and most notably in 2009. In the remainder of this paper, we will give details of the new observations presented for XX Cyg, examine some of the many reasons for timing errors in O – C diagrams, and conclude this analysis by taking a closer look at the data sets presented in 2009 before making our concluding remarks.

2. Observations

2.1 The West Mountain Observatory

The new observations presented in this study were secured at the Brigham Young University (BYU) West Mountain Observatory (WMO) shown in Figure 2. WMO is a well-maintained research facility located about one hour away by car from the main BYU campus in Provo, Utah. It should be noted that the last 5.5 miles to the observatory are on a rough gravel road.

Figure 2. The main building at the BYU West Mountain Observatory looking toward the west.

WMO is a research facility that is operated primarily by undergraduate students during the spring and summer observing seasons. The primary goal of having undergraduate student observers operate the observatory is to enable them to gain research experience in a mentored environment on a regular basis for a period of several months. The student observers generally work in small teams for a couple of nights at a time and secure observations needed for different student projects while also working on observations for their own research. This cooperative observing practice leads to each student ending up with the observations they need despite missing nights due to weather, instrumentation, or other unforeseen random problems at the observatory. Additionally, working to assist with various projects allows undergraduate student researchers to gain experience working on targets ranging from asteroids to active galaxies and just about everything in between.

2.2 The 0.32-meter Telescope

The new observations of XX Cyg presented in this paper were made at WMO using the 0.32-meter f/9 Ritchey-Chrétien reflecting telescope (see Figure 3) housed in one of the smaller domes to the west of the main building. For 2024, all observations were obtained with the same instrumental system. The telescope was equipped with standard Johnson/Cousins BVRI filters from Astrodon and an FLI ML 16200 CCD camera. The ON Semi KAF-16200 Front Illuminated CCD is a 4500 x 3600 array with 6.0 μ pixels. The plate scale of the 0.32-meter telescope is 72.2 ”/mm. This yields 0.433 ”/pixel when using the KAF-16200 CCD. For this project, it was decided to operate the CCD binned 2 x 2. This resulted in a scale of 0.866 ”/pixel and a field of view 32.5’ x 26.0’.

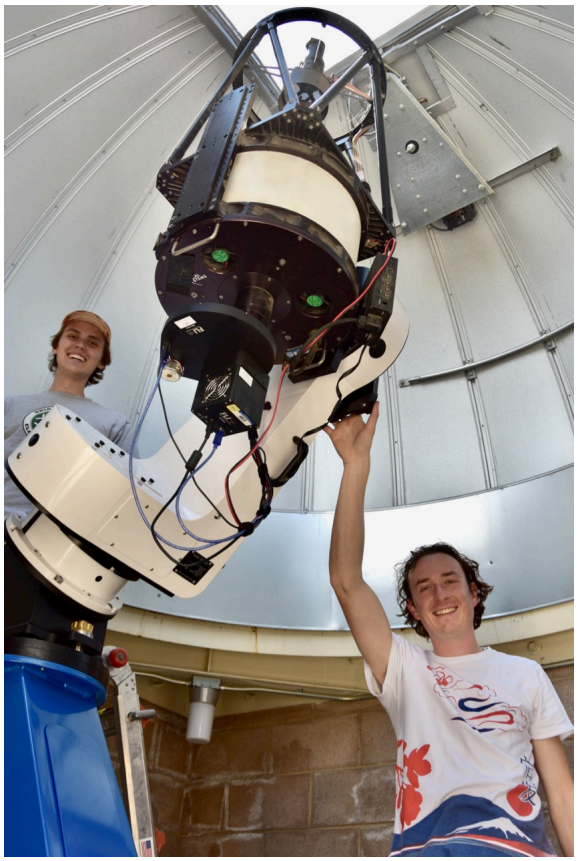

Figure 3. Students Oliver Hancock (left) and Denzil Watts (right) during the installation of a new PlaneWave L-series mount on WMO's RCOS 0.32-meter f/9 Ritchey-Chrétien reflecting telescope.

For the most recent 2024 observations presented in this paper, we used 15 times of maximum light from 10 nights of observations. Two times of maximum light were recorded on each of the last five nights of observations. The raw data frames were processed using standard IRAF routines to produce nightly master dark and zero frames along with master flat frames for each filter made weekly from evening and morning twilight sky flats. There is no pier flipping correction needed when using the PlaneWave L-series mount. The master flat frames would typically utilize at least 50 individual twilight flats. The processing was done with the IRAF task *ccdproc.* The heliocentric corrections were made for all frames using the *setjd* command.

3. Investigating O – C Data Scatter

3.1 Stability of XX Cygni Light Curve

Observations of XX Cyg from the Transiting Exoplanet Survey Satellite (TESS) provide ample evidence for the light curve stability of XX Cyg. At this time, observations have been released for eight observational sectors secured in 2019, 2021, and 2022. An examination of the different data runs shows a light curve that is remarkably stable as was noted previously in the reference to the work of Niu et al. (2023). A plot of approximately 24 hours of data from the Sector 14 observations in July of 2019 is shown in Figure 4. For the sector 14 test data, the data for XX Cyg

shows the same regular single period that is dominant. In a test that used 58 of the times of maximum light (about every third cycle) for Sector 14, we found that the standard deviation for the times of maximum light was 0.00038 day (about 33 seconds). We noted that this was more than 20 times smaller than the dispersion in the 2009 data reported in Yang et al. (2012). The TESS times of maximum light are plotted in the O – C diagram shown in Figure 5. Later in this section we use times of maximum light from three years of TESS data.

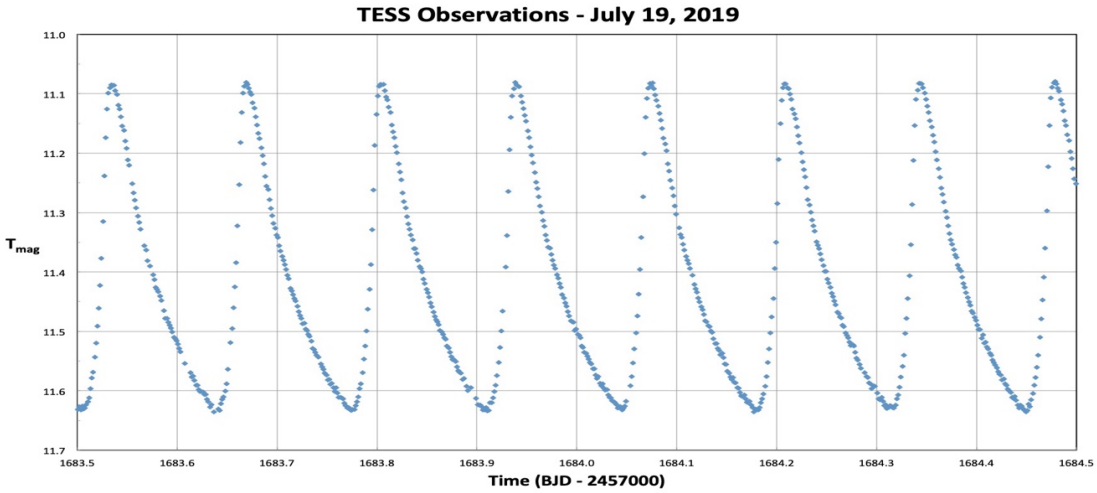

Figure 4. TESS magnitude versus BJD for the approximately one day of typical data of XX Cyg for observations made by TESS on UT 2019-07-19.

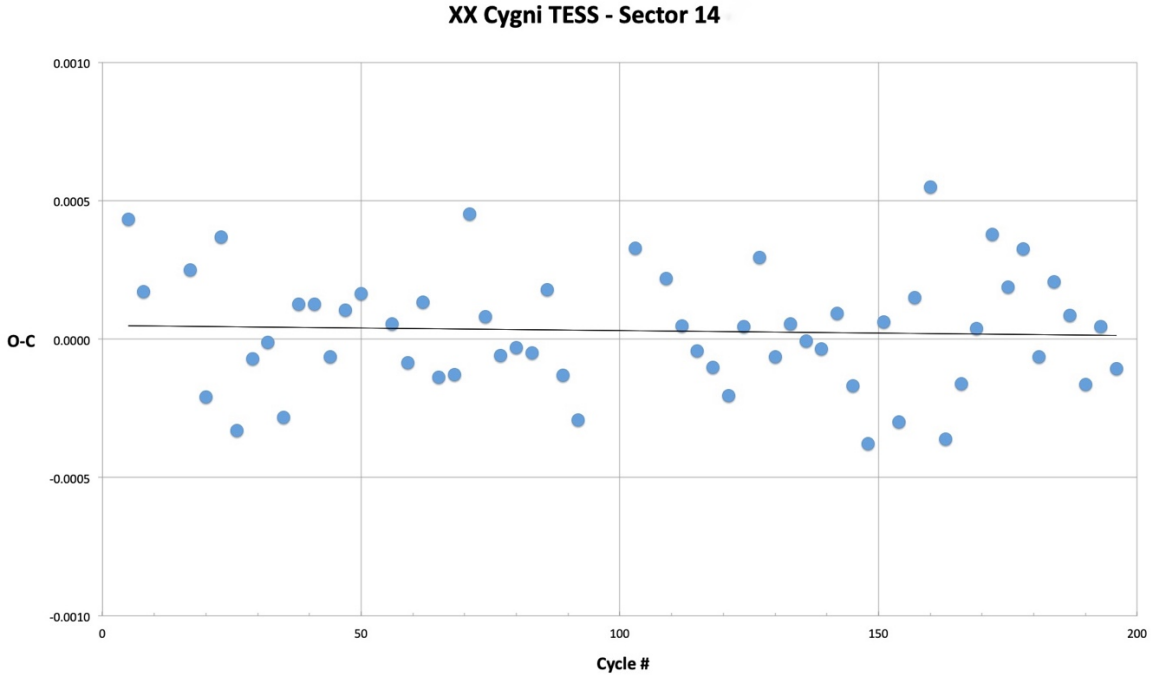

Figure 5. O – C diagram of the 2019 TESS Sector 14 times of maximum light for XX Cyg. There are 58 times (approximately every third cycle) of maximum light plotted in this figure. The standard deviation for these points relative to the line is 0.00038 day, or about 33 seconds.

3.2 Filter Wavelength Dependence

The primary focus of the original idea for this study was to look for a timing dependence. Due to the fact the that the amplitude of a light curve gets smaller as you move to redder filters and that the shape of the light curve is broader as a result of the diminished amplitude, it was suspected that the time of maximum light might be shifted slightly to a later time similar to what is seen for a radial velocity minimum in pulsating variable stars as shown in Figure 6. To determine if maximum light timings had any correlation with filter wavelength, we secured five nights of observations on XX Cyg using the 0.32-meter telescope and Johnson/Cousins BVRI filters during the last ten nights of July 2024. There were two times of maximum light observed on each of these nights. The phased data from the five nights of Johnson/Cousins photometry are shown in Figure 7. These curves illustrate the quality of nights, the observatory site, and the instrumental system used during this observing run. The phased data light curves also illustrate the often-observed stability of the light curve for XX Cyg.

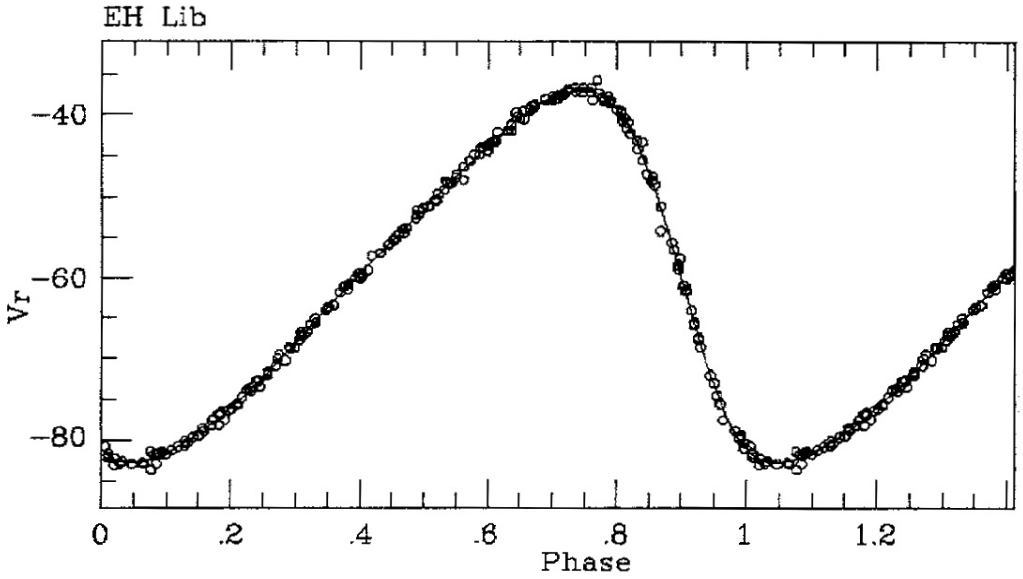

Figure 6. Radial velocity curve for the HADS, EH Librae as shown in Figure 11 from Schwendiman (2001). Note how the radial velocity minimum (similar to maximum light) occur near phase 0.05.

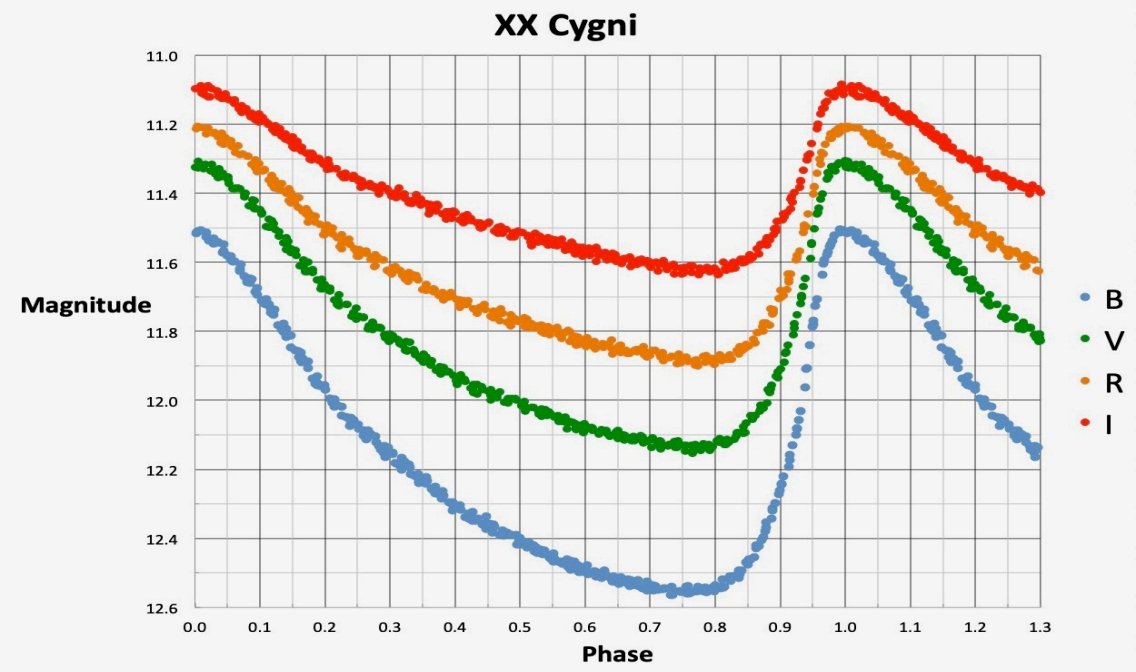

Figure 7. The light curves from phased Johnson/Cousins BVRI photometry of XX Cyg from late July 2024. A decreasing amplitude and broader light curves are seen when moving to redder filters.

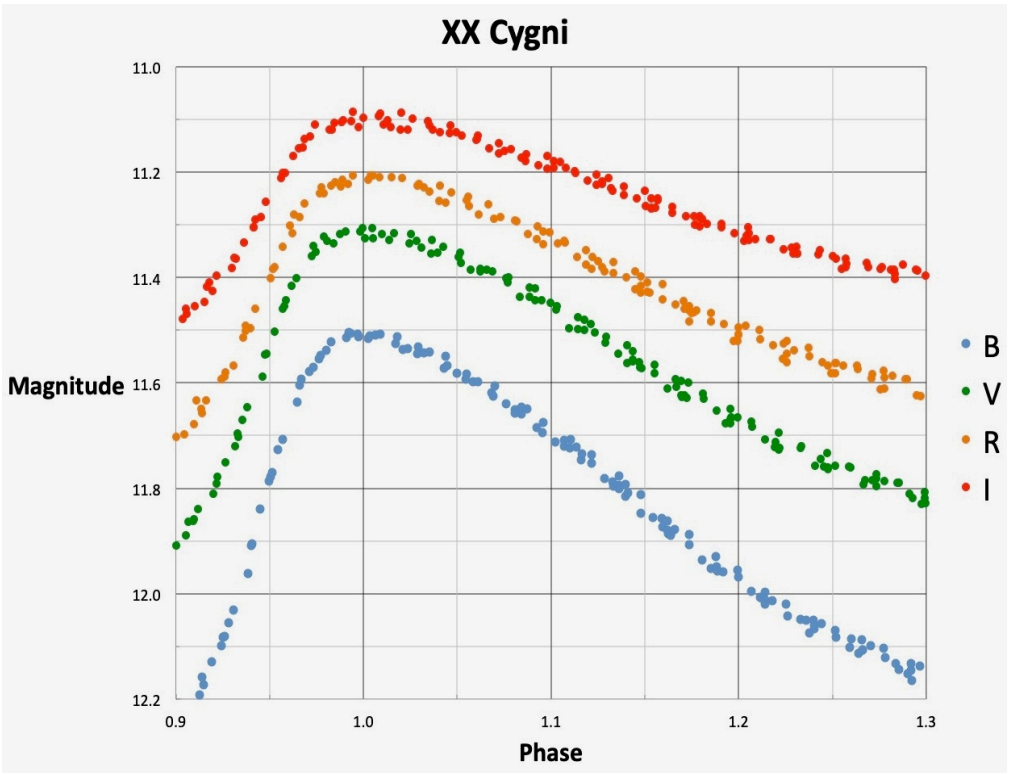

Figure 8. Zoomed view of the region of interest for the light curves shown in Figure 7 used to verify the lack of a correlation between maximum light timing and filter wavelength.

To verify what appears graphically to be nearly identical times of maximum light for each of the four filters examined, we have done curve fitting using the commercially available Peranso software developed for variable star analysis. The times of maximum light were determined from the restricted phase interval seen in Figure 8. The results of this analysis did not show a statistically significant difference in the maximum light timings or a repeatable dependence of the minor timing variations that were correlated with filter wavelength.

The results of the checks on maximum light timings did show differences between filters and at times the B filter times would even be slightly ahead of the V filter times. At the same time, the V times would be ahead of the R filter times. The I filter times did not generally follow that pattern, and in one case it was the earliest timing of the four filters. The standard deviation of the timings in the different filters for the individual maximum light measures ranged from between 35 to 90 seconds. For the combined phased data, the standard deviations for the different filter timings were 38, 53, 55, and 78 seconds for the B, V, R, and I filters, respectively. Results of trials for some of the interesting cases are shown in Figure 9. It is interesting to note that all the timing differences detected were within a 1σ envelope. It is reasonable to conclude that there is no trend in maximum light timings correlated with the choice of visual filter.

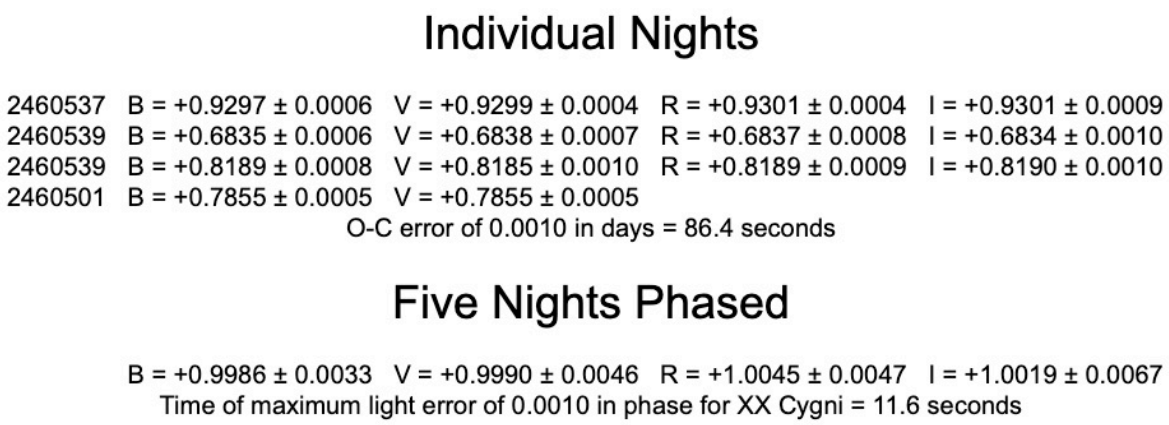

Figure 9. Selection of diverse results from the time of maximum light trials done to detect differences that could be filter dependent. There were no statistically significant or repeatable trends seen in these data.

3.3 Observational Cadence

The search for the possible causes of maximum light timing errors was extended to include looking at possible effects from observational cadence. This was accomplished by examining results from different observational cadences. We started with 18 data points from a well-determined time of maximum light in the B filter secured on JD 2460501. We increased the number of points in the original set to 35 by fitting a point to the light curve at the midpoint between each pair of original observations. Next, we added one more point on the descending part of the data set and then dropped every other point in that set to form a 10-point data set. We used every third point to form a seven-point data set and finally used every fourth point to

make the final five-point data set. Each of these five data sets were used to determine the time of maximum light for that epoch. This produced an interesting result in that each trial (including the expanded data set) was found to have a slightly later time of maximum light. The error in determining the maximum light time was smaller with a larger data set. The best determined time was for the 35-point set with an estimated error of about 35 seconds. The 10- and five-point data set were the poorest determinations, with each having an error of about 78 seconds. The difference in time between the 35-point and five-point determinations was 61 seconds. That difference is once again within the 1σ range. The results of these trials are shown in Figure 10. Observing cadence alone cannot account for timing errors as large as several minutes.

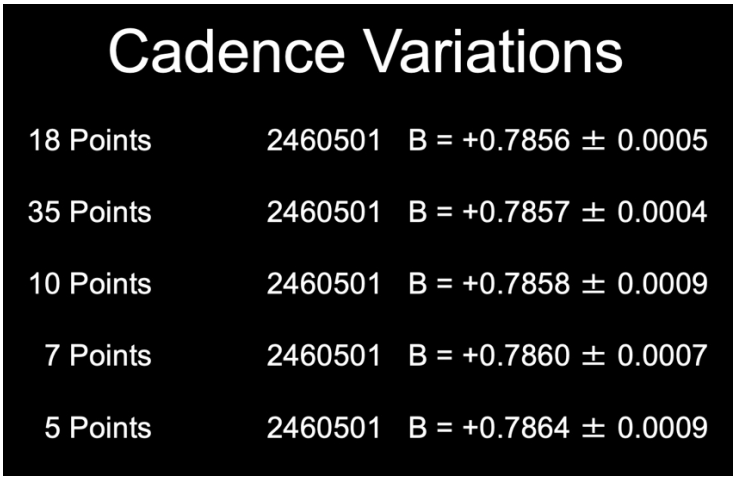

Figure 10. The results of the observing cadence trials for maximum light timings of XX Cyg.

3.4 Random Photometric Errors

Another possible source of maximum light timing errors that need to be examined are random photometric errors. It was decided that a quick way to check this possible source of error was to take a known light curve (again, JD 2460501) and lower three or four points near maximum light on either the steep rising branch or the more slowly changing descending portion of the light curve. We took points in the original data set and lowered the selected points by 0.02 to 0.03 magnitude. The resulting light curves do not appear anomalous to visual inspection. Most experienced observers have seen photometric errors this size or larger that occur even in conditions that appear to be suitable for doing quality photometry. However, when there is a period of rapid seeing variations or a quick passage of thin clouds that are not easily detected, photometric errors of this size can appear without being noticed by an observer. We found that errors of this type on the descending part of the light curve (we called this “added late”) change the maximum light determination by only 30 seconds or less. Introducing this modest error into the photometry on the rising branch of the light curve seems to be much more serious. We found in various trials that small errors introduced on the rising branch (we called this “added early”) can easily result in 2 or 3σ errors on the order of 2 or 3 minutes to the observed times. Typical results from these trials are shown in Figure 11. If photometric errors are regarded as an explanation for large dispersion in O – C diagrams, it is likely that the size of the errors would need to be much larger than those we introduced in these trials. Errors of that size should be

easily detected by a visual inspection of light curves as they are processed. It is becoming common practice to run data though an automated pipeline for much of the basic analysis. It is recommended that all light curves be visually inspected for obvious irregularities before they are committed to an analysis pipeline.

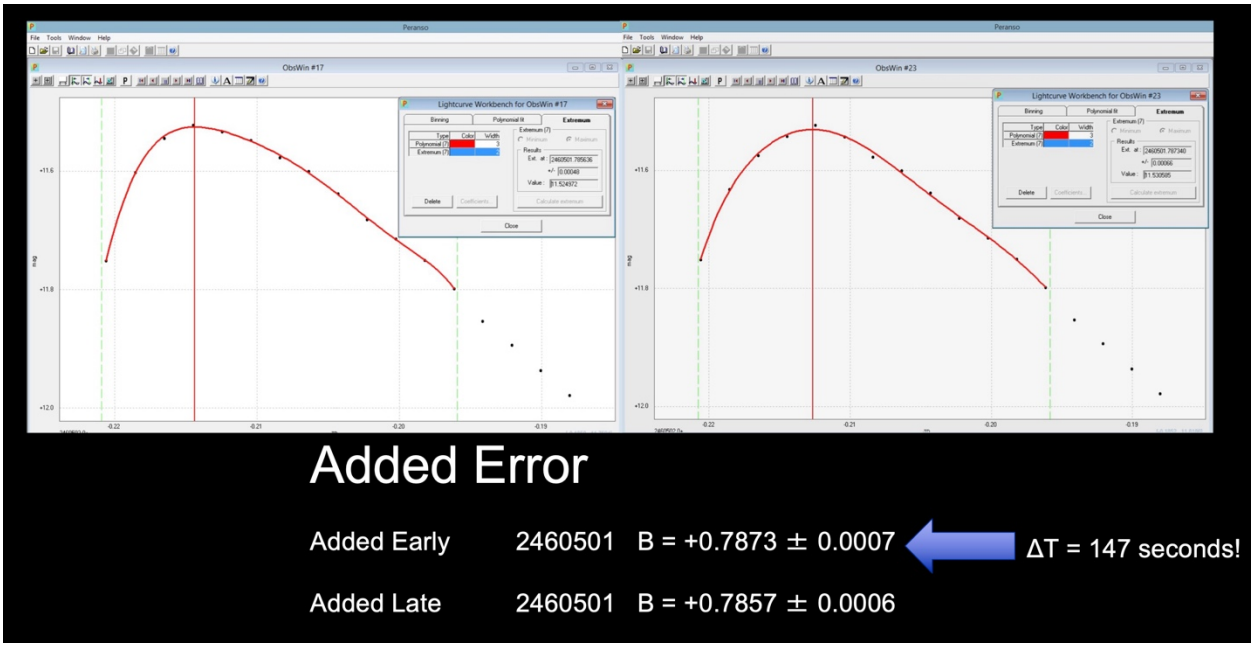

Figure 11. Light curves and results from the random photometric error test. The light curve with a few artificially lowered points on the descending portion (added late) of the curve is on the left. The light curve with a few artificially lowered points on the rising branch (added early) is on the right. Note that neither of the curves appears to be particularly atypical. However, the timing of maximum light for the two differ by more than two minutes in this 2σ example.

3.5 A Closer Look at the 2009 Data

After the results of the different trials designed to help explain the large timing irregularities evident in the more recent data sets in the O – C diagram for XX Cyg from Yang et al. (2012), we decided to take a closer look at the recent data. We were particularly drawn to the data from 2009. The data from 2009 are all modern CCD observations, but they have the largest scatter of all the data groups in the more than 100 years of maximum light timings. Yang et al. (2012) lists their paper, Fiacconi and Tinelli (2009), and Conidis et al. (2011) as the sources of data for 2009. It should be noted that the Conidis et al. (2011) paper is cited incorrectly in Yang et al. (2012). The listed authors are all incorrect (given as Georege, Sarahi, and Aaronj et al.), but the year, journal, volume, and page information are correct.

In Figure 12, we plot an O – C diagram for 2009 with an ephemeris formula of:

$$HJD_{max} = 2452115.73421 + 0.134865175 \times E \qquad (1)$$

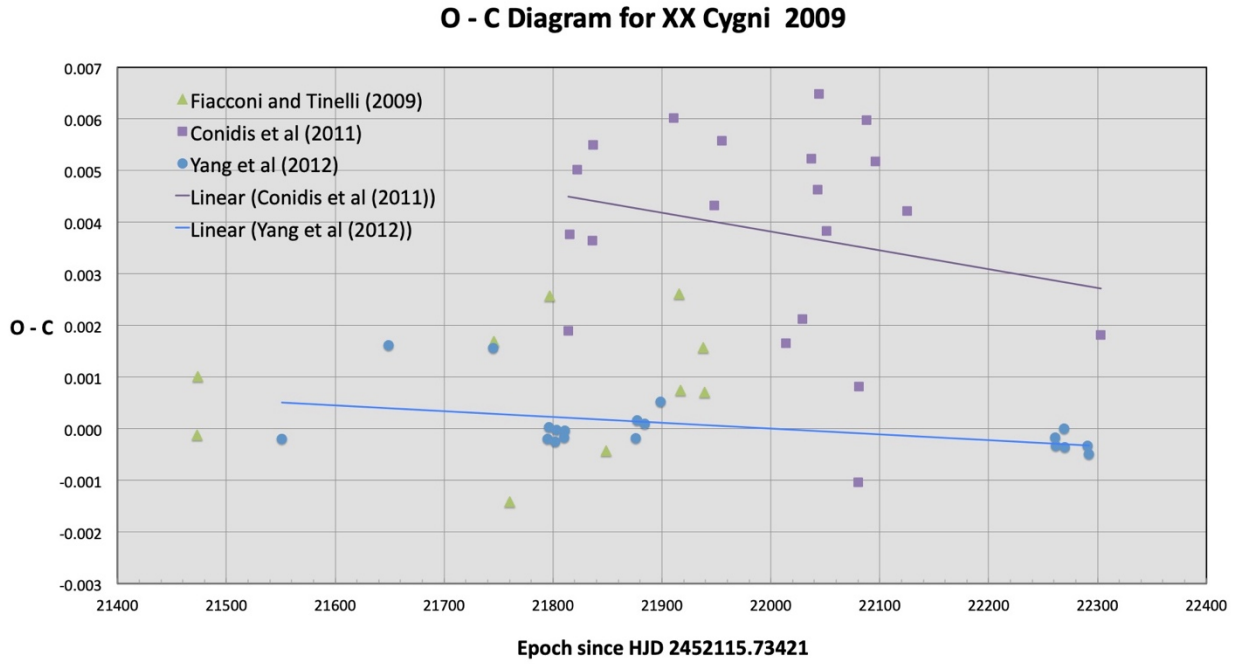

Figure 12. Plot of the 2009 O – C diagram for the three major data sets given in Yang et al. (2012). The period and epoch were selected to give a line with zero slope and an average residual of zero for the combined data set we introduce later for the years 2007 through 2024. The excessive scatter in the Conidis et al. (2011) data is evident in this plot. The teal-colored line and the purple line are the best fit line to the 2009 Yang et al. (2012) and Conidis et al. (2011) data sets, respectively. These lines are separated on average by more than a five-minute time difference.

In Equation (1), E is the cycle number since the original epoch, 2452115.73421. The epoch and period were calculated to give a zero slope and zero value average residual to the 2007 through 2024 data set that will be introduced in the next paragraph. The times of maximum light from Conidis et al. (2011) have striking differences from the data presented by Yang et al. (2012). They each have times of maximum light from the same night. For example, both have two times of maximum light that are only four cycles apart on JD 2455056, yet the O – C values for the Conidis et al. (2011) times are as much as 340 seconds later than the times of Yang et al. (2012) when compared to the calculated values for an epoch. Another comparison of the data points shows that the standard deviation derived for the multiyear O – C values of Conidis et al. (2011) is 0.00233 day (201 seconds). The standard deviation for the 2009 O – C values of Fiacconi and Tinelli (2009) is 0.00129 day (111 seconds). This level of accuracy is noteworthy since the Fiacconi and Tinelli observations were secured with an 80 mm refractor and a DSLR as the detector. The standard deviation for the multiyear O – C values of Yang et al. (2012) is 0.00040 day (35 seconds). This difference is evident in Figure 12 in the trendlines for Yang et al. (2012) and Conidis et al. (2011). The two lines have approximately the same slope but differ on average from each other by more than five minutes.

3.6 An XX Cygni O – C Diagram for Future Investigations

In Figure 13 we show a plot of the 2007 through 2024 O – C diagram for XX Cyg that includes the four data sets for these years given in Yang et al. (2012) along with additional data from TESS observations and WMO for the years 2019 through 2024. Again, the data from Conidis et al. (2011) stand out as having a much larger dispersion.

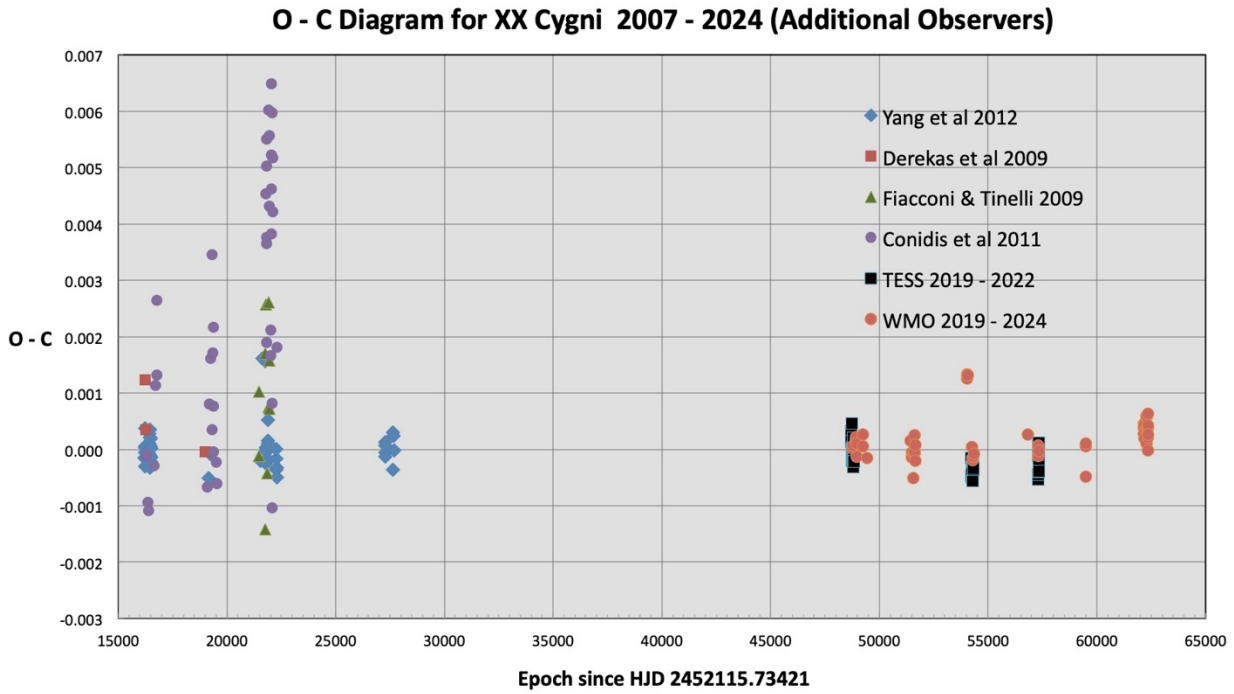

Figure 13. O – C diagram for XX Cyg using the calculated values from Equation (1). In addition to the four data sets given in Yang et al. (2012), additional data from TESS observations and data secured at WMO for the years 2019 through 2024 have been included to extend the diagram. The much greater dispersion in the data from Conidis et al. (2011) for the first three years is evident in this plot.

The WMO and TESS O – C values shown in Figure 13 have seasonal standard deviations of 0.00038 day (33 seconds) and 0.00025 day (22 seconds), respectively. This is comparable to what was found for the observations made by Yang et al. (2012). It seems unlikely that the timing values from Conidis et al. (2011) fit with the other five groups of data. At times when the observations were made on the same day or within a couple of days from each other, the points from Conidis et al. (2011) occur several minutes later. Once again, with two other observing teams in agreement during the 2009 season, it seems unlikely that the third team would repeatedly catch XX Cyg on nights when it was having a delayed maximum light. This seems especially true for times when two of the teams were observing at about the same time. It is also of note that Figure 2 in Conidis et al. (2011) is described as an example light curve of XX Cyg in a Johnson I-band filter. The light curve in that figure looks vastly different from the Cousins I filter light curve in Figure 7 above. In Figure 14, we include additional WMO observations along with available TESS

data and the observations of Yang et al. (2012) to produce a 2007 through 2024 O – C diagram for XX Cyg with a total standard deviation around the zero line of 0.00039 day (34 seconds).

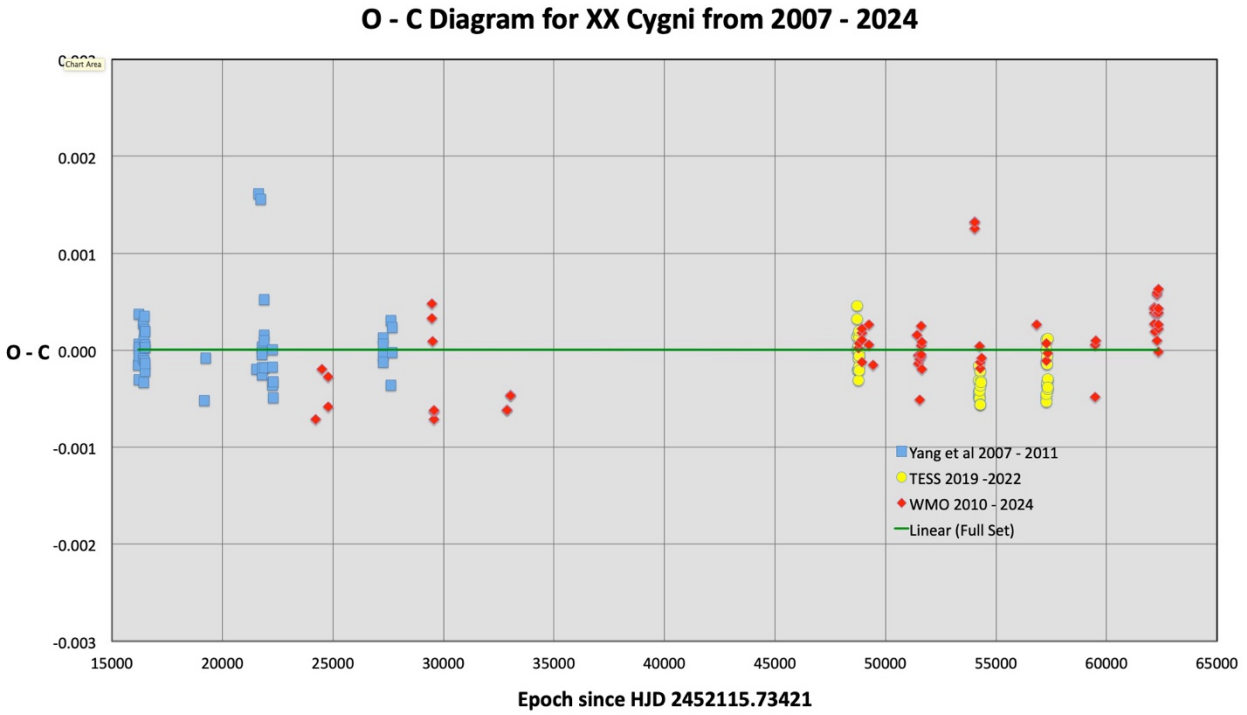

Figure 14. This graph uses the three data sets examined in this investigation with the smallest timing errors to produce an O – C diagram for XX Cyg with a combined standard deviation of 0.00039 day (34 seconds). This seems reasonable and consistent with the typical error for a time of maximum light derived from a well-defined light curve.

4. Conclusions

The are many possible sources of error that can appear in O – C diagrams. These are difficult to detect and can possibly be the product of several different factors acting together. In this investigation, we have examined several different sources of timing errors and concluded that most of them are insufficient by themselves to explain large amounts of seasonal scatter for seemingly stable pulsating variables.

Our tests showed that choice of filter has a small or non-existent effect on maximum light timings. It is also unlikely that observing cadence is a significant source of scatter in the determination of times of maximum light. Our tests showed little difference in the timings derived from the couple tenths phase interval on either side of a maximum that was defined by seven points or 35 points. As long as the magnitudes were precise and somewhat evenly spaced, the timings showed little variation. Photometric precision did seem to make a measurable difference in some cases. Timings for light curves with a steep rising branch appear to be affected by some combinations of random errors on the rising branch.

There are other factors that can have an impact on maximum light timings that were not addressed in this investigation. Omission or misapplication of the heliocentric correction can produce a significant seasonal timing error for stars with a period that is much less than a day. Of course, incorrect clock settings can cause many timing problems and be especially difficult to track down or correct. Other factors might include instrumental instability, inadequate flat fielding corrections, or poor baffling and internal reflections in the optical tube.

While XX Cyg may have gone through a time of great instability in the period from 2005 through 2010, it is difficult to explain why behavior like that was not more widely observed. It seems more likely that some other problem caused atypical timings like those reported in Conidis et al. (2011). Even though the differences between the two large data sets from that era are great, they remain unexplained, and it is likely the case that only careful monitoring in the future will validate the existence of large cycle-to-cycle timing variations. The lengthy time series observations of space-based surveys like TESS will hopefully help provide answers to these problems.

Acknowledgments

Many of the light curves shown in this paper and times of maximum light derived herein used photometry generated with the VPHOT program available through the AAVSO membership of several of the authors. Unless otherwise noted, the different authors of this presentation secured all photos displayed herein. This research utilizes data collected by the TESS mission and downloaded from the Mikulski Archive for Space Telescopes (MAST). Funding for the TESS mission is provided by NASA's Science Mission Directorate. Finally, this research made use of Peranso (www.peranso.com), a light curve and period analysis software.

We thank the Brigham Young University College of Computational, Mathematical, and Physical Sciences and Department of Physics and Astronomy for continuing support of undergraduate mentoring and the research done at the West Mountain Observatory.

References

Conidis, G. J., et al. 2011, PASP, 123, 26
Derekas, A. et al. 2009, MNRAS, 394, 955
Detre, L. 1936, Astronomische Nactrichten, 258, 329
Fiacconi, D., & Tinelli, L. 2009, Open Eur. J. Var. Stars, 114, 1
Joner, M. D. 1981, Thesis, Brigham Young University
Joner, M. D. 1982, PASP, 94, 289
Niu, Jia-Shu, Liu, Yue, and Xue, Hui-Fang, 2023, AJ, 166, 43
Schwendiman, L. R. 2001, Thesis, Brigham Young University
Szeidl, B., & Mahdy, H. A. 1981, Commun. Konkoly Obs., 75, 1
Yang, X. H., Fu, J. N., and Zha, Q. 2012, AJ, 144, 92

A Spectroscopic Investigation of the Interaction of Pleione with its Companion

Caleb Kettering and Dr. Melvin Blake

University of North Alabama Chemistry and Physics, 1 Harrison Plaza, Florence, AL, 35630, United States; ckettering@una.edu

Subject Keywords

AAVSO and Be-star International Database; Spectroscopy, Be stars; binary stars; variable stars

Abstract

Pleione is a Be/Shell star which exhibits photometric and spectroscopic variations. We have begun a study of its changes using the Be Star and AAVSO databases. We see that the times when its binary companion is near periastron show rapid changes in the equivalent width of the Hα line, coincident with changes in brightness. Superimposed on the short-term variations due to stellar encounters we see a long-term trend in the sense of the Hα equivalent width increasing. We also note the presence of OIII at 4932 angstroms near the Hβ line showing a P-Cygni type profile indicating the presence of a shell.

1. Introduction

Pleione is classified as a Be star, a type of star that remains in the hydrogen-burning phase of its life. This star is in the constellation Tauris within the Pleiades star cluster and is roughly 390 light years away from Earth. B_e stars are unique in their characteristics of experiencing significant mass loss due to high rotational speeds and stellar winds, affecting their evolutionary paths and potentially accelerating their lifespan. These rapid rotations are known to form disks of gas around the star and are believed to be the cause of Pleione's distinctive Balmer emission lines. These Balmer lines, especially Hα, Hβ, and Hγ, are important for studying stars like Pleione, as they show hydrogen transitions in the visible spectrum, ranging from red (Hα) to blue (Hβ) and violet (Hγ). Over the course of Pleione's lifetime, this disk formation has experienced spectroscopic and photometric variations. Since the end of its last diskless phase in 1937, the star Pleione has continually transitioned between B_e and B_e-Shell phases. These disturbances in the star's shell are believed to be caused by the passage of its companion star which occurs every 218 days.

2. Procedures

2.1 Methods

For this project we used spectroscopic and photometric data from the Be Star database and AAVSO databases respectively. We used a legacy IRAF installation to measure the equivalent

widths and the R/B ratio of the Hα, Hβ, and Hγ lines. After acquiring the equivalent widths, we plotted this data over the time to observe a trend in the data (Figures 1a-1f).

2.2 Results

Our data shows a varying ratio of violet and red emissions over time and long-term changes have been apparent in the star's R/B ratio over time. This suggests that the disk is either non-uniform or is experiencing velocity changes over time. Marr et al. (2022) suggest the disruption of this disk is likely due to the gravitational influence of Pleione's companion, component b, as the timing of changes in the Hα emission line seems to coincide with the companion's orbital period of approximately 218 days. Our results support this idea, since there is a disruption every 436 days which is roughly double the orbital period (Figures 1a-1f). There is a gap in the data due to the star being in the constellation Taurus, resulting in one disruption event taking place when the star is not observable.

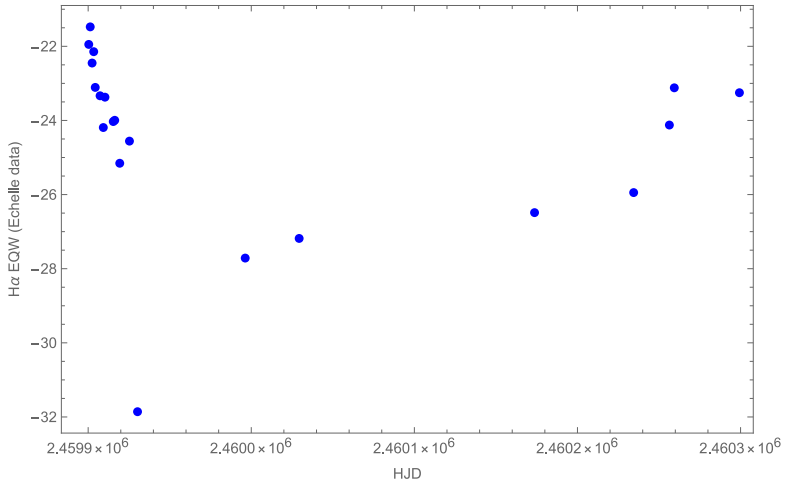

Figure 1a. Plot of EQW Hα over time.

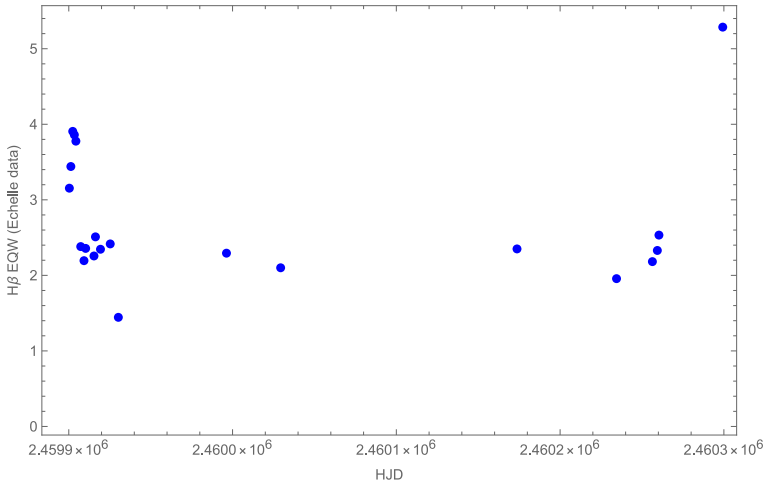

Figure 1b. Plot of EQW Hβ over time.

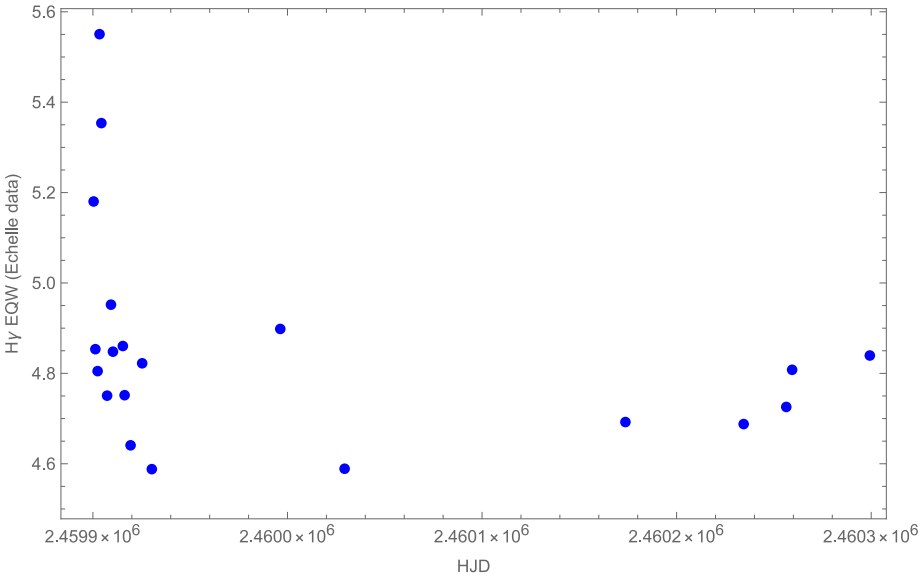

Figure 1c. Plot of EQW Hγ over time.

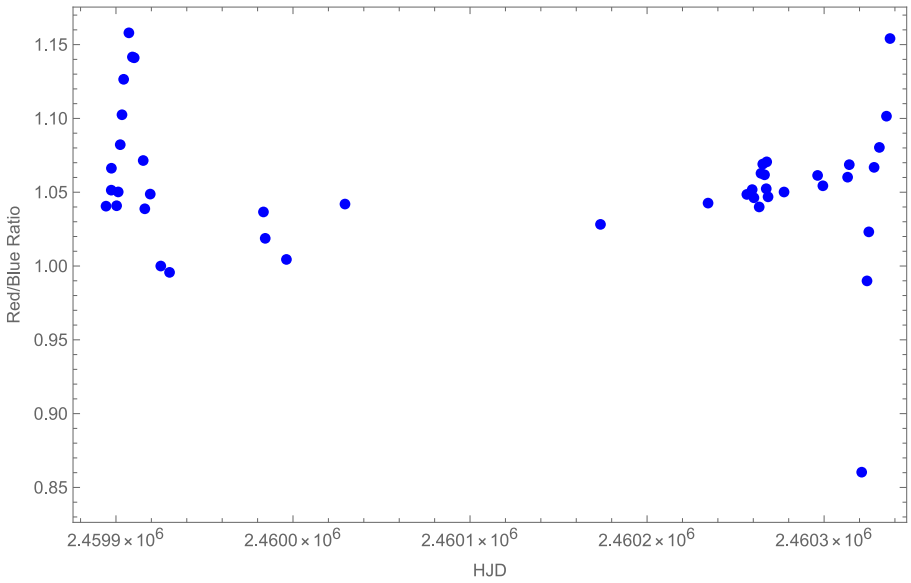

*Figure 1d. Plot of Hα red to blue ratio over time***.**

3. Conclusions

The results of our findings suggest the disk appears to be disrupted by the companion's close approach. Contrary to expectations, more Hα emission is not observed despite the star being brighter, which suggests that increased photon interaction could lead to faster gas dissipation and a decrease in disk density. We have noticed that the brightness over time does seem to coincide with the changes in the equivalent widths which would suggest a relationship between the two, more observation is needed. Lastly, we have noticed the presence of an O III line with a P Cygni profile in the H-beta region of our data. This is indicative of a surrounding shell of gas, rather than an outflow of material from the star.

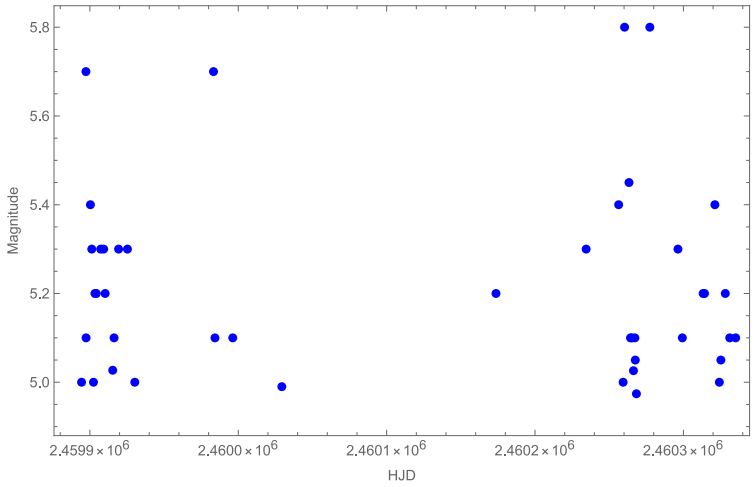

Figure 1e. Plot of Magnitude over time.

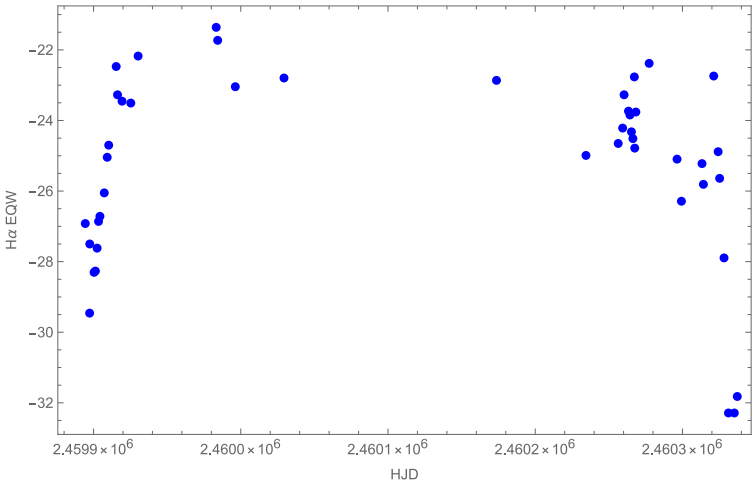

Figure 1f. Plot of EQW Hα over time.

Acknowledgements

We acknowledge with thanks the variable star observations from the AAVSO and Be-star International Database contributed by observers worldwide and used in this research.

References

Marr, K.C., et al. 2022, The Role of Disk Tearing and Precession in the Observed Variability of Pleione, ApJ 928, 145.

Suffak, M.W., Jones, C.E., and Carciofi, A.C. 2024, Disk Tearing in a Be star: predicted 3D observations, MNRAS, 527, 7515.

Katahira, J. 2023, Long-term evolution of the H-alpha emission line of Pleione between Jan 2009 and Mar 2023, BeSS database, SAG, 6, 1.

Empowering African Youths in Astronomy: The Impact of Pan-African Citizen Science e-Lab

Miracle Chibuzor Marcel[1], Kassamba Abdel Aziz Diaby[2], Meryem Guennoun[3], Betty Rose Nabifo[4], Mohamed Elattar[5], Andoniaina Rajaonarivelo[6], Privatus Pius[7], Molly Nkamogelang Kgobathe[8], Immanuel Luis[9], Sigrid Shilunga[10], Nejmeddine Etteyeb[11], Keketso Qhomane[12], Samuel Nyangi[13], Tresford Chilufya Kalunga[14], Nunes Alfredo Assano[15], Edson Domingos Jequecene[16], MAFUKA LUSALA JOSEPH[17], Esaenwi Sudum[18], Jorbedom Leelabari Gerald[19], Christopher Tombe Louis Gore[20], Kareem Waleed Hosny[21], Nagat Yasser[22], Jocelyn Franck[23], MAMOUDOU KOUROUMA[24], BABOUCARR BOBB[25], Kebab Jaiteh[26], Salma Sylla[27], Hans ESSONE OBAME[28], Dennis Kiyeng[29], Thobekile Sandra Ngwane[30], Tawanda Kelvin Simon[31], Saja Alhoush Sulayman[32], Salma Regaibi[33], Souley Yahaya[34], Tengwi Mogou Ornela[35], Henry Sanderson Viyuyi[36], Fortune Tatenda Matambo[37], Matthias Asare-Darko[38], Christian Kontoa Koussouwa Gbaba[39], Moisés da Silva[40], Ntahompagaze Joseph[41], Gilberto Gomes[42], Bongiwe Portia Mkhabela[43], Bauleni BVUMBWE[44], Tshombe Nkhowani[45], Mawugnon Axel Gahou[46], Sarah Abotsi-Masters[47], René Simbizi[48], Salomon Mugisha[49], Ahmed Saeed[50], Mohammed Yahya Alradi Eldaw[51], Allen Thomas[52], Ben Abdallah ridha[53], Dieumerci kaseha[54], Sherine Ahmed El Baradei[55], Nahla Hazem Hussein[56], BADO Fabrice[57], Ngozika Frances Anekwe[58], Arvind Ramessur[59], Mohamed Ali Koroma[60], Harold Safary[61], Oosthuizen Leonardo[62], Mdumiseni Wisdom Dabulizwe Dlamini[63], Mamadou Mahamat Djabbi[64], Nonofo Angela[65], Mamaja Jalloh[66], Mamadou Balde[67] , Joy Olayiwola[68], Elijah Ibharalu[69], Thierry Martial TCHANGOLE[70], Kirubel Memberu[71], Lidia Dinsa[72], Chidozie Gospel Ezeakunne[73]

1. Pan-African Citizen Science e-Lab, FCT, Abuja: info@pacselab.space, miracle.c.marcel@gmail.com; 2. Université Félix Houphouët-Boigny; 3. Oukaimeden Observatory; 4. National Curriculum Development Centre; 5. Bani-Suef University; 6. Haikintana Astronomy Association; 7. Department of Natural Science, Mbeya University of Science and Technology; 8. University of Botswana Astronomy Club; 9 & 10. Department of Physics, Chemistry and Material Science University of Namibia; 11. Tunisian Astronomical Society; 12. BlueCraneSpace Astronomy & Astrophysics Department - University of Pretoria; 13. Amateur Astronomical Society of Kenya; 14. Kabulonga Girls' Secondary School; 15 & 16. Detetives do Cosmos; 17. Astroclub Kongo Central; 18. The Astro Group of the Rivers State University; 19. The Astro Group of the Rivers State University; 20. Mayardit Academy for Space Sciences - University of Juba; 21 & 22. Paradox Team; 23. University Marien Ngouabi; 24. IT Dreams and Promises of the University of Bamgui; 25 & 26. Physics Dept. University of Gambia; 27. Orion Astrolab and Department of Physics, University Cheikh Anta Diop; 28. IAU - NAEC Gabon; 29. Space Partnerships and Applications Company Kenya; 30. Zimbabwe Astronomical Society; 31. Zimbabwe National Geospatial and Space Agency; 32. Amateur Astronomy Libya; 33. Steps Into Space Association; 34. Niger Space Surfer; 35. Astronomy Club of the University of Buea; 36. Zambia Space Explorers; 37. Zimbabwe National Geospatial and Space Agency; 38. PRAGSAC; 39. NGO Science Géologique pour un Développement Durable (SG2D); 40. Associação Angolana de Astronomia; 41. Physics Department, University of Rwanda, College of Science and Technology; 42. Angolan Space Program Management Office (GGPEN); 43. Galaxy Explorers; 44. Celestial Explorers; 45. Copperbelt University; 46. Sirius Astro-Club Benin; 47. Ghana Planetarium; 48 & 49. Physics Dept. University of Burundi; 50. Sudanese Asteroid Hunters; 51. Institute of Space Research and Aerospace (ISRA); 52. Center for Science Education; 53. Aljarid Astronomie; 54. Lubumbashi Astro Club; 55 & 56. Space - Water-Environment Nexus e - Center; 57. Laboratoire de Physique et de Chimie de l'Environnement, Université Joseph KI-ZERBO, Ouagadougou, Burkina Faso; 58. Phys. Dept. Chukwuemeka Odumegwu Ojukwu University Uli Campus Anambra State; 59. IAU - NOC Mauritius; 60. Cosmic Gazers Research Institute Sierra Leone; 61. Kenya Space Agency; 62. Night Sky Tours; 63. Destiny Stars of the Univesity

of Eswatini; 64. Toumaï; 65. Marang Junior Secondary School; 66. Sierra Leone Geospatial and Space Agency; 67. UNESCO Center for Peace USA in Guinea; 68. National Space Research and Development Agency, NASRDA HQ; 69. University of Benin; 70. CosmoLAB Hub Association; 71 & 72. Ethiopian Space Science Society; 73. University of Central Florida

Abstract

This paper summarizes the presentation delivered by the PACS e-Lab management team during the 113th Annual Meeting of the American Association of Variable Star Observers (AAVSO). The presentation outlined the rationale for founding PACS e-Lab, the various projects offered to the African public, and the research telescopes utilized, including the Las Cumbres Observatory, Slooh telescopes, and the MicroObservatory. It also highlighted the developmental impact of the organization and its future prospects, focusing on the establishment of an observatory that will serve as the center for the group's astronomy research, education, and outreach efforts.

1. Introduction

Welcome to the Pan-African Citizen Science e-Lab (PACS e-Lab) platform, Africa's leading hub for Astronomy Research, Education, and Outreach.

Many people grow up asking fundamental questions about the universe. However, in Africa, these curiosities often go unfulfilled due to a lack of accessible resources for learning about space science and astronomy. While some higher institutions in Africa offer astronomy and related courses, they tend to focus primarily on theory, leaving students without real-life, practical experiences. This disparity often leads to doubts and skepticism about astronomical science.

To address this challenge, the PACS e-Lab was established December 4th, 2020 as an online platform designed to bridge the gap in astronomy practices in Africa through our research, education and outreach projects. Through our platform, we collaborate with NASA and other related organizations in developed countries to engage the African public, including teachers, students, and space enthusiasts, in hands-on space science and astronomy activities, free of charge.

As a result, we have engaged over a thousand individuals across 50 countries (and still counting) in our projects. Many of our participants, whom we proudly call citizen scientists or citizen astronomers, have made significant discoveries, conducted observations using robotic telescopes, and published their findings in research papers undergoing peer review or already published in reputable journals. They have been featured in several local, regional, and international news media outlets and have presented their work at regional and global conferences.

2. Project Highlights

Asteroid Search: The asteroid research citizen science project is part of NASA's planetary defense program, which monitors asteroids in our solar system, including those that could potentially impact Earth in the future. To engage the public in this defense program, Dr.

Patrick Miller at Hardin-Simmons University established the International Astronomical Search Collaboration (IASC) in 2006 (Miller, 2018).

PACS e-Lab is IASC's largest partner in Africa. This partnership enabled the founding of PACS e-Lab, and has since become a prerequisite for all projects we offer. When new members join our amateur research community, they are encouraged to form groups and are trained in using the Astrometrica program to search for asteroids using practice datasets. Participants learn to analyze these datasets, prepare Minor Planet Center (MPC) reports, and submit them to IASC. Once trained, PACS e-Lab registers these groups with IASC's Pan African Asteroid Search Campaign to receive fresh datasets for analysis.

The datasets are provided to IASC by the Panoramic Survey Telescope & Rapid Response System (Pan-STARRS) (Chambers et al., 2016) at the University of Hawaii's Institute for Astronomy and the Catalina Sky Survey (CSS) (Larson et al., 2003) at the Lunar & Planetary Laboratory at the University of Arizona. These telescopes use automated pipelines to detect asteroids; however, faint asteroids with low signal-to-noise ratios often evade detection by these systems, necessitating manual analysis by citizen scientists (Miller et al., 2024).

The campaign operates monthly, and participating teams receive certificates of participation from IASC. Reports submitted are evaluated within a week to determine if the asteroid observations are valid. Valid observations are designated as preliminary discoveries, which undergo further evaluation for six months to a year. If confirmed as real asteroids, these become provisional discoveries and are assigned provisional numbers before being cataloged in the MPC database, maintained by the International Astronomical Union (IAU) in Paris. This data is also shared with NASA's JPL Small-Body Database, where orbital parameters and other details are refined and made publicly available.

After several years, teams may have the opportunity to name their discoveries, marking a significant achievement in their contribution to planetary defense and asteroid research.

Exoplanet Observation & Photometry: Exoplanet detection began in the 1990s, and to date, over 5,500 exoplanets have been discovered using space-based surveys such as the Kepler Space Telescope, Transiting Exoplanet Survey Satellite (TESS), Spitzer Space Telescope, CoRoT (Convection, Rotation, and Planetary Transits), etc., and ground-based missions like the Keck Observatory, Very Large Telescope (VLT), Gemini Observatory, etc.

The next phase of exoplanet research focuses on understanding the composition of these distant worlds. Although some existing telescopes have been used to study exoplanetary compositions, they face limitations, such as an inability to detect vital faint signals from these planets.

New and upcoming instruments like the James Webb Space Telescope, Nancy Grace Roman Space Telescope, the Magellan Telescopes, etc., are designed to overcome these limitations. These advanced telescopes will be used for follow-up observations of previously detected exoplanets, enabling scientists to study their compositions and other parameters in detail.

To achieve this, it is crucial to refine the mid-transit periods of exoplanets so that observations can be precisely timed, avoiding wasted telescope time. This is where the NASA Exoplanet Watch, founded by Zellem et al., 2020; 2023, comes in. The initiative allows citizen scientists to contribute observational data to refine the transit periods of exoplanets.

Our organization is part of these efforts, engaging teachers, students, and STEM enthusiasts from Africa. Our Citizen scientists receive training in observing and capturing images of stars using the 0.4m Las Cumres Observatory (Brown et al., 2013) and MicroObservatory (MOBS) robotic telescopes (Sadler et al., 2001; Gould et al., 2006; Dussault et al., 2018). They also learn to conduct photometry using the EXOTIC software to generate light curves and submit observational reports to the American Association of Variable Star Observers (AAVSO).

Double-star astrometry: This project involves observing close double stars' position angles and separations (Marcel et al., 2024). As part of this research project, we offer training using the 0.4m Las Cumbres Observatory, a network of robotic web-based telescopes, to observe a close double star listed in the Washington Double Star Catalog, then use software tools such as AstroImageJ or Afterglow Access to measure the position angle and separation distances between the primary and secondary stars.

Our trainees also learn how to request historical records of the system to compare changes over time with their observations. Additionally, they will access Gaia data for the system to determine the nature of their gravitational binding.

As part of the project, our citizen researchers will draft a research paper to be submitted to the *Journal of Double Star Observations* for peer review and publication. They also have the opportunity to present their results at conferences, either through talks or posters.

Astro-photo visual development: This refers to processing space images using computer programs and software to produce stunning, colorful visuals. This project empowers our citizen scientists to learn how to process images captured by both ground-based and space telescopes (e.g., JWST, Hubble, and Las Cumbres Observatory) through various software tools and techniques.

As part of this project, our citizen astronomers learn how to schedule observations of celestial objects like galaxies, star clusters, and nebulae using the 0.4m Las Cumbres Observatory telescope. They also use software tools such as Photoshop, GIMP, and FITS Liberator to process the images. Once they are proficient with the LCO platform, you will progress to accessing and processing FITS data from the Hubble Space Telescope (HST) and the James Webb Space Telescope (JWST). The goal of this project is to inspire and educate the African public about the beauty and diversity of the universe through astrophotography.

ARISS-Amateur Radio on the International Space Station: The Amateur Radio on the International Space Station (ARISS) event allows students and the public to connect directly with astronauts aboard the ISS via amateur radio, engaging in live Q&A sessions about space science, life in space, and current missions (Bauer, 2019). This initiative aims to inspire interest in STEM fields through real-time interactions with space professionals.

While some schools in Morocco and South Africa have previously hosted ARISS projects with their students, PACS e-Lab is the first organization to host the event with participation from individuals across the entire continent. Through this initiative, PACS e-Lab involved students and citizens throughout Africa by collaborating with its regional partners to enhance access. These regional collaborators help extend the event's reach and impact, engaging schools and communities continent-wide and establishing ARISS as a recurring educational experience across Africa.

Telescope Donation Project: Through our Telescope Donation Project, we collaborate with international donors to equip our teams across Africa with telescopes, empowering them to bring astronomy education and outreach to their communities. These telescopes allow participating groups to conduct public stargazing events, educational workshops, and training programs, enhancing local engagement in astronomy and space science.

3. Our Research Telescopes

At PACS e-Lab, our science engagements with the African public also include active participation from those in academic institutions. To support our astronomical research endeavors, we submitted telescope time proposals to educational and outreach entities such as the Las Cumbres Observatory, Slooh, and MicroObservatory. These organizations empower groups like ours to operate their robotic telescopes for educational and research purposes. These telescopes are strategically located at some of the best astronomical sites worldwide and offer optimal viewing conditions for various celestial observations.

With internet connectivity, we can access and control these telescopes remotely from various locations across Africa using smartphones or computers, making astronomical research both accessible and convenient. Through these telescopes, our citizen astronomers engage in real-time data collection and conduct meaningful research projects, including monitoring variable stars, observing double stars, and contributing to exoplanet studies.

4. PACS e-Lab's Developmental Impacts in Africa

We have recruited and engaged over a thousand individuals in over 50 African countries at various levels, educational institutions, space agencies, and astronomy organizations across Africa, in several of the projects described above and are continually developing new ones and forging new collaborations. Our projects contribute to Africa's development by addressing 7 out of the 17 Sustainable Development Goals (SDGs): Quality Education (SDG 4), Gender Equality (SDG 5), Decent Work and Economic Growth (SDG 8), Industry, Innovation, and Infrastructure (SDG 9), Reduced Inequality (SDG 10), Peace, Justice, and Strong Institutions (SDG 16), and Partnerships for the Goals (SDG 17). By engaging the African public in these activities, we aim to enhance astronomy knowledge and research skills within underrepresented African communities, fostering a new generation of astronomers and space scientists.

5. Future Prospects

We have achieved tremendous milestones since the inception of PACS e-Lab on December 4, 2020, and we are now looking forward to having an observatory that will serve as an operations center for our astronomy research, education, and outreach endeavors.

Additionally, we are forging new collaborations to expand the range of projects we offer to the African public.

Acknowledgments

The PACS e-Lab management extends heartfelt gratitude to Ms. Kalee Tock, affiliated with Stanford Online High School and a member of the Las Cumbres Observatory Global Sky Partner program, for facilitating PACS e-Lab's membership to the AAVSO.

We also appreciate Dr. Domingos Barbosa and his team at ATLAR Innovation for their sponsorship for us to attend the 113th Annual Meeting of the American Association of Variable Star Observers (AAVSO).

References

Bauer, F. H., Taylor, D., White, R. A., & Amend, O. (2019). Educational outreach and international collaboration through ARISS: Amateur radio on the international space station. Space Operations: Inspiring Humankind's Future, 827-856. https://link.springer.com/chapter/10.1007/978-3-030-11536-4_33

Brown, T. M., Baliber, N., Bianco, F. B., Bowman, M., Burleson, B., Conway, P., ... & Willis, M. (2013). Las Cumbres Observatory global telescope network. Publications of the Astronomical Society of the Pacific, 125(931), 1031-1055. https://iopscience.iop.org/article/10.1086/673168/meta

Chambers, K. C., Magnier, E. A., Metcalfe, N., Flewelling, H. A., Huber, M. E., Waters, C. Z., Denneau, L., Draper, P. W., Farrow, D., Finkbeiner, D. P., Holmberg, C., Koppenhoefer, J., Price, P. A., Saglia, R. P., Schlafly, E. F., et al. (2016). The Pan-STARRS1 Surveys. arXiv preprint arXiv:1612.05560v3.

Dussault, M., Wright, E., Sadler, P., Sonnert, F., & ITEAMS II Team. (2018, January). The impact of an authentic science experience on STEM identity: A preliminary analysis of YouthAstroNet and MicroObservatory telescope network participant data. In American Astronomical Society Meeting Abstracts (Vol. 231). https://mo-www.cfa.harvard.edu/OWN/pdf/YAN_Poster2017_AAS.pdf

Gould, R., Dussault, M., & Sadler, P. (2006). What's Educational about Online Telescopes?: Evaluating 10 Years of MicroObservatory. Astronomy Education Review, 5(2). https://mo-www.cfa.harvard.edu/OWN/pdf/10yearsofMicroObservatory_AER.pdf

Marcel, M. C., Gerald, J. L., Bvumbwe, B., Sani, I. A., Pius, P., Ekwu, O. M., ... & Olayiwola, J. U. (2024). Measurement of the double star system WDS 03286+ 2523 BRT 133 with a web telescope. Journal of Double Star Observations, 20(1), 48-55. http://www.jdso.org/volume20/number1/Marcel_48_55.pdf

Marcel, M. C., Sani, I. A., Gerald, J. L., Pius, P., Ekwu, O. M., Bvumbwe, B., ... & Olayiwola, J. U. (2024). New astrometric measurements of the position angle and separation of the

double star system WDS 03245+ 5938 STI 450. Journal of Double Star Observations, 20(1), 39-47. http://www.jdso.org/volume20/number1/Marcel_39_47.pdf

Miller, J. P. (2018). International Astronomical Search Collaboration: An Online Outreach Program in Astronomical Discovery for High School & College Students. RTSRE Proceedings, 1(1). https://rtsre.org/index.php/rtsre/article/view/27

Miller, P., Weryk, R., Wainscoat, R., Perret, J., Hartung, S., Vorobjov, T., ... & Pennypacker, C. (2024). The International Astronomical Search Collaboration (IASC)—Citizen Scientist System for Asteroid Discovery. Publications of the Astronomical Society of the Pacific, 136(2), 024502. https://iopscience.iop.org/article/10.1088/1538-3873/ad11a0/meta

Larson, S., Beshore, E., Hill, R., Christensen, E., McLean, D., Kolar, S., McNaught, R., and Garradd, G. (2003). The CSS and SSS NEO surveys. In Bulletin of the American Astronomical Society, volume 35, page 982.

Sadler, P. M., Gould, R., Leiker, P. S., Antonucci, P., Kimberk, R., Deutsch, F., & Hoffman, B. (2001). MicroObservatory Net: A network of automated remote telescopes dedicated to educational use. Journal of Science Education and Technology, 10(1), 39

Zellem, R. T., Pearson, K. A., Blaser, E., Fowler, M., Ciardi, D. R., Biferno, A., ... & Malvache, A. (2020). Utilizing small telescopes operated by citizen scientists for transiting exoplanet follow-up. Publications of the Astronomical Society of the Pacific, 132(1011), 054401. https://iopscience.iop.org/article/10.1088/1538-3873/ab7ee7/meta

Zellem, R. & Exoplanet Watch (2023, January). Exoplanet Watch: Inviting Citizen Scientists to Observe Transiting Exoplanets. In American Astronomical Society Meeting Abstracts (Vol. 55, No. 2, pp. 126-01). https://ui.adsabs.harvard.edu/abs/2023AAS...24112601Z/abstract

MESA Modeling of Blue Supergiants and Alpha Cygni Variables

Ava H. Moore and Joyce A. Guzik

Los Alamos National Laboratory, Los Alamos, NM, 87545, USA; ahmoore@lanl.gov

Subject Keywords

Techniques: stellar modeling; stars: variable: Alpha Cygni; stars: individual (alpha Cyg)

Abstract

Alpha Cygni variables are a subset of supergiant stars with spectral types A and B that show variations in their luminosity and radial velocities (Saio et al. 2013a,b). How these stars proceed through their evolution depends on their helium core mass, as well as on poorly understood phenomena such as mixing, overshooting, and wind mass loss (Saio et al. 2013a,b). For our research, a study of the parameters that affect a star's evolution through the red supergiant phase and determine whether a star returns to the blue supergiant region is performed using the MESA (Modules for Experiments in Stellar Astrophysics) code (Paxton et al., 2011; Jermyn et al., 2023) for models with mass fraction of elements heavier than hydrogen and helium Z = 0.015.

1. Introduction

Massive star evolution is relatively uncertain compared to that of other stars. Evolutionary processes within massive stars depend on several physical processes in the stellar interior, such as mixing, rotation, and magnetic fields (Georgy et al. 2014). Mass loss can also play an important role throughout the evolution and has a diversity of implementations in evolutionary codes. Ekstrom et al. (2012) show that some massive red supergiant models with rotation and a metallicity of Z = 0.014 will cross the H-R diagram a second time from the red supergiant phase back to the blue during core helium burning if the mass-loss rate during the red supergiant phase is high enough.

Knowing this, there should be two different populations of blue supergiant stars: those that evolve to the red supergiant branch after leaving the main sequence and those that were previously on the red supergiant branch and cross the H-R diagram back toward the blue. The second group have been shown to have a series of excited modes of radial pulsations due to the high luminosity-to-mass ratio in their blue supergiant phase (Saio et al. 2013a,b).

Alpha Cygni variables, a type of BA supergiant, show variations of less than 0.1 magnitude in their luminosity which are believed to be irregular pulsations. Deneb is one of the most well-known and best-studied Alpha Cygni variables, with periodicity between 10 to 100 days (Gautschy 2009).

Stellar models for Deneb have been unable to match observations, indicating an uncertainty in the excitation mechanism for radial or nonradial modes. Modeling by Gautschy (2009) showed that Deneb's pulsations might be explained by low-degree nonradial modes excited as the star evolves toward the red supergiant phase. These nonradial modes propagate like gravity modes below the iron opacity bump at around 200,000 K in the stellar envelope but propagate as pressure modes in layers above the iron bump. Saio et al. (2013a) found excited radial and nonradial pulsations only after significant mass loss in the red supergiant phase caused the models to evolve towards the blue supergiant phase, with the periods of the excited modes longer than the range of Deneb's observed periods.

Here, we present the results of a systematic study of modeling parameters for Alpha Cygni variables to better understand the differences with observation. Our goal is to determine which models show radial or nonradial pulsations and compare predicted periods to those observed in Alpha Cygni stars, and therefore whether pulsations can help to explain the variability in these stars. We also aim to determine if these models have similar mechanisms for their variability, which will aid in determining whether the group of Alpha Cygni variables are a homogenous class or not.

2. Methods

Modules for Experiments in Stellar Astrophysics (MESA, Paxton et al. 2011; Jermyn et al. 2023) is an open-source code used for stellar evolution calculations for a broad range of research topics in astrophysics. Here, we study the effects of different modeling options in MESA for Alpha Cygni variables.

An input file (inlist) with the default treatment for each physics option was run for models between 15 and 40 solar masses with a metallicity of Z=0.015 (see Fig. 1). This mass range was also studied by Saio et al (2013a) based on the instability boundaries of similar supergiant stars that show excitation of radial modes. The boundaries for these regions depended on metallicity, with Saio et al (2013a) calculating instability boundaries for models with metallicities between Z = 0.014 (which was used for models in Saio et al. 2011) and Z = 0.02. MESA's OPAL a09 opacities were used alongside the FreeEOS option. Convective mixing was done using the Henyey treatment with a mixing length (alpha) of 1.82 and gamma of 0.333. Semi-convection was set to an efficiency of 0.1. The overshooting treatment used MESA's exponential treatment.

We explored the effects of overshooting, semi-convection, rotation, and mass loss via stellar winds. We first ran a set of models with these options turned off. Then we explored turning each of these on in isolation with the other options switched off.

```
&star_job
  show_log_description_at_start = .false.

  create_pre_main_sequence_model = .true.
  pre_ms_guess_rho_c = 0
  pre_ms_d_log10_P = 0

  set_initial_age = .true.
  initial_age = 0

  set_initial_model_number = .true.
  initial_model_number = 0

  set_initial_cumulative_energy_error = .true.
  new_cumulative_energy_error = 0d0

  pgstar_flag = .true.
  save_pgstar_files_when_terminate = .true.
/ ! end of star_job namelist


&eos
  use_FreeEOS = .true.
/


&kap
  Zbase = 0.015 !check if connected to initial_z, these tables use the value of Zbase for Z, unless
use_Zbase_for_Type1 = .false..

  kap_file_prefix = 'a09' !can set to oplib tables using oplib_agss09, true
  kap_lowT_prefix = 'lowT_fa05_a09p' !check tables for matching profile, matched
  kap_CO_prefix = 'a09_co' !check tables for matching profile, check if needed, matched

  use_Type2_opacities = .true.
/ ! end of kap namelist
```

Figure 1. An image of the first three sections of the MESA inlist file.

Once isolated tests of each individual option were finished, and no models were found to have blue looped, models were run with a combination of options turned on to see if they would evoke a blue loop (i.e., a blue supergiant phase following the red supergiant phase). For simulations with only one option turned on, studies were done for masses between 15 and 40 solar masses. However, once testing started to combine more than one option, results were obtained for only 15 and 20 solar-mass models.

3. Results

Figure 2 (left) shows evolutionary tracks with none of the additional physics options turned on. Several of the evolutionary tracks show unphysical behavior at the end of the main sequence phase that was mitigated with semi-convection turned on (Figure 2, right), so semi-convection was used for the remaining parameter studies. Figures 3 and 4 show results for models with either overshooting, rotation or mass loss turned on in addition to semi-convection. Blue looping was found to occur in two 15 solar-mass models (Fig. 5), one which applied overshooting and mass-loss parameters to more closely fit results of Saio et al. (2013a), and one with overshooting, mass-loss, and rotation. Figures 2 through 5 were models calculated using the MESA version 24.03.1. However, 20 solar-mass models with these same parameters, calculated using MESA 24.08.1, did not complete a full blue loop (Fig. 6).

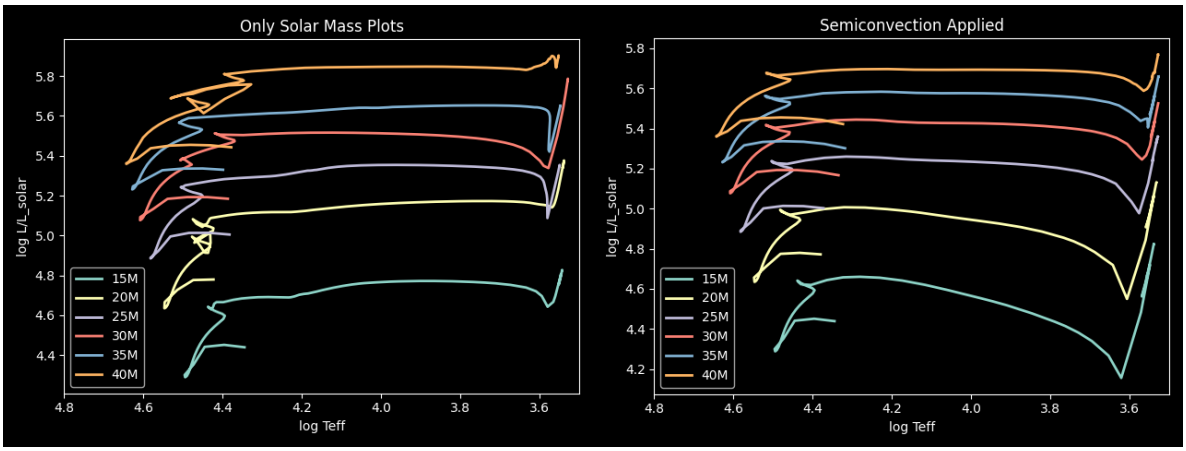

Figure 2. a) Evolutionary tracks for 15-40 solar masses with no additional options applied (left); b) Evolutionary tracks for 15-40 solar masses with only semi-convection (right).

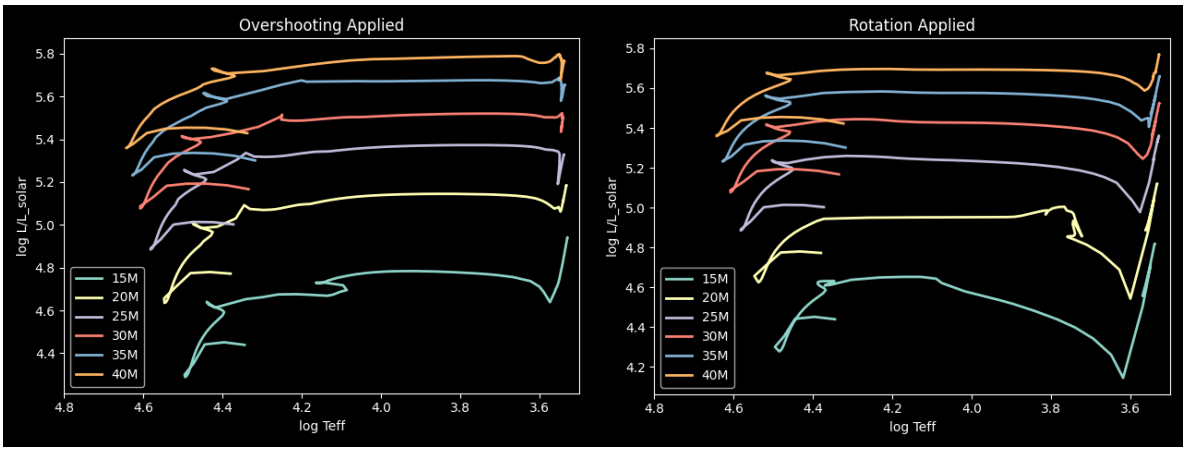

Figure 3. a) Evolutionary tracks for 15-40 solar-mass models with semi-convection and overshooting (left); b) Evolutionary tracks for 15-40 solar masses with semi-convection and rotation (right).

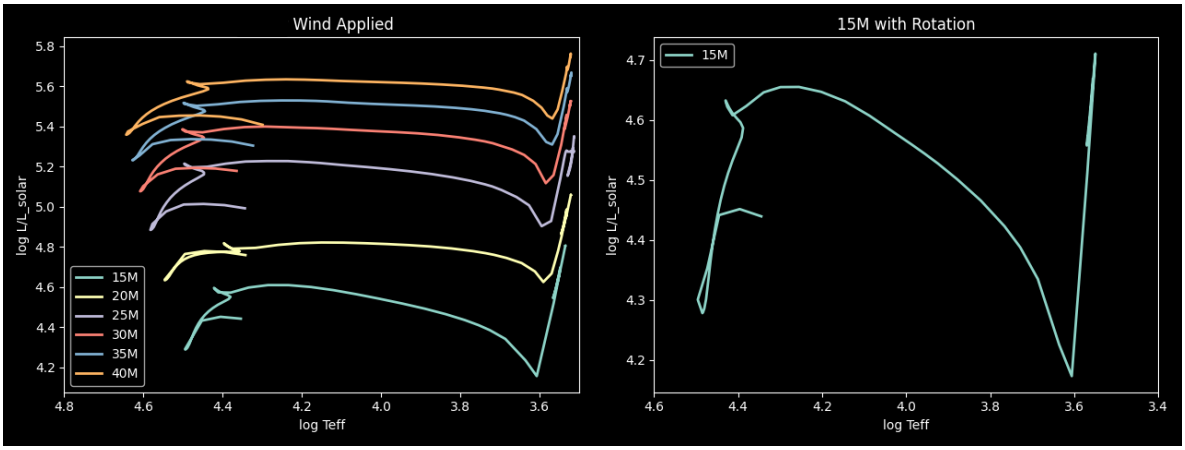

Figure 4. a) Evolutionary tracks for 15-40 solar-mass models with semi-convection and mass loss (left); b) Evolutionary track for a 15 solar-mass model with semi-convection, mass loss and rotation (right).

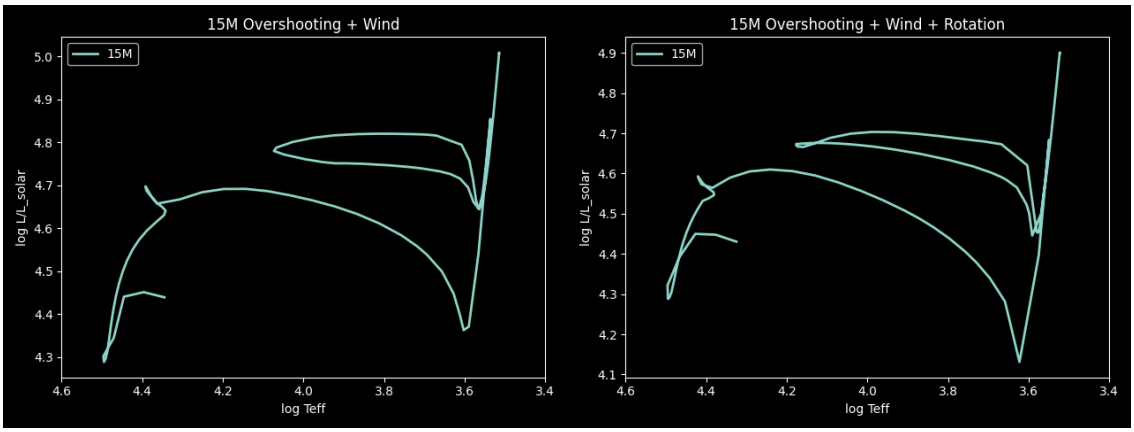

Figure 5. a) Evolutionary track for a 15 solar-mass model with semi-convection, overshooting and mass loss (left); b) Evolutionary track for a 15 solar mass model with semi-convection, overshooting, rotation, and mass loss (right).

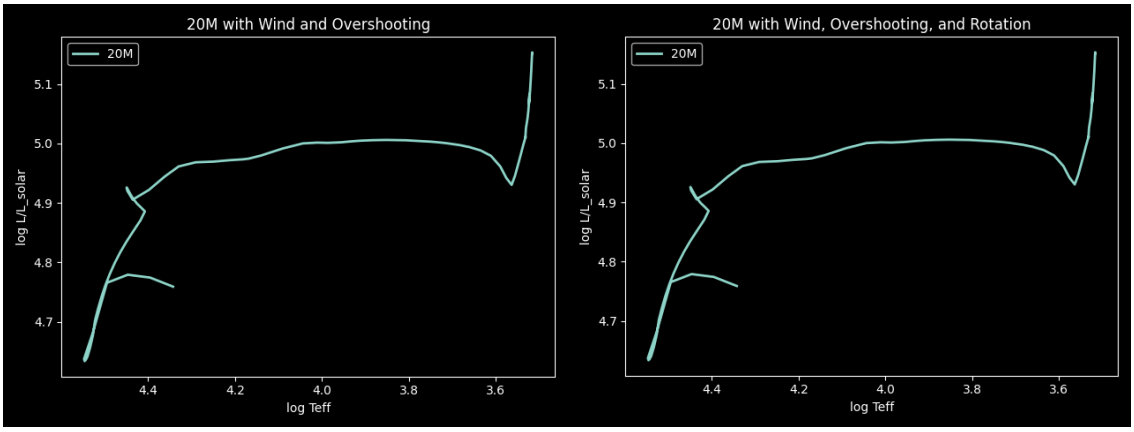

Figure 6. a) Evolutionary track for a 20 solar-mass model with semi-convection, mass loss and overshooting; b) Evolutionary track for a 20 solar-mass model with semi-convection, mass loss, overshooting, and rotation (right).

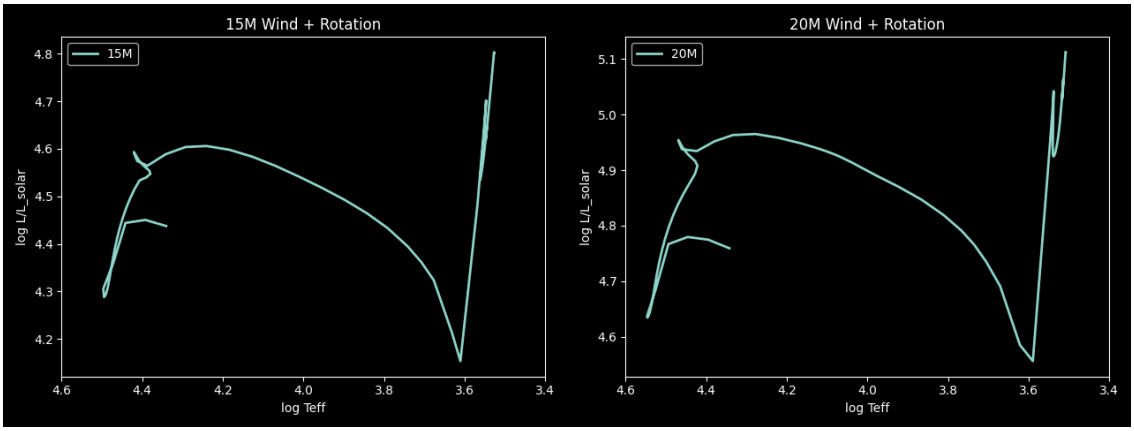

Figure 7. a) Evolutionary track for a 15 solar-mass model with semi-convection, rotation and mass loss (left); b) Evolutionary track for a 20 solar-mass model with semi-convection, rotation and mass loss (right).

Figure 7, calculated using MESA version 24.03.1, shows results for a 15 and 20 solar-mass model with mass loss and rotation, both of which have not completed a blue loop. However, these models do show movement along the red giant branch, losing luminosity before they make a second ascent.

3. Conclusions

Evolution from the red supergiant phase back to the blue supergiant phase is seen in a 15 solar-mass model using overshooting and stellar winds, neglecting rotation, as done in Gautschy (2009), and for a 15 solar-mass model using overshooting, stellar winds, and rotation, as done with some models by Saio et al. (2013a). However, this blue supergiant phase is not repeated in equivalent 20 solar-mass models. For 15 and 20 solar-mass models with mass loss and rotation applied, movement is seen along the red giant branch but there is no resulting blue loop. Analysis of the model's pulsations is ongoing and will hopefully provide insight into the possible causes of variations in Alpha Cygni variables.

Acknowledgements

We acknowledge the developers of the Modules in Stellar Astrophysics code who work relentlessly to create an environment that allows any type of user to become engaged with stellar astrophysics.

References

Aufdenberg, J. P., Hauschildt, P. H., Baron, E., et al. 2002, ApJ, 570, 344, doi: 10.1086/339740

Ekström, S., Georgy, C., Eggenberger, P., et al. 2012, Astronomy and Astrophysics, 537, A146, doi: 10.1051/0004-6361/201117751

Georgy, C., Saio, H., and Meynet, G., 2014, Monthly Notices of the Royal Astronomical Society: Letters, 439, 6–10, https://doi.org/10.1093/mnras/slt16

Gautschy, A. 2009, Astronomy and Astrophysics, 498, 273, doi: 10.1051/0004-6361/200911666

Jermyn, A. S., Bauer, E. B., Schwab, J., et al. 2023, ApJS, 265, 15, doi: 10.3847/1538-4365/acae8d

Paxton, B., Bildsten, L., Dotter, A., et al. 2011, ApJS, 192, 3, doi: 10.1088/0067-0049/192/1/3

Saio, H. 2011, Monthly Notices of the Royal Astronomical Society, 412, 1814-1822, doi: 10.1111/j.1365-2966.2010.18019.x.

Saio, H., Georgy, C., and Meynet, G. 2013a, Monthly Notices of the Royal Astronomical Society, 433, 1246–1257, doi: 10.1093/mnras/stt796

Saio, H., Georgy, C., and Meynet, G. 2013b, Astronomical Society of the Pacific Conference Series, 479, 47, doi: 10.48550/arXiv.1305.4728

Pulsating White Dwarfs: Probing the Instability Strip

Ava H. Moore

Los Alamos National Laboratory, Los Alamos, NM, 87544, US; ahmoore@lanl.gov

Subject Keywords

Techniques: Photometry; Techniques: CCD; stars: variable: V777 Her; stars: individual (V777 Her); stars: individual (DDE 156)

Abstract

Using time series photometry, Figures of pulsating helium white dwarf GD 358 and other white dwarf candidates were processed looking for variability. Variability found in white dwarf candidates was used to help better restrict the boundaries of the DB instability strip. The 0.4-meter reflecting telescope at Brooks Astronomical Observatory was used, and it helped assess whether a facility geared towards teaching was useful for detecting variability and performing asteroseismolgy of pulsating white dwarfs. Pulsations were easily detected in GD358, as well as PHL 970. There was no evidence, above the noise level, for pulsations in the white dwarf candidates GD 93, KUV 07540+4015, KUV 09538+3405, LP 207-7, LP 313-16, FBS 0808+435, CBS 92, and HZ 10.

1. Introduction

White dwarfs are the final evolution stage of roughly 98% of all stars, and thus are structurally influenced by their previous stages of evolution. A white dwarf's atmospheric composition can have two distinct compositions: a DA composition (exhibiting hydrogen absorption lines in its spectrum) or a DB composition (exhibiting only helium absorption lines in its spectrum) (Agnes Bischoff-Kim et al. 2019). Roughly 20% of white dwarfs will have a DB composition, compared to approximately 80% of white dwarfs that have a DA composition. DB white dwarfs are known to pulsate at effective temperatures between 21,000 K and 31,000 K (Beauchamp et al. 1999), while DA white dwarfs pulsate at temperatures between 11,750 K and 13,500 K (Van Grootel et al. 2012), known as the DB instability strip and DA instability strip, respectively.

However, there is uncertainty in the location and width of the instability strip for both the DA and DB white dwarfs. In 1999, Beauchamp et al. attempted to map the location of the DB instability strip by analyzing spectroscopic data of 23 known DB stars. Then, theoretical models of the stellar atmospheres of the DB stars were performed using either a pure helium composition or an atmosphere with hydrogen traces. It was found that the hotter, blue edge of the instability strip was sensitive to convection treatment of the atmosphere, and to the total stellar mass of the helium envelope.

Depending on the assumption for atmospheric composition, stars that defined the instability strip theoretically did not match those that defined the instability strip based on observations. The helium models predicted the edge to be at 27,800 K which is 3700 K cooler than the star PG 0112 +104, a non-variable white dwarf that defines the coolest edge of the DB stage at 31,500 K. When including traces of hydrogen in the atmosphere, the temperature of the blue edge dropped considerably from that of pure helium models to 24,700 K. These models put the hottest variable DB star as GD 358, which was determined to spectroscopically have a temperature of 27,000 ± 1000 K.

More analysis was done on the instability strip in 2011 by Bergeron et al. using models that were built from synthetic spectra which allowed free-free absorption at low temperatures of negative helium ions and considering spectroscopic observations at Hα that constrained hydrogen abundances. Calculations were done using atmospheres with traces of hydrogen between H/He of 3.162e-7 and 0.01, as well as calculations of pure helium atmospheres. The models showed that there was a distinction to be made between DB white dwarfs and DBA white dwarfs, with DBA stars indicating the presence of hydrogen lines. For pure helium envelopes, a blue edge was predicted close to the observed edge at around 30,000 K depending on the convective efficiency used while a red edge was predicted near 25,000 K. The boundaries of the DBA stars were unclearly defined due to a lack of observations of non-variable DBA stars.

Thus, to resolve the purity of the instability strip of DB pulsators, it is vital to obtain observations of as many white dwarfs as possible, with correct effective temperature measurements. Although white dwarfs are faint, they can still be observed using ground-based telescopes. Since large observatories are often over-subscribed, it is useful for independent and smaller observatories to participate in these observations. This allows further progress towards a pure instability strip.

2. Methods

The Brooks Astronomical Observatory is a small, teaching observatory located on Central Michigan University's campus in the middle of downtown Mount Pleasant, MI, and as such is highly susceptible to light pollution. It houses a 16-inch Cassegrain reflector with a 13.3 µm, 13-pixel square CCD for basic visual observations.

One target studied using the Brooks Astronomical Observatory is GD358. It is one of the brightest and best-studied helium atmosphere white dwarf stars, with 15 observed independent radial overtones. It works well as a test subject due to its extensive study and accurate temperature and surface gravity measurements, which place it near the red edge of the instability strip.

A series of observations on GD358 were performed on 35 nights over the course of ninety days, giving roughly 200 hours of usable data. Observations of additional known variable white dwarfs were taken, as well as some candidate white dwarf targets which were chosen to see if they could be classified as variable white dwarf stars.

Source selection was a vital aspect of determining whether a target was truly varying. Observations of white dwarfs can be influenced by many factors, such as instrument sensitivity, site location, weather, and climate. It was important to observe a known variable first, GD358, to determine if its frequency spectrum was reproducible by the equipment available. Having previous studies to reference for variable targets was important, as it helped determine whether our analysis was accurate or not.

Once this was confirmed, there were several considerations for white dwarf candidates. Since multiple telescope sites were used, targets were limited by RA and DEC of the site locations. For the on-campus telescope, the guide system limited targets to above 25 degrees DEC. The RA varied for all locations based on the month of observations.

It was also important to consider targets that lie strictly outside of the instability strip. To argue for redefining the strip's edges, targets needed to be observed fluctuating in magnitude outside of the range of known variability.

Observations of all target stars in the V band lasted between 1 and 4 hours, depending on the weather conditions. To minimize aliasing in the target's light curve, observing sessions were conducted at least three days per week with exposure lengths lasting 90 seconds or more to combat poor visibility. Observations on remote telescopes (located in Chile, Poland, and North Carolina) had shorter exposure lengths, roughly 60 seconds or less.

Figures were reduced using AstroFigureJ to remove spatial variations and artifacts, and differential photometry was conducted to find the target magnitude. The target's light curve was compiled using the time-dependent magnitude measurements, and a Fourier transform was performed on the data points to produce a frequency spectrum.

3. Results

3.1 GD358

Over three decades of analysis of GD358's pulsation spectrum has identified 15 radial overtones (k) with periods between 400 and 1100 seconds, all for angular degree $\ell = 1$. GD358's nonlinear multiperiodic light curve has been found to show varying amplitude in individual modes over time. When translating the light curve to a Fourier transform, the frequencies identified have been shown to not be observed in all seasons and are not identical between years in terms of width and amplitude (Bischoff-Kim et al. 2019).

Data was collected over 90 days across three months: September, October, and December, getting 35 nights of data in total or roughly 200 hours. As such, we decided to decompose the data into different collections of nights. The full frequency spectrum for all days of observation is shown below.

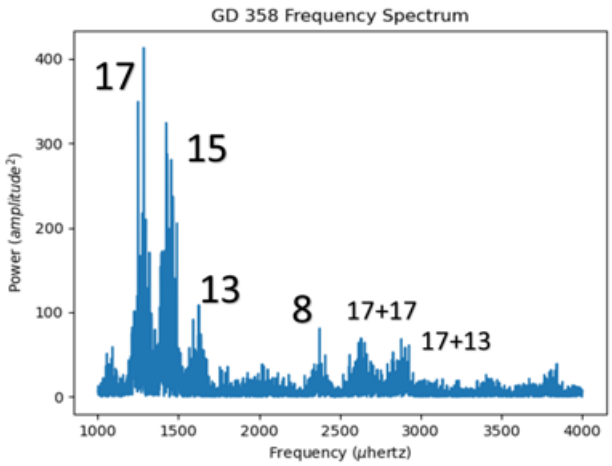

Figure 1. A Fourier transform of GD358's light curve over the 3-month observation period.

In the frequency spectrum, there are four identifiable frequencies of k = 8, 13, 15, and 17, corresponding to periods of 423.13 s, 617.40 s, 699.82 s, and 769.74 s respectively (Bischoff-Kim et al. 2019). There are also two combination periods of k = 17+17 and k = 17 + 13.

The decomposed spectra by grouping of observation week are shown below.

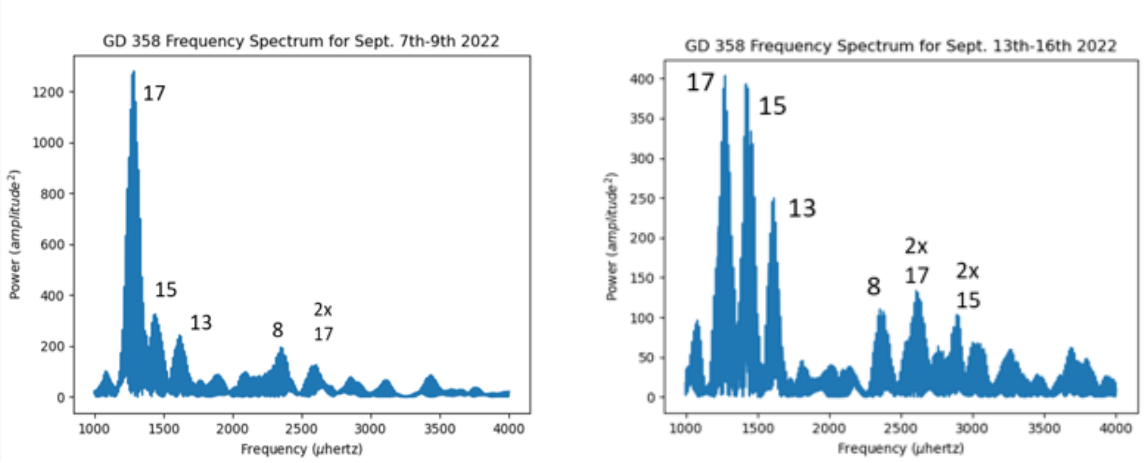

Figure 2. a) A Fourier transform of GD358's light curve over the week of September 7th-9th (left); b) A Fourier transform of GD358's light curve over the week of September 13th-16th (right).

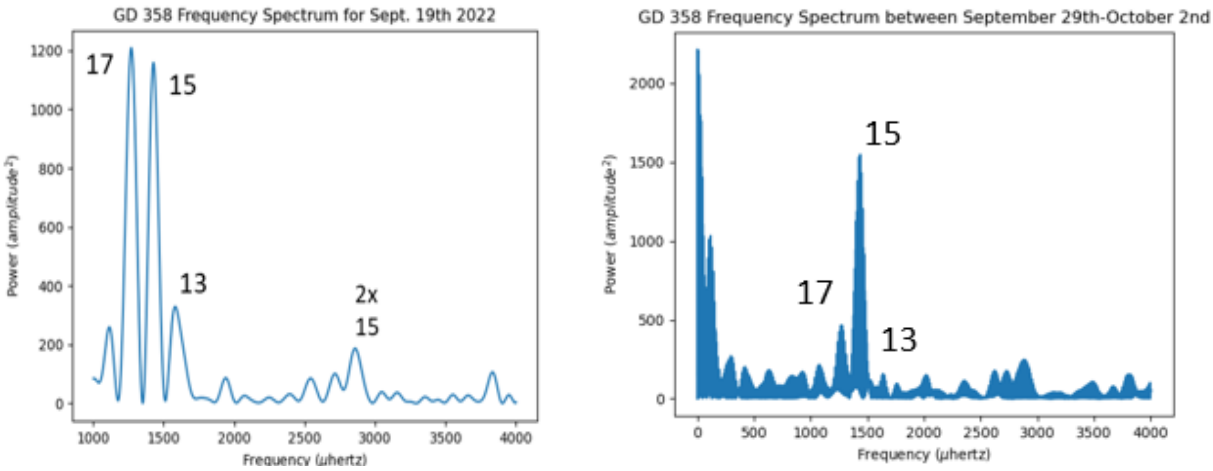

Figure 3. a) A Fourier transform of GD358's light curve for September 19th (left); b) A Fourier transform of GD358's light curve for the week of September 29th-October 2nd (right).

As the frequencies evolve, we can see that between the first set of observations and the second set of observations, the power scale (measured in squared milli-modulation amplitude) has decreased by nearly a third. As this is occurring, the k = 17 mode is becoming less prominent in the following weeks. It decreases in power to roughly 400 mma^2. Its power jumps back up to just over 1200 mma^2 during the third week before then decreasing again on the last week of observations to below 500 mma^2.

By the third week, the k = 8 mode has disappeared completely from the spectrum. It does not reappear in later observations. This is possibly because, as found by Bischoff-Kim et al. (2019), there is no detected amplitude for k = 18 above 15 mma^2. This would give a peak power of 225 mma^2. With the both the k = 17 and k = 15 overtones having peaks near 1200 mma^2, it would be difficult to confidently observe any peak for k = 8.

We eventually see the k = 15 mode dominant over the k = 17 mode on the last week of observations, for the week of September 29th into October. At this point, all linear combinations of modes have disappeared as well and only periods of 600 seconds or higher are observable. It's possible that the short observing runs prevented observations of higher frequencies and other radial overtones.

As the telescope is in an area with a humid climate and drastic temperature changes, transparency and seeing are greatly affected late in the calendar year. With these conditions, it is necessary to take in as much light in as possible, increasing the exposure time. Since the frequencies modulation on periods of seconds, it is possible that certain periods are being missed due to long exposure length.

3.2 PHL 970

PHL 970 is a DOZ white dwarf first identified in 2000 by the Montreal-Cambridge-Tololo Survey of Southern Subluminous Blue Stars (Lamontagne et al. 2000), with a magnitude of roughly 15.8.

In 2021, Reindl et al. (2021) showed variability in available TESS, CSS, and ATLAS data of PHL 970, giving a period of about 2.32 days.

There is not much known about PHL 970's variability or what causes it. However, it is theorized that the variability is due to rotation since periodograms of its variability show equal period humps, common for rotating stars (Reindl et al. 2021). Ultra-high excitation lines of C IV, detected in Reindl et al. (2021), suggest external factors could contribute to the features of the star such as stellar winds, or, as suggested by Bergeron et al. (2021), a magnetosphere around the star. However, Heinze et al. (2018) first characterized the star as variable in 2018, categorizing it as a sinusoidal variable for its simple sine-like light curve.

The light curves captured by our team are shown below.

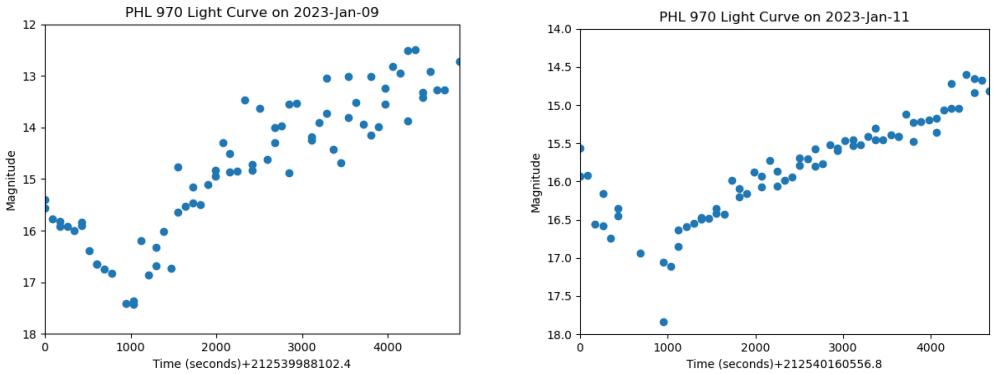

Figure 4. a) PHL 970's light curve on January 9th, 2023 (left); b) PHL970's light curve on January 11th, 2024 (right).

PHL 970 was observed using remote capabilities at Cerro Tololo Inter-American Observatory. From these observations, a Fourier Transform was produced to see if there were any identifiable frequencies.

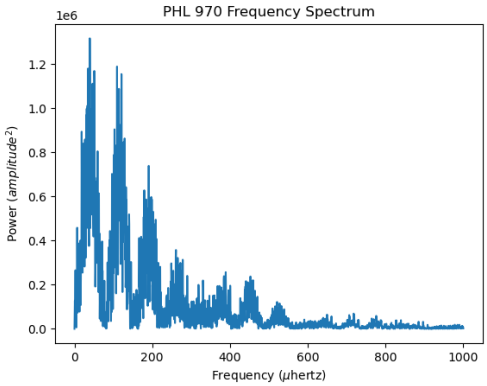

Figure 5. A frequency spectrum for PHL 970. Frequency is shown in microhertz while power is shown in mma².

As seen in Figure 5, there is a large prominent frequency approximately 50 µHz, which would correspond to roughly 0.231 days or a tenth of PHL 970's known period. This is likely a linear combination or overtone of the longer period but could also be an artifact of sampling. Since the star was only observed on 3 separate nights due to scheduling issues with the telescope, it would not be possible to see the full period without further observation.

The overall Fourier series of PHL 970 is rather simple, with steady variation between 10 and 600 µhz. Periodograms in Reindl et al. (2021), Figure 3, show a similar steady variation with one large peak around 2 days followed by steadily decreasing peaks on either side. Though the frequency spectrum does not give much further insight into PHL 970's variability, it does show us that its variation is still detectable in shorter periods. It also shows us that detection of its potential frequencies is possible despite its faint magnitude.

Further inspection into the frequencies and their amplitude is needed to say anything more, as well as a false alarm test to ensure the frequencies detected aren't due to noise.

3.3 Variable Candidate Targets

To obtain potential targets for observation, a SIMBAD search was conducted using a few limiting parameters: location of the telescope proposed for us and spectral type (mainly classification as a White Dwarf or a White Dwarf Candidate; SIMBAD does not separate white dwarfs by their spectral classifications).

Roughly 500 potential targets were obtained and were then plotted into a rough H-R diagram using surface gravity measurements and plotted against a rough surface temperature estimate based on the star's B-V magnitude. Any targets with grade C or lower surface gravity or surface temperature measurements were discarded. Using Beauchamp et al. (1999), the best fit for the blue edge of the instability strip was drawn on the diagram, which designated a model with a mixing length about half the pressure scale height in the convective zone, or ML2, and included traces of hydrogen. The best fit for the theoretical red edge of the instability strip from Thejll et al. (1991) (using the ML2 and pure helium model), was also included in the diagram.

Stars on either side of the blue edge of the instability strip were chosen for observation within a certain fraction of the magnitude defined by the edges. The final candidates were GD 98, KUV 07540+4015, KUV 09538+3405, LP 207-7, LP 313-16, FBS 0808+435, CBS 92, and HZ 10. Candidates with a V magnitude higher than 14.8 were observed using the remote telescope due to issues resolving magnitudes fainter than 15 with the on-site telescope. The resulting light curves and Fourier transforms are below.

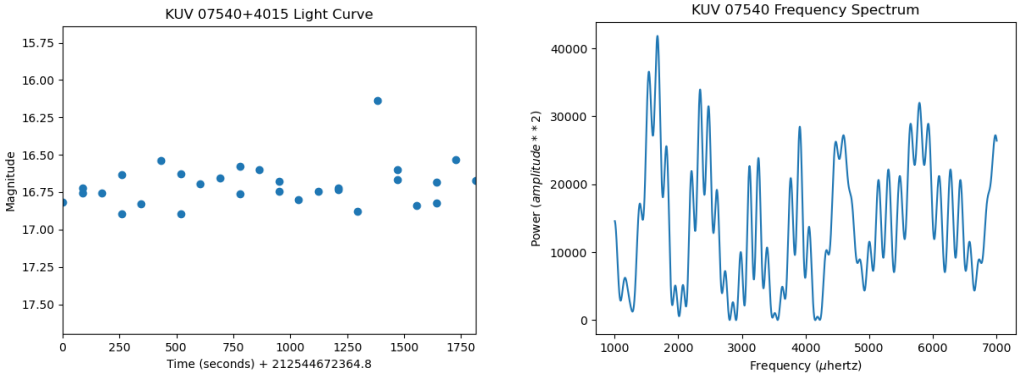

Figure 6. Light curve of magnitude vs. Julian date for KUV 07540+4015 (left) and the resulting Fourier transform (right).

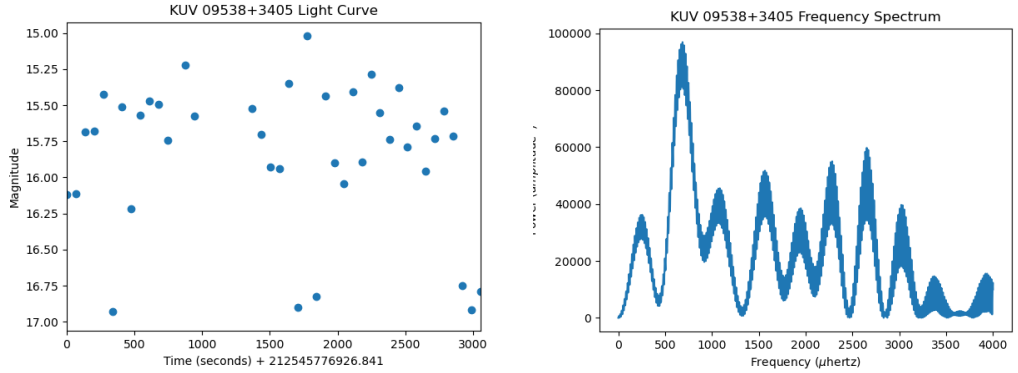

Figure 7. Light curve of magnitude vs. Julian date for KUV 09538+340 (left) and the resulting Fourier transform (right).

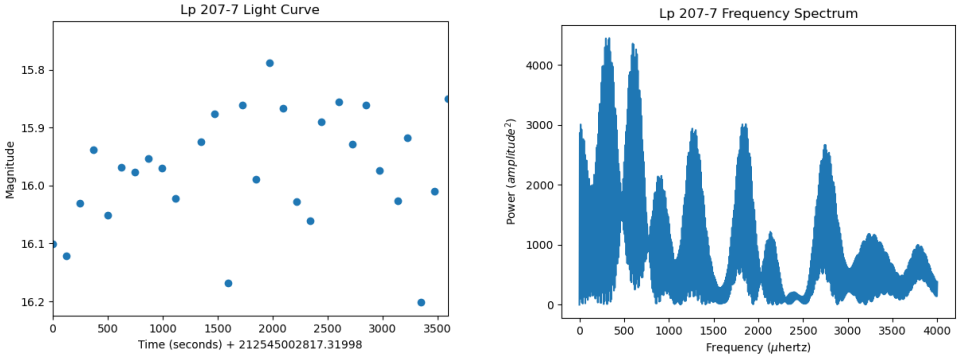

Figure 8. Light curve of magnitude vs. Julian date for LP 207-7 (left) and the resulting Fourier transform (right).

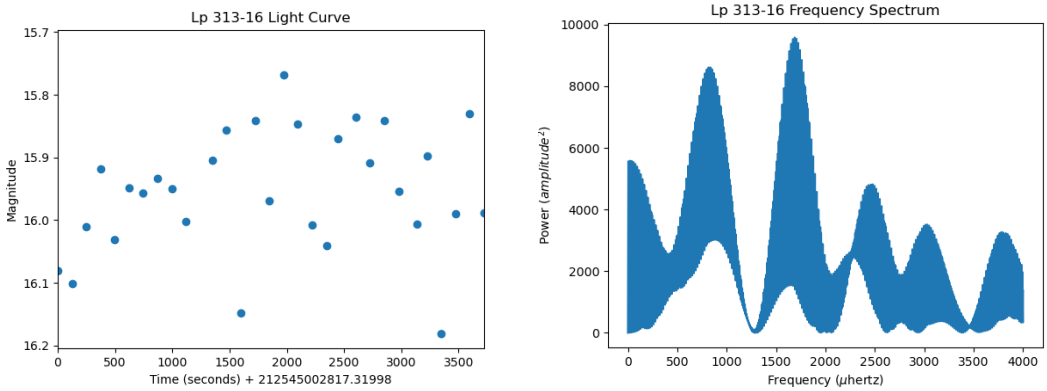

Figure 9. Light curve of magnitude vs. Julian date for LP 313-16 (left) and the resulting Fourier transform (right).

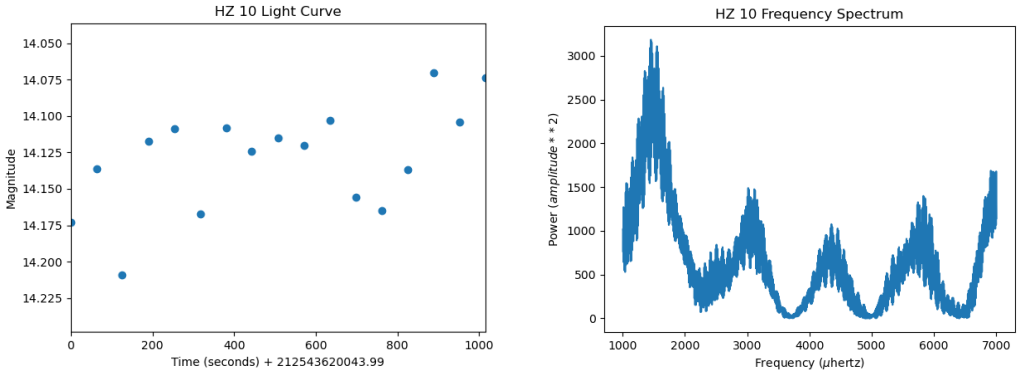

Figure 10. Light curve of magnitude vs. Julian date for HZ10 (left) and the resulting Fourier transform (right).

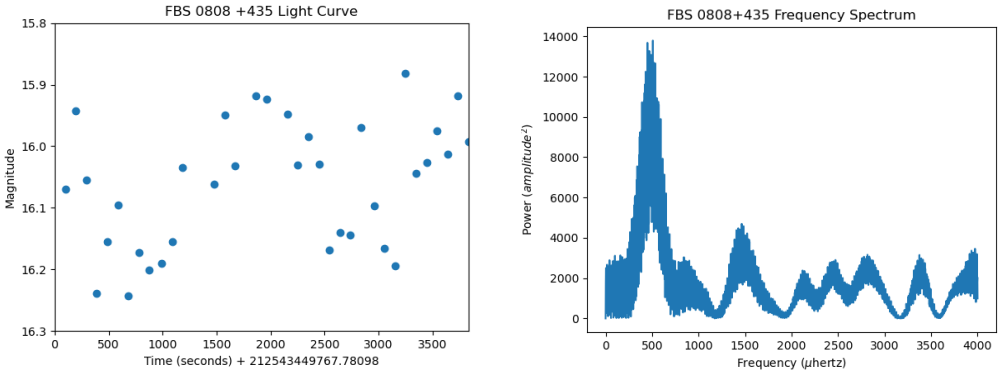

Figure 11. Light curve of magnitude vs. Julian date for FBS 0808+435 (left) and the resulting Fourier calculation (right).

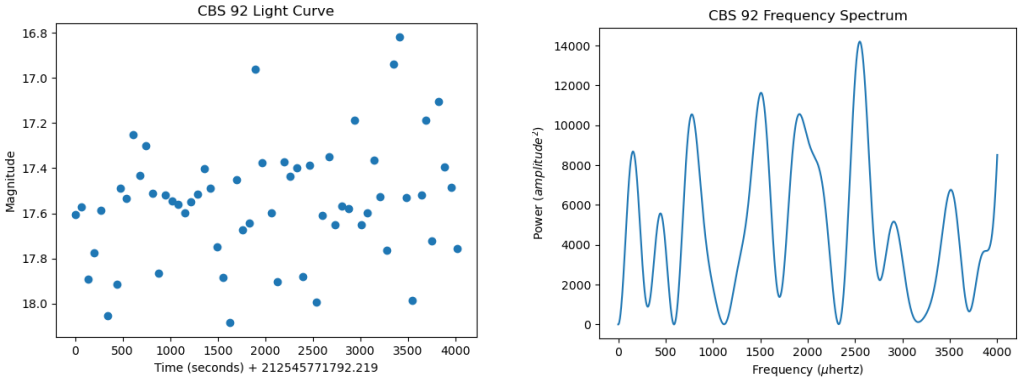

Figure 12. Light curve of magnitude vs. Julian date for CBS 92 (left) and the resulting Fourier calculation (right).

None of the variable candidate targets show obvious evidence of variability above the noise level. There are a few potential candidates, such as FBS 0808+435 and KUV 09538+340, that would benefit from further inspection and false alarm testing.

Though the stars were screened ahead of time, it would be interesting to clarify whether these stars exhibit signs of being white dwarfs by obtaining spectra of their stellar atmospheres. If there were non-white dwarfs in the candidate pool, it would be easier to reduce the potential targets and select better candidates for observation.

4. Conclusions

Asteroseismology is an observational method that allows us to determine a star's composition, as well as many other properties of the star, but its ability to help produce accurate periods of variable stars means it can also serve as a method of constricting the instability strip.

As shown in this paper, modest telescopes, such as the one at the Brooks Astronomical Observatory, can provide reliable data and detect frequencies found in known variable stars even with marginal observing conditions. These telescopes are also capable of producing results that distinguish between variable and non-variable targets. Given the ability to continue with further study, it is recommended that a comprehensive campaign be developed to identify additional targets as well as to produce uninterrupted observations of other targets that show potential variability.

Acknowledgements

This work was done in collaboration with Dr. Aaron LaCluyze at Central Michigan University and Paul Bradley at Los Alamos National Laboratory.

References

Beauchamp, A., Wesemael, F., Bergeron, P., et al. 1999, The Astrophysical Journal, 516, 887–891,

doi: 10.1086/307148
Bergeron, P., Wesemael, F., Dufour, P., et al. 2011, ApJ, 737, 28, doi: 10.1088/0004-637X/737/1/28
Bergeron, P., Wesemael, F., Fontaine, G., et al. 2021, The Astronomical Journal, 162, 188, doi: 10.3847/1538-3881/ac22b1
Bischoff-Kim, A., Provencal, J., Bradley, P., et al. 2019, The Astrophysical Journal, 871, 13, doi: 10.3847/1538-4357/aae2b1
Central Michigan University. 2024, Brooks Astronomical Observatory, https://www.cmich.edu/academics/colleges/college-science-engineering/centers/brooks-astronomical-observatory
Fontaine, G., & Wesemael, F. 2001, White Dwarf, 1st edn., ed. P. Murdin (CRC Press INC)
Gavras, P., Rimoldini, L., Nienartowicz, K., et al. 2023, Astronomy & Astrophysics, 674, doi: 10.1051/0004-6361/202244367
Heinze, A. N., Tonry, J. L., Denneau, L., et al. 2018, The Astronomical Journal, 156, 241, doi: 10.3847/1538-3881/aae47f
Kepler, S. O., Nather, R. E., Winget, D. E., et al. 2003, Astronomy & Astrophysics, 401, 639–654, doi: 10.1051/0004-6361:20030105
Lamontagne, R., Demers, S., Wesemael, F., Fontaine, G., & Irwin, M. J. 2000, The Astronomical Journal, 119, 241–260, doi: 10.1086/301181
Reindl, N., Schaffenroth, V., & et. al, S. F. 2021, Astronomy & Astrophysics, 647
Thejll, P., Vennes, S., & Shipman, H. L. 1991, The Astrophysical Journal, 370, 355, doi: 10.1086/169822
Van Grootel, V., Dupret, M.-A., Fontaine, G., et al. 2012, Astronomy & Astrophysics, 539, doi: 10.1051/0004-6361/201118371
Winget, D. E., Robinson, E. L., Nather, R. D., & Fontaine, G. 1982, The Astrophysical Journal, 262, doi: 10.1086/183902

Analysis of RR Lyrae Stars in the Globular Cluster NGC 3201

Nicholas Peh, Maiya Qiu, Eden Li, and Kalée Tock

Stanford Online High School, Redwood City, CA 94063;
nicholaspeh27@yahoo.com; kaleeg@stanford.edu

Abstract

We selected the RR Lyrae stars V6, V26, V51, and V66 in the globular cluster NGC 3201 for analysis in B, V, SR, and SI filters. These four stars are Blazhko candidates due to their modulating period or amplitude. We found possible Blazhko candidacy for V66 by comparing past literature and archival data with our images, finding the best period changing from 0.6675 days in 2021 to 0.6667 days in 2024. V6, V26, and V51 do not appear to have clearly modulating periods between studies from 2021 and 2024; however, for these stars, we present an update to the Clement's Catalog periods which were taken from older observations. Light curves were fitted using point spread function photometry, which was found to produce significantly cleaner light curves compared to those created by source extractor photometry. We also present the amplitudes of the target stars and situate them in their stellar environments using a Color Magnitude Diagram (CMD) and Bailey diagram of the NGC 3201 cluster. Isochrone fits used the software Astromancer, whose metallicity output was converted from [M/H] to [Fe/H] for comparison with past literature. The resulting metallicity was lower than expected although the uncertainty range here does not necessitate a recategorization from the Oosterhoff dichotomy Type I to Type II.

A paper on this work was published in 2024 in the Journal of the Association of the American Association of Variable Star Observers, https://apps.aavso.org/jaavso/article/3941/

Long Secondary Periods in Red Giants: AAVSO Observations and the Eclipse Hypothesis

John R. Percy and Melanie Szpigiel

Department of Astronomy & Astrophysics, and Dunlap Institute for Astronomy and Astrophysics, University of Toronto, 50 St. George Street, Toronto ON M5S 3H4; john.percy@utoronto.ca

Subject Keywords

AAVSO International Database; Photometry, CCD; Photometry, visual; Long-period variables; Semi-regular variables; Period analysis; Amplitude analysis; Stars: individual (SS Cep, AF Cyg, U Del, EU Del, TX Dra, UW Her, OP Her, Y Lyn, W Ori, W Tri, ST UMa)

Abstract

At least a third of red giants show a long secondary period (LSP), 5 to 10 times longer than the pulsation period. There is strong evidence that the LSP is caused by eclipses of the red giant by a dust-enshrouded low-mass companion. We have used long-term AAVSO observations of 11 stars to study two aspects of the eclipse hypothesis: the relation between the LSP phase (eclipse) curve and the geometry of the eclipse, and the long-term (decades) changes in the LSP phenomenon in each star. The stars with the largest LSP amplitudes show evidence of a dust tail on the companion, but most of the 11 stars show only a small-amplitude sinusoidal phase curve. The LSP amplitudes of all the stars vary slowly by up to a factor of 8, suggesting that the amount of obscuring dust varies by that amount, but there is no strong evidence that the geometry of the system changes over many decades.

1. Introduction

Red giant stars are unstable to low-order pulsation modes, generally the fundamental and/or first overtone mode. About a third of such stars also have a "long secondary period" (LSP), 5 to 10 times the pulsation period, depending on whether the pulsation is in the fundamental or first overtone mode. The cause of these LSPs was unknown for almost a century. Recently, Soszynski et al. (2021) have presented strong evidence that they are due to eclipses of the red giant by dust-enshrouded companions which were originally planets, but which subsequently accreted gas and dust from the star and became brown dwarf or low-mass stars. Figure 1 shows an artist's conception of an LSP system.

A simple model of the system would then include the red giant (probably pulsating), the low-mass companion with a halo of dust and gas, perhaps trailing a dust tail which merges with a uniform (or not) ring of gas and dust around the red giant. But, as Figure 1 suggests, the situation can be more complicated. The outer layers of the red giant are not uniform and symmetric, but consist of large, random convection cells. The pulsation amplitude of the red giant varies by up

to a factor of ten, so the gas and dust flows are patchy. The system may be seen at any angle, not necessarily edge-on; this would affect the interpretation.

Figure 1. Artist's conception of the LSP process. Source: Matylda Soszynska

Despite the success of the Soszynski et al. mechanism for explaining the LSP phenomenon, there are still some puzzling aspects, and those have been the topic of some previous papers by our group. The present paper deals with two aspects of the LSP process: (1) the relationship between the LSP (eclipse) phase curve and the geometry of the eclipse process, and (2) changes (if any) in the LSP process in the star over a period of decades. We can study such changes because of the existence of the American Association of Variable Star Observers (AAVSO) International Database (AID) of visual and photoelectric photometry, which extends back in time for many decades. We have previously used some of this data in several studies of LSPs in red giants (e.g. Percy and Diebert (2016)), but we realized that there was even more information which could be derived.

1.1 Eclipse phase curve and the eclipse geometry

Let us consider how the LSP system, as seen in Figure 1, produces the observed light and phase curves. If the LSP system is seen flat-on, there will be no eclipses. If the system is seen at an angle – 45 degrees, for instance – the dusty companion may eclipse the top or bottom of the face of the red giant, producing a relatively short "partial" eclipse with a flat maximum. If the system is seen edge-on, there are several possibilites. If the companion is small and opaque, the minima and maxima will both be flat. The depth of the eclipse will depend on the ratio of the areas of the two objects. The length of the eclipse will depend on the relative sizes of the red giant and its companion. If the companion and its halo are large and relatively transparent, the eclipse will be slow and symmetric; the egress will be a reflection of the ingress. If the companion has a dust tail behind it, the ingress will be relatively shorter and the egress with be longer because of absorption by the tail, as seen in Figure 2. Figure 1 shows a tail which is extended into a disc or torus, which may completely encircle the red giant. In that case, the disc of the red giant may never be completely unobscured.

Figure 1 in Soszynski et al. (2021) and the Introduction to that paper are instructive. The figure shows eclipse (LSP) phase curves for a selection of stars in the Galactic bulge and LMC. The smallest-amplitude stars have short, rounded eclipses and flat maxima. The largest-amplitude stars have a more rapid ingress, a slower egress, and pointed minima. Soszynski and Udalski (2014) had demonstrated that such a phase curve could be produced by a dusty cloud with a comet-like tail. One caveat: the stars in this figure are chosen to have small pulsation amplitudes,

to highlight the LSP variations; this may introduce some bias in the shape of the eclipse curves shown, such as preferentially including lower-luminosity stars.

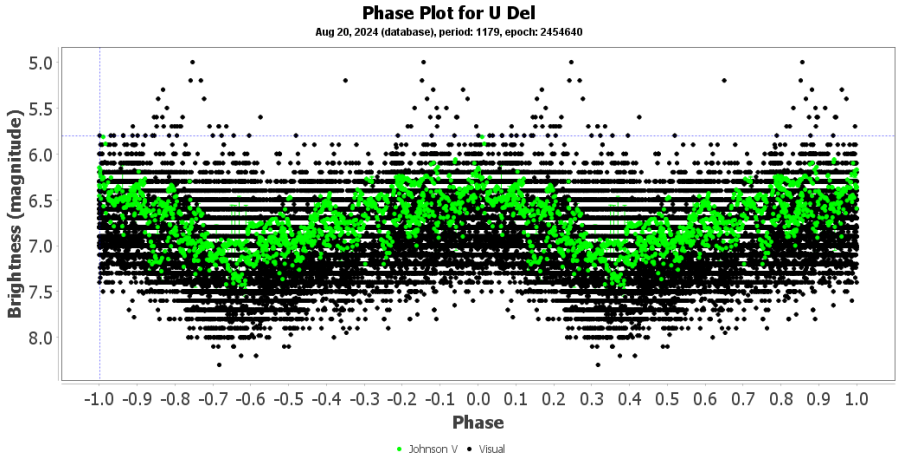

Figure 2. The phase (eclipse) curve for U Del. The black points are visual, the green points are Johnson V. The LSP is 1178 days. Source: AAVSO.

1.2 Long-term changes in the LSP phenomenon

Visual data in the AID goes back almost a century for some red giants; photoelectric Johnson V photometry extends about half as far back. To study long-term changes in the LSP process, we require stars for which the data are dense and sustained. We drew most of the stars from a recent compilation by Percy and Zhitkova (2023), which analyzed data from the AAVSO Binocular Observing Program. One problem is that the pulsational variations act as "noise" in studying the LSP variations, adding to the usual observational error noise. Table 1 lists the 11 stars that we considered suitable for our study. The last column lists the ratio of the LSP amplitude LSPA to the pulsation amplitude PA. This is a measure of the "signal-to-noise" for studying the LSP variation.

Why does all this matter? Because red giants are common; the AAVSO monitors hundreds of them. The sun will become a red giant; will it exhibit the LSP process? There is much interesting physics in the processes by which the red giant produces dust, and its dust-enshrouded companion. And LSPs are a stellar mystery which AAVSO data have helped to solve.

2. Data and Analysis

Visual and Johnson V observations of the 11 stars in Table 1 were downloaded from the AID, and analyzed using careful light-curve analysis, and time-series analysis with the AAVSO VSTAR software package (Benn 2013). The LSPs and pulsation periods, and their amplitudes were taken from Percy and Zhitkova (2023) and checked, if necessary, with the Fourier routine in VSTAR. Note that the amplitudes given by VSTAR, and quoted in this paper, are actually semi-amplitudes, not max-to-min ranges.

Table 1. Red giants with LSPs and sustained observations in the AID. The table gives the starname, LSP period and mean, maximum, and minimum amplitude, pulsation period and amplitude, ratio of LSP to P, and ratio of LSP amplitude to pulsation amplitude.

Star	LSP(d)	LSPA	LSPAmax	LSPAmin	PP(d)	PA	LSP/P	LSPA/PA
SS Cep	947	0.11	0.21	0.07	170	0.17	5.57	0.65
AF Cyg	913	0.08	0.17	0.02	93	0.18	9.82	0.44
U Del	1179	0.21	0.26	0.14	120	0.08	9.83	2.63
EU Del	630	0.05	0.10	0.03	63	0.10	10.00	0.50
TX Dra	700	0.14	0.19	0.10	76	0.12	9.21	1.17
UW Her	986	0.07	0.11	0.06	182	0.17	5.42	0.41
OP Her	699	0.10	0.14	0.03	74	0.06	9.45	1.67
Y Lyn	1245	0.35	0.44	0.15	135	0.09	9.22	3.89
W Ori	2358	0.20	0.23	0.18	432	0.13	5.46	1.60
W Tri	768	0.07	0.10	0.06	109	0.04	7.05	1.75
ST UMa	615	0.06	0.14	0.04	90	0.13	6.83	0.46

The visual observations were analyzed preferentially, since they were more numerous and extend back the furthest. Note that the visual and V passbands are slightly different, so the V observations are offset from the visual ones, as you can see in the light and phase curves. Eclipse phase diagrams were constructed with VSTAR (e.g. Figure 2). For some of the stars, the shape of the LSP phase curve was apparent from visual inspection. In addition, the phase curves could be fitted with low-order (typically 4) polynomials, using the polynomial function in VSTAR. The shape of the phase curve could be then described, very simply, by the phase difference between maximum and minimum – or the fraction of the LSP cycle in which the star is decreasing in brightness. If the phase curve was symmetrical, this parameter would be 0.50. If the ingress was faster that the egress, it would be less than 0.50. The depth of the eclipse could be measured from the difference between maximum and minimum of the fitted polynomial. For stars with dense, sustained data, changes in these parameters with time could be determined by dividing the data into time segments and analyzing each segment separately. Changes in the depth of the eclipse could also be determined using the wavelet routine within VSTAR. A helpful strategy for detecting cycle-to-cycle changes in some of the LSP light curves was to average the measurements in bins equal to the pulsation period. It cuts down, partially, on the pulsation "noise".

3. Results

The 11 stars in our sample are listed in Table 1, along with some results. Notes on individual stars follow:

- SS Cep: LSPA is only 0.11; PA is 0.17. The former varies by a factor of three. Early in the dataset, the phase curve seems to show a slower decline to minimum and a faster return to maximum; later in the dataset, the phase curve is more sinusoidal.

- AF Cyg: LSPA is less than half PA, so there is significant pulsation "noise" in the LSP analysis. The LSPA variation – 0.02 to 0.17 – is proportionally the largest in our sample. The phase curve is small-amplitude, sinusoidal, and essentially constant over the period of the dataset.
- U Del: LSPA is relatively large, and PA is relatively small, so the LSP is easier to analyze and interpret; it is one of our two best cases, along with Y Lyn. The phase curve (Figure 2) has a distinctive shape, with a more rapid decline to minimum and a slower return to maximum; this would be consistent with a tail following the companion as it eclipses the red giant. Also, the star spends about half the LSP at or near maximum, which suggests that the star may be relatively unobscured in this interval. Early in the dataset, the phase curve was slightly more sinusoidal; this may be because the LSP amplitude was lower at that time (Figure 3).
- EU Del: LSPA is small; PA is twice as large. This star has extensive photoelectric coverage, and is aprototype for SARVs: small-amplitude red variables. It is much easier to analyze the pulsation than the LSP. LSPA varies by a factor of three. The polynomial fit suggests that the star has a slow decline to minimum and a more rapid rise to maximum, but the effect is very small and is affected by the strong pulsational noise.
- TX Dra: LSPA and LSPA/PA are moderate. LSPA varies by a factor of two. The shape of the phase curve remains uniformly sinusoidal over the period of the dataset.
- UW Her: LSPA is moderate, but PA is relatively large (0.17) so the pulsation "noise" level is high. LSPA varies from 0.06 to 0.11, but the phase curve remains uniformly sinusoidal over the period of the dataset.
- OP Her: LSPA and LSPA/PA are moderate. There is a large range in LSPA – from 0.03 to 0.14 – but the phase curve is uniformly sinusoidal over the course of the data.
- Y Lyn: LSPA is large, and much larger than PA so, not surprisingly, this was the easiest star to analyze and interpret. This star's phase curve (Figure 4) has the same distinctive properties of that of U Del (see above) and can be interpreted in the same way -- in terms of a trailing dust tail.
- W Ori: LSPA is small, but PA is smaller. Because of the longer length of LSP and P, it is easy to see the effect of the pulsation "noise" in the phase curve.
- W Tri: LSPA is small, but PA is smaller. LSPA varies from 0.06 to 0.10; the phase curve remains sinusoidal over the course of the data (Figure 5), typical of many of the stars in our sample.
- ST UMa: LSPA and LSPA/PA are both small, so the data are difficult to analyze and interpret. LSPA varies from 0.04 to 0.14; the phase curve remains sinusoidal over the period of the dataset.

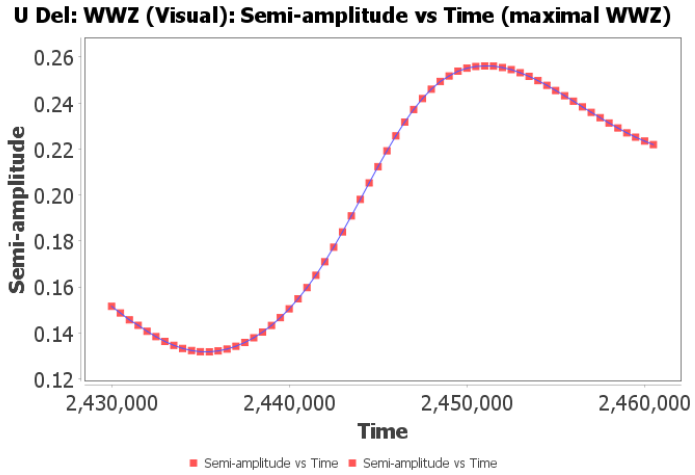

Figure 3. The semi-amplitude of the U Del LSP – which is a measure of the depth of the eclipse – versus time. Source: AAVSO.

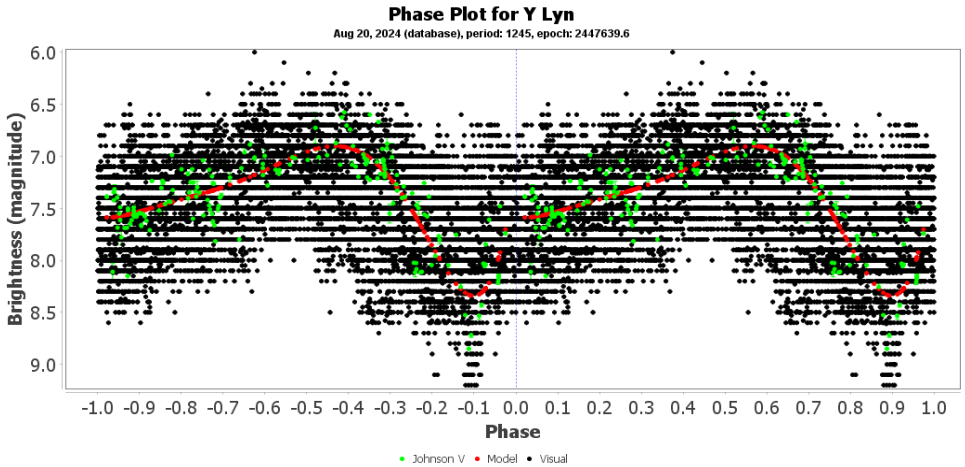

Figure 4. The phase (eclipse) curve for the LSP in Y Lyn. The black points are visual, the green points are Johnson V, and the red curve is a fitted fourth-degree polynomial. The LSP is 1245 days. Source: AAVSO.

4. Discussion and Conclusions

Mass loss in Mira stars is usually associated with their pulsation. It is somewhat puzzling that, in stars with small pulsation amplitudes -- U Del and Y Lyn for example – the star can drive off sufficient dust and gas to increase the companion mass, and produce its envelope of dust, and its tail.

The pulsational "noise", on top of the observational noise make the analysis in this project difficult. For many of the stars in Table 1, the signal-to-noise for the LSP analysis is less than one. It might be worthwhile to repeat this analysis using only V data on stars with dense photoelectric/CCD coverage, even though that data extends back by only 3-4 decades.

It is somewhat puzzling that, in stars with small pulsation amplitudes -- U Del and Y Lyn for example – the star can drive off sufficient dust and gas to increase the companion mass, and produce its envelope of dust, and its tail.

Nevertheless, the relatively small scatter in the phase curves for U Del and Y Lyn – especially the V data -- supports the conclusion that the phase curse, and the eclipse geometry do not change significantly over a few decades.

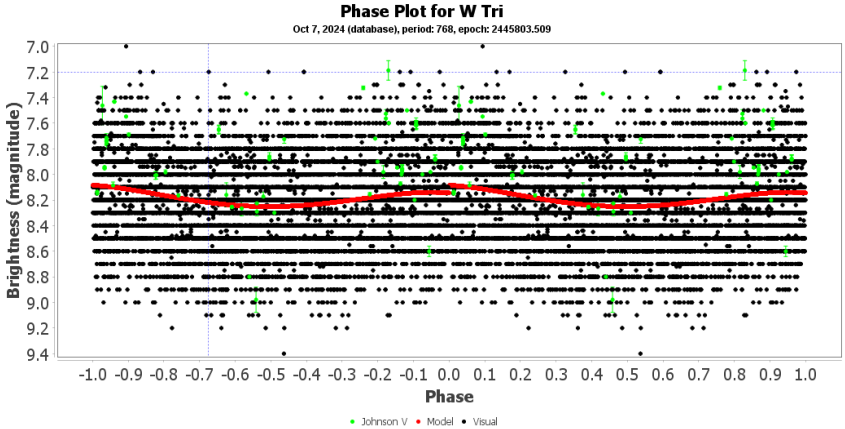

Figure 5. The phase (eclipse) curve for W Tri. This, with its small amplitude and sinusoidal shape, is typical of over half the stars in our sample. The red curve is a polynomial fit. Source: AAVSO.

The amount of obscuring dust, as indicated by the LSP amplitude, can vary by a factor of up to eight, and does so on a time scale of decades. The eclipse geometry, as reflected by the uniformity of the light curve, and the relatively small scatter in the phase (eclipse) curve, appears not to change significantly over the time interval of our data, despite the dust variation. At least two of our larger-LSPA stars show an asymmetrical phase curve which can be interpreted as due to a dust tail following the companion. For most of our stars, however, the LSP amplitude is small, and the phase curve is sinusoidal. None show “classical” eclipse curves with flat maxima.

Acknowledgements

We acknowledge with thanks the variable star observations from the AAVSO International Database contributed by observers worldwide and used in this research. We also thank the AAVSO HQ staff who have maintained the database over many decades, and the staff and others who have created and maintained the VSTAR time-series analysis package. This project was supported by the University of Toronto Work-Study Program, and the Dunlap Institute. We thank Professor Igor Soszynski and Matylda Soszynska for providing Figure 1.

References

Benn, D. 2013, VSTAR data analysis software (http://www.aavso.org/node/803)
Percy, J.R. and Deibert, E. 2016, J. Amer. Assoc. Var. Star Obs., 44, 94.
Percy, J.R. and Zhitkova. 2023, J. Amer. Assoc. Var. Star Obs., 51, 230.

Soszynski and Udalski, A. 2014, Astrophys. J., 788, 13.
Soszynski, I., et al. 2021, Astrophys. J. Lett., 911, L22.

Wideband Photometry of the Semiregular Variable RZ Arietis

Dr. Richard W. Schmude, Jr. and Qasim Ahmed

Gordon State College, 419 College Dr., Barnesville, GA 30204; Schmude@gordonstate.edu

Abstract

The writers made 69 V-filter brightness measurements of RZ Arietis since late 2023. One conclusion of this work is that the primary period may change by over 35% in just two months. Periods range from 27.7 days up to 76 days. The mean length of the primary period is 51 days with a standard deviation of 12 days. This is based on 23 measured periods. We also conclude that this star's mean brightness dropped by 0.1 to 0.2 magnitudes in 2022.

Subject Keywords

RZ Arietis; photoelectric photometry

1. Introduction

Astronomers have learned several things about RZ Arietis over the last 50 years. Burnham (1978) classifies it as an irregular variable with a brightness range between 5.9 and 6.3. After considerable study by members of the AAVSO and the British Astronomical Association, we have a better understanding of how its brightness changes. With this information, Hirshfeld and Sinnott (1985) classify this star as an "SRb" with a brightness range of 5.62-6.01. The "SRb" means a semiregular variable classification with a "poorly expressed period" (Hirshfeld and Sinnott, 1985). Scovil (1990) lists it as a semi-regular variable with a brightness range of magnitude 5.6 to 6.0. North (2004) describes a semi-regular variable star as a giant or supergiant that shows some periodicity in its brightness but also may show irregularities. RZ Arietis has shown a combination of regular and irregular changes in both its brightness and brightness period and, hence, fits this description well. Astronomers have also measured its distance. Tabur et al (2009) list a parallax of 9.28 milliarcseconds with an uncertainty of 0.30 milliarcseconds. This is consistent with a distance of 108 parsecs. Therefore, one may compute the absolute magnitude of this star and use this to determine its position on the Hertzsprung-Russell diagram. Richichi and co-workers (2018) report an angular size of 10.6 milliarcseconds (with an uncertainty of 0.2 milliarcseconds) based on the lunar occultation method. They used near-infrared light in their measurement. From this information one may then compute the diameter of RZ Arietis as 171 million km with an uncertainty of around seven million km.

Lee (1970) summarizes the brightness measurements (in magnitudes) of RZ Arietis in the wavelength range between 0.35 and 3.4 μm. He reports eight different color indices for it including B – V = 1.51 and V – R = 2.42. There is a chance that the color indexes change as this star dims.

The earliest visual brightness estimates of RZ Arietis in the American Association of Variable Star Observers (AAVSO) Database are from 1954 and the earliest photometric measurements in the V filter are from 1983 (AAVSO, 2024). All V-filter measurements in the AAVSO Database have been corrected for both extinction and color transformation. To simplify time changes, the Julian Date (JD) is used as the time standard in this paper.

In this report, an uppercase V (Johnson system) means a color correction has been included, whereas a lowercase v means a color correction has not been included. In all cases, brightness values are on the Johnson system.

The purpose of this study is firstly to measure the length of the primary period of variability for RZ Arietis and report how it changes. This will be done in a wavelength close to the Johnson V-filter. Secondly, the results from this study will be compared to reported V-filter brightness values in the American Association of Variable Star Observers (AAVSO) Database. Finally, the mean period, the mean V-filter magnitude and absolute V-filter magnitude will be reported.

2. Methods

An SSP-5 photometer manufactured by Optec (Optec, 1995) is used for all brightness measurements along with a 0.080 m refractor telescope. The brightness values of the comparison star, Rho Arietis (V = 5.616, B – V = 0.433) are from Westfall (2008). In all cases, Delta Arietis was used as a check star. The writers are confident that the comparison star magnitude remained constant to within 0.03 magnitudes because of the good agreement of measured magnitudes of Delta Arietis.

Our brightness values were typed into a Microsoft Excel spreadsheet. The V-filter brightness values for RZ Arietis (as listed in the AAVSO Database) were also typed into the spreadsheet. This software package was used in determining the mean brightness of our values and those from the AAVSO Database. It was also used in generating the graphs in this report.

3. Results

The results from our studies covering 2023-2024 are presented first. Afterwards, our results are compared to those in the AAVSO Database and from this, selected values for RZ Arietis are reported.

3.1. Our Results

Figure 1 shows brightness measurements of RZ Arietis made up to JD 2,460,648. The left half shows two well-developed cycles of brightness maxima, but the brightness maxima show variations of 0.1 magnitudes. The writers summarize this work elsewhere (Schmude and Ahmed, 2024). The more recent data show two brightness maxima with the second one being 0.2 magnitudes fainter than the first one near JD 2,460,556. The data before JD 2,460,400 are consistent with a primary period of 58.4 days. This is not the case for data collected after JD

2,460,500. The certain periods are 58.4, 58.4, 38.1 and 37.7 days. Percy et al. (2003) and Percy and Deibert (2016) report periods of 37.7 and 56.5 days which are in good agreement with our results. These two periods are also evident in a power spectrum reported by Percy et al. (2008). Tabur et al. (2009), however, report periods of 49.9 and 54.8 days.

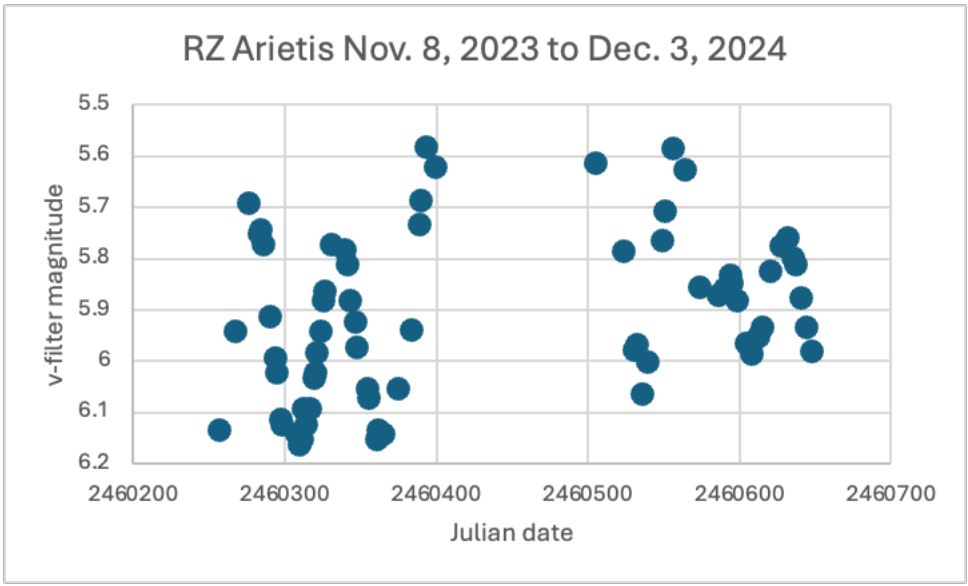

Figure 1. Brightness measurements collected by the authors between November 2023 and December 2024. Color corrections have not been added to the results.

The mean v-filter brightness for the points in Figure 1 is v = 5.91. Using a B – V value of 1.51 (Lee, 1970), a color transformation correction of -0.043 magnitudes is added to this result to obtain a mean V-filter magnitude of 5.87 for the period covered in Figure 1. The transformation coefficient for the V filter is -0.0402 and is computed from the two-star method (Hall and Genet, 1988). The V-filter brightness ranges from 5.54 to 6.12 in Figure 1 (after the color transformation correction is added). This is a range of 0.58 magnitudes, which is a little larger than those reported by Burnham (1978), Hirshfeld and Sinnott (1985) and Scovil (1990).

3.2. Combining 2023-2024 results with AAVSO Database results

The results in Figure 1 may be compared to those in the AAVSO Database (AAVSO, 2024), which has 909 V-filter measurements between JD 2,445,653.7 and 2,460,379.6.

One of the findings from the AAVSO database is that the length of a cycle of brightness maxima to the next maxima can change in two months. Figure 2 shows measurements from this database recorded in the mid-1990s. Two large changes took place in a few months. Firstly, the peak brightness dropped from 5.58 (JD 2449,709) to 5.82 (JD 2,449,774). A second large change is that the time difference between successive brightness maxima changed from 49 days to 65 days in two months.

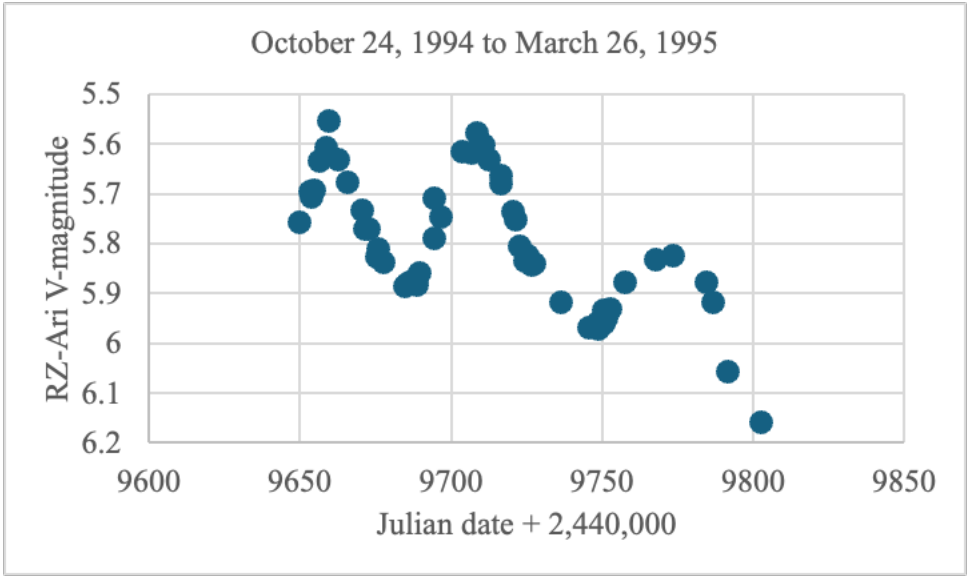

Figure 2. Data from the AAVSO data base for RZ Arietis. Note the large changes in brightness maxima, and period between successive brightness maxima.

The AAVSO Database was examined for information on the primary periods of RZ Arietis. A total of 19 periods (in days) were measured and are given in Table 1. The mean period from just the AAVSO Database is 52 days with a standard deviation of 13 days. These values are consistent with those measured by the writer and his students. The mean primary period length for the AAVSO Database plus the four measured periods from this study is 51 days with a standard deviation of 12 days.

Table 1. Periods measured from the AAVSO Database. Approximate date is JD + 2,440,000.

Date	Period (days)	Date	Period (days)	Date	Period (days)
8590	27.7	10,070	62.9	12,270	49.1
8620	34	10,420	45.9	16,320	52
8660	48.1	10,760	62.9	18,850	76
9360	35	10,810	47.1	19,240	57
9680	65	11,190	54.1	19,580	71.9
9740	48.9	11,540	46.9	19,960	59.6
10,020	44.9				

The mean V-filter magnitude from values in the AAVSO Database is 5.77. This is brighter than the mean of the color-corrected values made by the writers. The most likely explanation for this is that a recent brightness drop took place.

One of the questions the writers want to answer is: Is there more than one period of brightness change for RZ Arietis? A Long Secondary Period (LSP) of a few hundred days has been reported. For example, Percy and Deibert (2016) report an LSP of 479.4 days. There also appears to be an even longer period of variability (~3000 days) based on the light curve of RZ Arietis in Figure 6.32 of Percy (2007). Accordingly, the AAVSO Database was examined apparition by apparition. An

apparition for RZ-Arietis lasts from July to the following March. If an apparition had at least one well-defined brightness maxima and one well-defined minima,, a mean V-filter magnitude was computed for it. A total of 24 mean apparitional brightness values were computed plus an additional two from the left portion of Figure 1. The resulting mean brightness values are plotted in Figure 3. There is probably an LSP of a few hundred days; however, part of the difficulty is that an apparition lasts for ~270 days with a 90-day gap. In some cases, the data gap is even larger or, worse yet, there are very few brightness measurements for an apparition. The mean apparitional brightness values fluctuated a little for 1983-2021, which is probably the results of an LSP. Nevertheless, the mean apparitional magnitude for 1983-2021 was brighter until JD 2,458,000; afterwards, there is a 0.1 – 0.2 magnitude drop for this value. The writers believe that this drop is significant and warrants further study. This drop is probably the reason why the mean brightness in Figure 1 is lower than the corresponding value for 1983 – 2024.

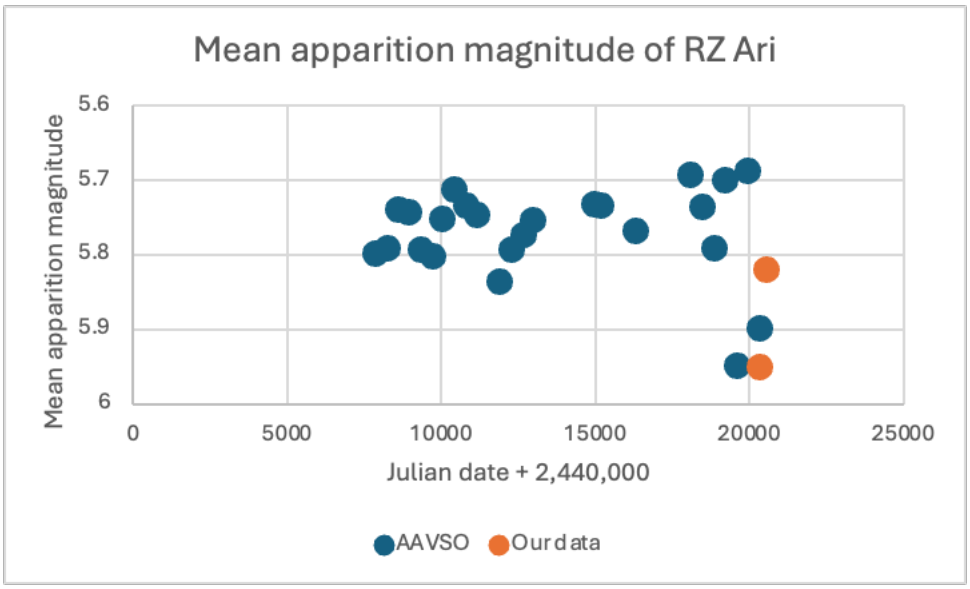

Figure 3. Mean apparition magnitude versus time for the AAVSO Database and the results in the first half of Figure 1. Gaps in the data are the result of a lack of measurements for some apparitions.

4. Discussion

RZ Arietis shows a combination of consistency in its brightness along with unexpected changes. More measurements of this star are needed along with spectroscopic measurements to better understand it. Power spectra of ten-year increments of the AAVSO Database measurements may be fruitful showing long-term trends in brightness and period change. There is a chance that this star changes in color as it brightens and dims. It would be difficult though to measure color corrections for this star since its color index is so high. One possibility is to measure the b-v or r-v values of this star without color corrections. These values could reveal a periodic a color change.

The writers plan to continue measuring the V-filter brightness of RZ Arietis. There are also plans to look at the visual brightness measurements of this star to search for long term changes going back to the 1950s.

5. Conclusions and Future Work

It is concluded that the primary period of RZ Arietis may change by over 35% in just two months. The values in Table 1 show that the primary period of brightness change can range from less than 28 days to 76 days. It is also concluded that a sudden brightness drop in the V filter apparently happened in 2022. This change means that more data should be obtained.

Table 2 summarizes the selected constants of RZ Arietis as of late 2024.

Table 2. The selected constants of RZ Arietis as of late 2024.

Constant	**Value (uncertainty)**
Mean V-filter brightness	5.78
Absolute magnitude*	0.62
Mean primary period (all values)	51 days (standard deviation of 12 days)

*Based on a parallax of 9.28 milliarcseconds as reported in Tabur et al. (2009)

6. Acknowledgements

The writers are grateful to Rebecca Smiley and Denis Martinez for their assistance.

7. References

AAVSO. 2024, Observations from the AAVSO International Database (http://www.aavso.org).

Burnham, R. Jr. 1978, Burnham's Celestial Handbook", Vol. 1, Dover, New York.

Hall, D. S. and Genet, R. M. 1988, "Photoelectric Photometry of Variable Stars" Second Revised and Expanded Edition, Willmann – Bell, Inc., Richmond.

Hirshfeld, A. and Sinnott, R. W. 1985, Sky Catalog 2000.0 Volume 2 Double Stars, Variable Stars and Nonstellar Objects," Sky Publishing Corp., Cambridge MA.

Lee, T. A. 1970, The Astrophysical Journal **162**, 217.

North G. 2004. "Observing Variable Stars, Novae and Supernovae," Cambridge University Press, Cambridge UK.

Optec Inc. 1995, "Model SSP-5 Photoelectric Photometer" 1995, Lowell MI. Optecinc.com/astronomy/archive/manuals/SSP-5_first_generation_rev3_march_1995.pdf

Percy, J. R. 2007, "Understanding Variable Stars," Cambridge University Press, Cambridge UK.

Percy, J. R., Besla, G., Velocci, V. and Henry, G. W. 2003, Pub. Astron. Soc. Pacific, **115**, 479.

Percy, J. R. and Deibert, E. 2016, JAAVSO **44**, 94.

Percy, J. R., Mashintsova, M., Nasui, C. O., Palaniappan, R. and Seneviratne, R. 2008, Pub. Astron. Soc. Pacific, **120**, 523.

Richichi, A., Fors, O., Merino, M., Otazu, X., Nunez, J., Prades, A., Thiele, U., Perez-Ramirez, D. and Montojo, F. J. 2018, arxiv.org/pdf/0908.3228.

Schmude, R. Jr., Ahmed, Q., Smyly, R. and Martinez, D. 2024, in The Society of Astronomical Sciences, 43rd Annual Symposium on Telescope Science, June 20-22, 2024, Ontario, CA.

Scovil, C. E. 1990, "The AAVSO Variable Star Atlas", 2nd edition, AAVSO, Cambridge MA.

Tabur, V., Bedding, T. R., Kiss, L. L., Moon, T. T., Szeidl, B. and Kjeldsen, H. 2009, Mon. Not. Royal Ast. Soc., **400**, Issue 4, 1945.

Westfall, J. E 2008, "A.L.P.O. Monograph Number 12" who cites Mermilliod, J.-C. Photoelectric Photometric Catalog of Homogeneous Measurements in the U B V system," NASA Astronomical Data Center, Selected Astronomical Catalog, Volume 1 (CD-ROM).

Astrometric Measurement of Binary Star Systems Using Speckle Interferometry

Dinesh Shetty, Francisco Vasquez

Ferris State University, 820 Campus Drive, Big Rapids, MI, 49307, USA; dineshshetty@ferris.edu

Pat Boyce, Grady Boyce, Mark Harris

Boyce Research Initiatives and Education Foundation, 3540 Carleton Street, San Diego, CA, 92016, USA; pat@boyce-astro.org

Subject Keywords

Binary Stars; Astrometry; Speckle Interferometry; Washington Double Star Catalog; Orbital Elements

Abstract

Astrometric measurements of the physical systems WDS 14153+0308, WDS 18031-0811, WDS 18540+3723, WDS 20182+2912, 20210+4437, and WDS 2155+1053 were performed using speckle interferometry. The measurements were done using the 17" Boyce Astro Research Observatory's Plane Wave CDK telescope. The orbital plots and the elements for many of these systems were published in the Washington Double Star catalog about two decades ago. The measurements yielded a mean separation distance and mean separation angle of, 1.136" ± 0.008" and 28.288° ± 0.147°, respectively, for WDS 2155+1053, and a mean separation distance and angle of, 0.930"± 0.003" and 28.92° ± 0.21°, for WDS 20210+4437. The measurement for WDS 2155+1053 agrees well with the published sixth orbital catalog. Other systems show minor changes in their published orbit. However, the measurement for WDS 20210+4437 shows a significant departure indicating a refinement of the current orbital solution.

1. Introduction

The position angle and the separation distance characterize the apparent orbit of a binary star system. The Sixth Catalog of Orbits of Visual Binary Stars maintained by the United States Naval Observatory 2023 (Wash2023) contains information on the separation angles and distances, along with the orbital elements and the plot, from measurements carried over many decades. As new measurements become available, it is important to refine the orbital plots and the elements for predicting future positions (ephemerides) of known binary stars.

This work studies the binary star systems, WDS 14153+0308, WDS 18031- 0811, WDS 18540+3723, WDS 20182+2912, 20210+4437, and WDS 2155+1053. The orbital elements and the plots for these systems were optimized several years ago using the then-available data. Since then, there have been several new measurements, and it is important to include these measurements in the orbit optimization to obtain refined orbital elements. Table 1 shows the

systems studied in this work and the reference for the last optimization that was carried out. Also, shown in the table is the orbit grade defined by the Washington Double Star catalog. Grades range from 1 to 5 with 1 for the best-defined orbits. It is observed that some systems were last optimized as late as 1996 (Hei1996a) and some as recent as 2019 (Izm 2019).

Table 1. References for the last optimization of the orbit for the systems studied.

System	Discoverer Number	References	Grade
WDS 14153+0308	STF 1819 AB	Sca2012b	2
WDS 18031-0811	STF 2262 AB	Sod1999	3
WDS 18540+3723	BU 137 AB	Izm2019	4
WDS 20182+2912	A 1205	WSI2006b	5
WDS 20210+4437	A 725	Hrt2009	4
WDS 21555+1053	BU 75 AB	Hei1996a	2

2. Methods

The data were collected using the Boyce Research Initiative and Education Foundation's (BRIEF) 17" Plane Wave CDK BARON telescope at Sierra Remote Observatory in California and a QHY 600 CMOS camera with a 2x Powermate compound lens for imaging. This configuration yields a resolution of approximately 0.13 arcseconds per pixel. The BARON telescope system is fully automated and can effectively measure binary stars with separation as low as 0.8 arcsec using speckle interferometry. The NINA (Night Imaging 'N' Astronomy) control software was used with the Speckle Interferometry plugin written by Nick Hardy. The BARON NINA script took a full frame 30-second exposure (4,599 x 4,599 pixels) of the field of view centered on the target to ensure correct pointing and to measure the plate scale and camera rotation angle using Plate Solve 3.80 by Dave Rowe. The speckle images were taken with a 512 x 512 field called the Region of Interest (ROI) centered on the target at an exposure suitable for the target's magnitude. The 30-second exposure followed by speckle images was repeated for a nearby "reference star" to apply in the speckle interferometry data reduction. The NINA plugin managed this entire process including the selection of the reference star from the Smithsonian Astrophysical Observatory Star Catalog (SAO).

The science images were processed using the speckle interferometry technique. This technique is known to be effective for studying very close binary stars where the diffraction criteria of the telescope and atmospheric distortions (seeing) impose a strict limit on the resolution. This technique consists of taking a series of very short exposure (on the order of 10 – 100 ms) images that eliminate atmospheric smearing in telescope images and then processing these images mathematically via a complex bispectrum analysis to produce a final image where the optical distortions are removed, and the stars completely resolved.

A speckle reduction software (Speckle Toolbox) developed by Dave Rowe (Har2017) was used for this process. The process began with all 500 images being compiled into FITS cubes which results in a single file that is smaller in size and faster to process during speckle reduction. The smaller

file was then processed using the bi-spectrum phase analysis algorithm in the latest version (10.03) of the speckle toolbox with the calibration parameters previously obtained to extract the position angle (θ) and the separation distance (ρ).

Figure 1 shows an example of the bi-spectrum analysis for the binary system WDS 18540+3723. The star at the bottom (with a green circle around it) is the primary star and the one at the top (with a red circle around it) is the secondary star.

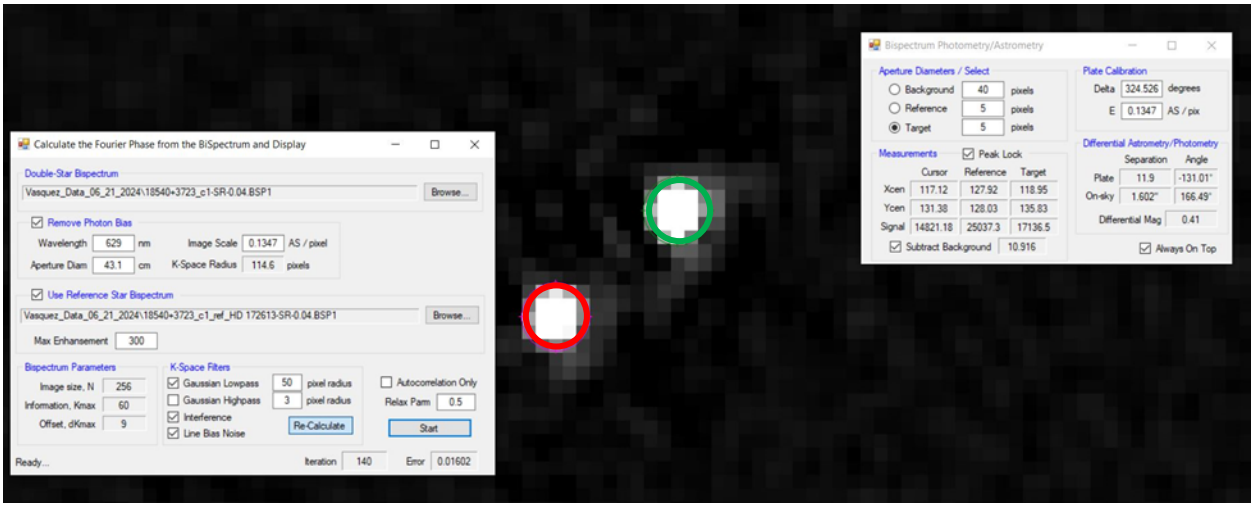

Figure 1. Screenshot of the data reduction on WDS 20210+4437.

The measurements were carried out for three nights (June 21, 2024 (2024.474); June 23, 2024 (2024.479); and June 25, 2024 (2024.485)). Five hundred images (science images) with an exposure time of 0.04 s and 0.06s were collected for various binary systems using the Sloan r filter. Each image was collected in two cycles.

The data was analyzed using the speckle reduction technique as described above. To minimize the effect of sky conditions and other related factors and the inherent biases in the analysis process from person to person, the reduction results from various nights and different people were averaged for each system.

3. Results

The results from this work were overlayed on the plot published by the WDS Sixth Orbital Catalog. Figure 2 shows this plot for each system. The results from the present work are represented by the red solid dot and labeled as BARON2024. The solid ellipse in each plot is the orbit published decades ago as discussed earlier and shown in Table 1. The data from other measurements (Wash2023) that have been carried out since the last optimization are also shown in the plot. These are shown in the figure by symbols with other colored labels.

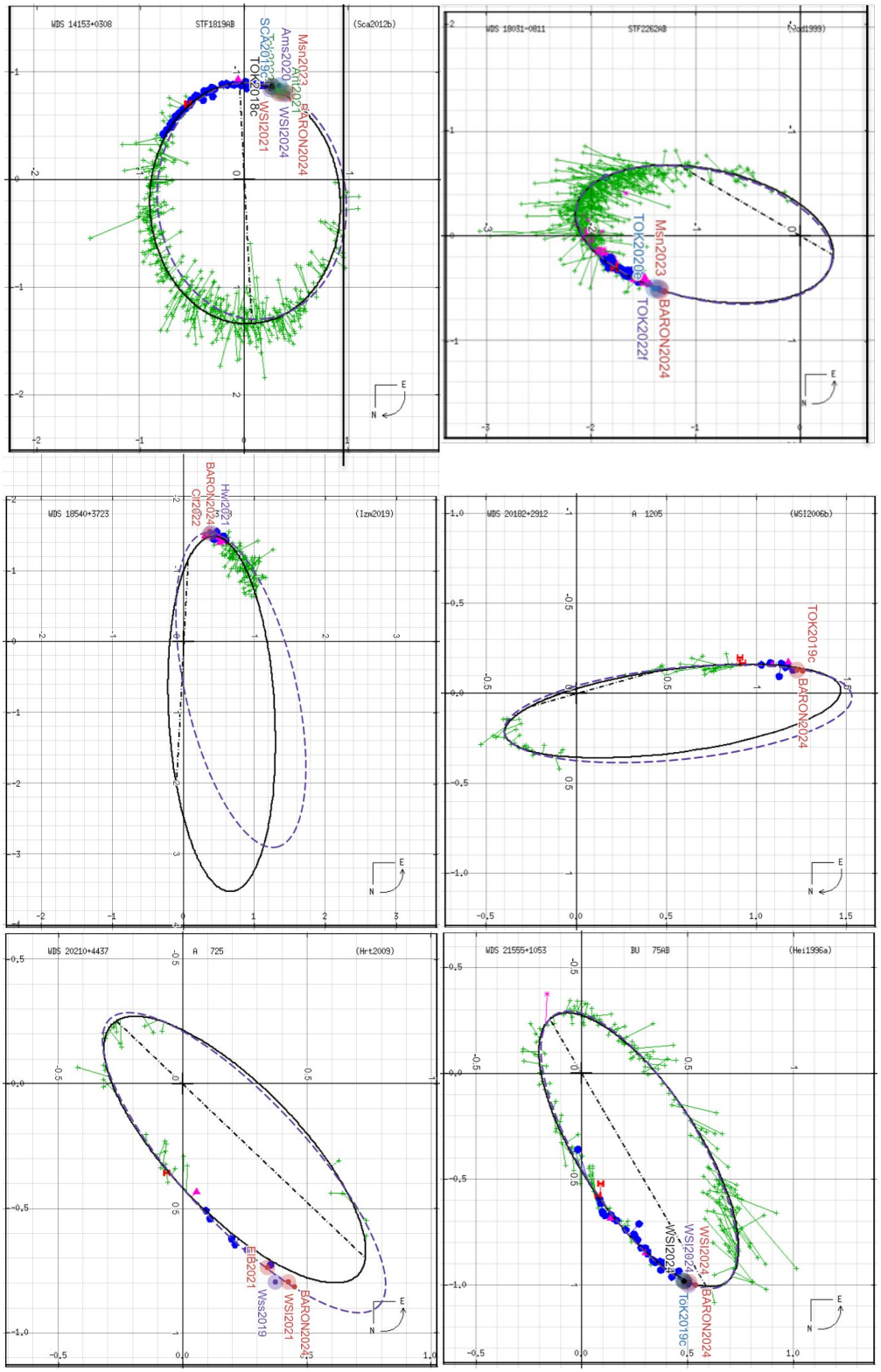

Figure 2. Apparent orbits (solid ellipses) with historical data from the Sixth Orbit Catalog for the six systems. The red solid point (BARON2024) is the observation from the present work. The dashed ellipses are the new apparent orbits discussed in Section 5.

4. Discussion

The dashed ellipse in each plot in Figure 2 is the proposed new orbit. The orbit was obtained by optimizing all the data to date using the optimization program in the speckle toolbox 10.03 by Dave Rowe. The optimization program works by finding local minima in the seven-dimensional space defined by the seven orbital parameters using the gradient descent and randomization process. For the present work, the optimization was performed by loading the Washington Double Star historical data with the present data into the optimizing program in the Speckle Toolbox. The program was then run through various iterations until an optimization determined by the minimum Weighted Root Mean Square Deviation (WRMSD) was reached between the observation and the calculated orbit. To avoid bias toward past data that were less precise (such as micrometer measurements), equal weights were assigned to all data, and no data was excluded from the optimization process. Figure 2 also includes data that was not included in the last optimization carried out. These are shown by the colored labels in Figure 2. The variance between the current ephemeris and those obtained from the present measurement is much smaller for the Grade 2 target than the Grade 4 and Grade 5 targets. The Grade 2 measurements are therefore a validation of the accuracy of our measurements. The new orbits for Grade 4 and Grade 5 targets are thus indicative of the important deviation from the ephemeris predicted by the Sixth Orbital Catalog.

The apparent orbit parameters a, b, h, k, and q for each system obtained from the optimization are shown in Table 2.

Table 2. Apparent orbital parameter values for various systems.

System	a (")	b (")	h	k	q (deg)
WDS 14153+0308	1.102	0.897	0.207	0.048	7.1
WDS 18031-0811	1.25	0.62	-0.9	-0.19	77.4
WDS 18540+3723	2.212	0.837	-1.169	0.65	53
WDS 20182+2912	0.971	0.255	-0.55	0.17	-84.2
WDS 20210+4437	0.789	0.252	0.4	-0.035	43.0
WDS 21555+1053	0.753	0.28	0.45	0.04	31.9

a (") - Semi-major axis in arcseconds
b (") - Semi-minor axis in arcseconds
h - x offset for the primary star
k - y offset for the primary star
q (deg) - Angle of the major axis in degrees

The apparent orbit is the projection of the true orbit onto a plane perpendicular to the observer's line of sight. It is related to the true orbit via seven parameters known as orbital elements. The orbital elements for the true orbit from the optimization are shown in Table 3.

Table 3. Orbital elements of the true orbit for the new apparent orbit (dashed ellipse) in Figure 2.

System	*P*	*a*	*e*	*i*	W	T_o	w
WDS 14153+0308	225.34	1.1010	0.1933	145.89	6.87	2002.879	172.85
WDS 18031-0811	279.52	1.5855	0.765	63.47	62.97	1833.51	53.98
WDS 18540+3723	1138.11	3.61	0.8087	76.57	186.51	2115.547	74.46
WDS 20182+2912	508.45	1.8606	0.9067	98.86	285.47	1970.746	72.88
WDS 20210+4437	189.51	0.7964	0.5259	68.23	225.11	1960.241	344.73
WDS 21555+1053	150.37	0.7597	0.5763	63.77	29.66	1969.252	193.92

The optimized apparent orbit parameters were used to plot the new orbit shown by the dashed ellipse in Figure 2 using DESMOS (Gen2024). The results show that the systems WDS 14153+0308, WDS 18031-0811, and WDS 21555+1053 show some minor changes in their orbit, whereas the systems WDS 18540+3723, WDS 20182+2912, and WDS 20210+4437 show significant departure from those published by the Sixth Orbital Catalog. The results from Figure 2 indicate that WDS 20210+4437 and WDS 18540+3723 may be more eccentric. Continued observation of these systems will help improve the orbital elements further for these systems.

5. Conclusions

We have studied several binary star systems to check whether there has been any change in the orbit since it was last published in the Washington Double Star catalog. We found that minor changes in the published orbit for some systems may be in order, while others needed significant changes. The improved orbital elements will aid in predicting future positions (ephemerides) of known binary stars. The present analysis did not apply any weight to the historical measurements during optimization, and all data was treated equally. The Orbital Elements in Table 3 may be optimized further by adjusting the weights applied to the historical measurements in future analyses. In particular, systems WDS 20210+4437, WDS 18540+3723, and WDS 20182+2912 warrant further investigation for their ephemeris.

6. Acknowledgments

Dinesh Shetty and Francisco Vasquez thank the Boyce Research Initiatives and Education Foundation (BRIEF) for providing the training materials, extensive guidance, and use of the BARON telescope. We would also like to acknowledge Ferris State University's sponsored research office for the funds provided under the Summer Student Research Fellowship for this work. We also thank Nick Hardy for his Speckle Interferometry Plug-in for NINA. This research used the Washington Double Star Catalog maintained at the U.S. Naval Observatory. It also utilized Dave Rowe's Plate Solving algorithm and Speckle Toolbox for data reduction and analysis. The work also used the Desmos graphing calculator for plotting.

References

Genet, R., McCudden, P., & Ellis, M. 2024. Desmos Analysis of Known Binaries: WDS 16212+2259, Journal of Double Star Observations, 20(2), 264

Harshaw, R., Rowe, D., and Genet, R. (2017). The Speckle Toolbox: A Powerful Data Reduction Tool for CCD Astrometry. Journal of Double Star Observations, 13(1), 52
Heintz, W.D., ApJS 105, 475, 1996 11
Hartkopf, W.I. & Mason, B.D., AJ 138, 813, 2009
Izmailov, I.S., Ast. Lett. 45, 30, 2019
Smithsonian Astrophysical Observatory Star Catalog, http://tdc-www.harvard.edu/catalogs/sao.html
Scardia, M., Prieur, J.-L., Pansecchi, L., & Argyle, R.W., Inf. Circ. 177, 1, 2012
SIMBAD Astronomical Database. https://simbad.cds.unistra.fr/simbad/
Soderhjelm, S., A&A 341, 121, 1999
Washington Double Star Catalog (2023). United States Naval Observatory, http://www.astro.gsu.edu/wds/
Mason, B.D., Hartkopf, W.I., Wycoff, G.L., & Holdenried, E.R., AJ 132, 2219, 2006
Mason, B.D., Williams, S.J., Matson, R.A., Josties, J.D., Eakens, P.D., Justice, M., Kilian, C.M. & Warner, R., AJ 162, 53, 2021

Utilizing Sky Surveys to Corroborate the Blazhko Period of EY UMa

Emily Watson and Dr. Matthew Craig

Department of Physics and Astronomy, Minnesota State University Moorhead, 1104 7th Ave S, Moorhead, MN 56563; Emily.Watson@go.mnstate.edu

Subject Keywords

Blazhko Effect; Lomb-Scargle Periodogram; RR Lyrae Variables; stars: individual (EY UMa)

Abstract

This project builds on prior work done determining the primary and Blazhko periods of the RR Lyrae star EY UMa. This year, data from the Catalina Real-Time Transient Survey (CRTS), NASA's Transiting Exoplanet Survey Satellite (TESS), and the All-Sky Automated Survey for Supernovae (ASAS-SN) were analyzed to compare sky survey and satellite results with observations at the Paul P. Feder Observatory. The current estimate for the primary period of this star is 0.54906 ± 0.000023 days. With the aid of sky surveys, the current estimate for the Blazhko period was found to be 94.2 days. There is evidence that this star is experiencing phase modulation along with the amplitude modulation studied thus far, though more analysis is needed to determine its period.

1. Introduction

The purpose of this project is to analyze the star, EY UMa, an RR Lyrae type variable. Almost every year since 2012, the star EY UMa has been observed using the Paul P. Feder observatory, which is at the Minnesota State University Moorhead Regional Science Center. Initially, EY UMa was analyzed by the student Hollee Klesh along with Dr. Matt Craig. This was done to try to accurately determine its period, as it was not precisely measured at that time. During this time, they noticed that the star exhibited more variability than the primary period could account for. This was determined to be due to the Blazhko Effect. Seen in approximately 1/3 of all RR Lyrae variables, this effect is a long-term modulation in the amplitude if the light curve, seen over a period of days to months. It is not currently known what the cause behind this effect is. Heidt (2015) estimated the Blazhko period to be 93 ± 4.5 days.

Work done on this project in 2023 determined the primary period to be 0.549 days. The calculated value of the short-term period is in line with the period given in the Variable Star Index (VSX). Throughout that analysis, a few potential Blazhko frequencies were determined: 0.308/day, 0.017/day, and 0.1211/day, with corresponding periods of 32.5 days, 58.82 days, and 82.569 days, respectively (Watson et al. 2023).

The goal with this project currently was to see if a more accurate primary period and a Blazhko period could be determined. To do this, additional data was taken at the Paul P. Feder observatory. Additionally, data from the Catalina Real-Time Transient Survey (CRTS; Drake et al.

2009), NASA's Transiting Exoplanet Survey Satellite (TESS; Ricker et al. 2015), and the All-Sky Automated Survey for Supernovae (ASAS-SN; Shappee et al. 2014). These data sources are then analyzed to determine the periods present within the star.

2. Methods and Results

2.1 Methods

There were four main data sources utilized throughout this project. First, data on EY UMa has been collected at the Paul P. Feder Observatory. The telescope is a 16" Cassegrain and the camera from 2018 to present is an Andor Apogee Aspen CG16M. All the analyzed data from 2018 to present was taken in the Sloan r filter. This data analyzed were calibrated using flat, dark, and bias images using standard calibration techniques using the package ccdproc (Craig 2023). Aperture photometry was done using the photutils package (Bradley 2023). Along with this, data from the TESS satellite, and the ground-based CRTS and ASAS-SN surveys were used as comparison to the observations from Feder.

All of the data was analyzed in Jupyter notebook environments. To analyze the data a Lomb-Scargle periodogram was used (Lomb 1976; Scargle 1982). Then, taking light curves of each data source, the data was folded over the period found by that data source (LightKurve Collaboration 2018). This was used to check the accuracy of the found period on the data.

2.2 Results

2.2.1 Primary Period

Starting with the data from the Paul P. Feder observatory analyzed in 2023, the resulting periodogram can be seen in Figure 1. This data is significantly less clean than some of the other data sources utilized in this project. This is due to aliasing. With periodograms detecting periodicity in unevenly sampled data, it is easy for the algorithm to pick up on patterns that an observer would know to not be a relevant period. For example, being a ground-based telescope, it can only observe at night, when it is clear, and when the star is high enough in the sky, above approximately 30 degrees. Among other factors, all of these "periods" are factored into the final periodogram, making it hard to determine the real primary frequency at play within the star. While the Feder observatory may not be reliable to determine the primary period of EY UMa on its own, combining its data with sky surveys increases confidence in the final result if both sky surveys and ground-based observing give the same primary period.

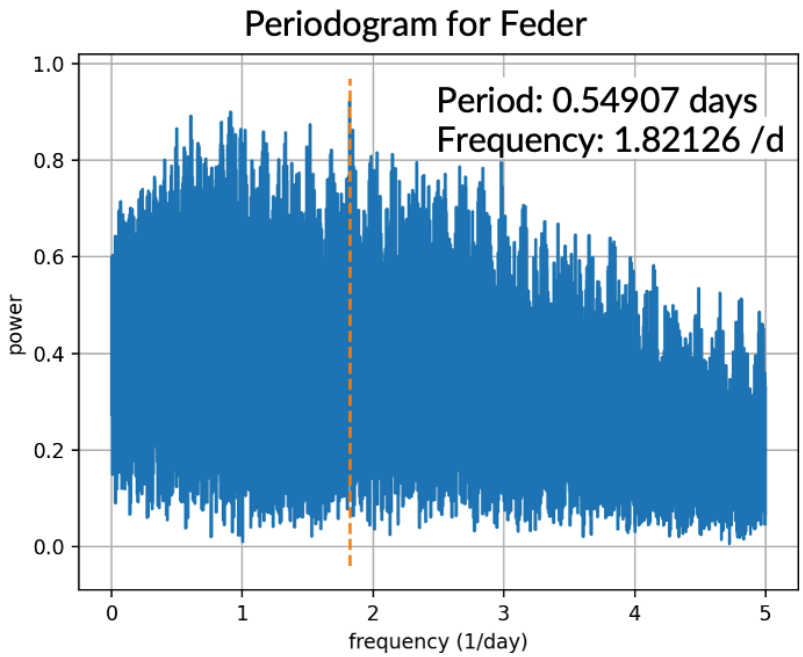

Figure 1. Periodogram for the data taken at the Paul P. Feder observatory from 2018 to 2023.

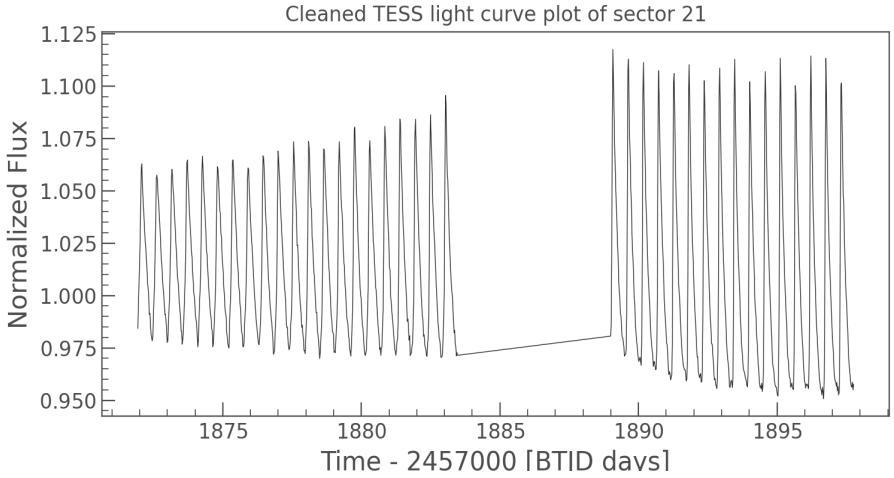

Figure 2. The normalized light curve diagram of sector 21 TESS data after cleaning the data.

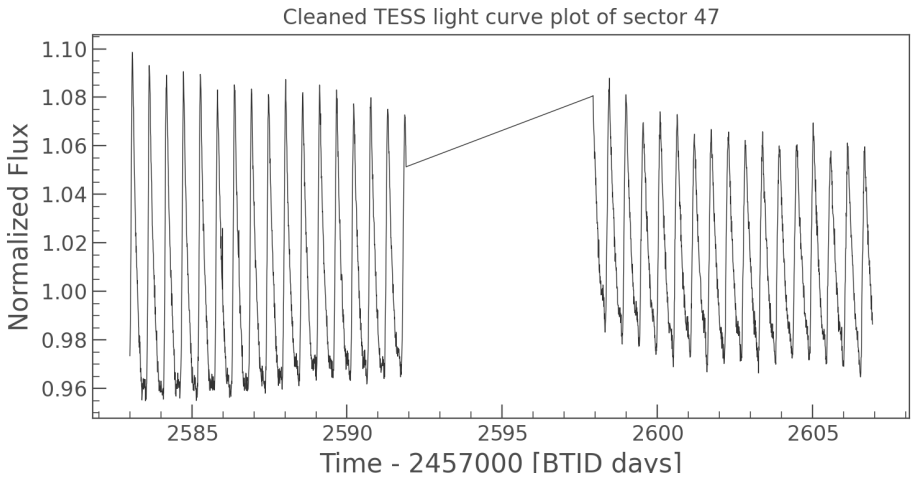

Figure 3. The normalized light curve diagram of sector 47 TESS data after cleaning the data.

In Figures 2 and 3, it can be seen that the amplitude of oscillation in the two 28-day sectors is changing with time. In addition to increasing confidence that the Blazhko effect is present in this star, seeing that sector 21 is only decreasing and sector 47 is only increasing in amplitude shows that this long-term period is much longer than 28 days.

The light curves from TESS can then be combined and analyzed in a Lomb-Scargle periodogram, as seen below in Figure 4. With there being two sectors, each having nearly continuous data for 28 days, the noise level is low in the periodogram. The primary frequency and its harmonics are clearly visible. Along with this, the smaller side peaks on either side of the primary, indicative of the Blazhko effect, are also visible. While the TESS data accurately determines the primary period, without having data spanning an entire presumed Blazhko period, this data cannot accurately give a Blazhko period.

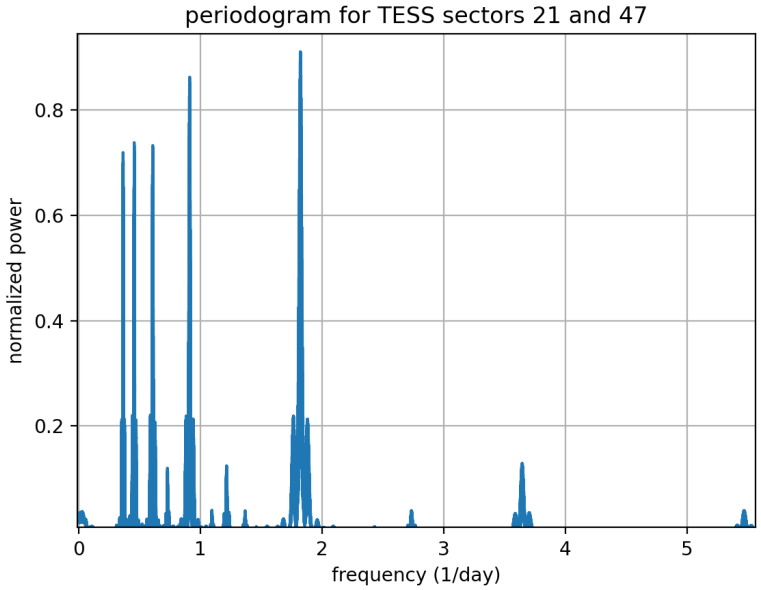

Figure 4. The Lomb-Scargle periodogram for the combined sectors of TESS data.

This same analysis was then done on the data from CRTS, ASAS_SN, and the Paul P. Feder observatory. Along with the data sources being analyzed separately, the data from CRTS, ASAS_SN, and Feder were also combined to be analyzed simultaneously. Two main steps were needed to combine this data properly. Firstly, all of the data needed to be transformed into the same filter. ASAS-SN and CRTS use the Johnson Cousins V filter, while Feder used the Sloan r filter.

$$\boldsymbol{Sloan\_r\_mag} = \boldsymbol{mag} - (\mathbf{0.046} * (\boldsymbol{B} - \boldsymbol{V}) + \mathbf{0.11})$$

The equation above can be used to transform all of the data sources to the same filter (Jester et al. 2005). Using known magnitude values for EY UMa in Johnson Cousin B and V, the formula can be applied.

Along with this, to get comparable amounts of data from each source, the data from Feder was binned to 0.1-day increments. With this being done, the three data sources could now be analyzed on one periodogram. While there is still aliasing in this data, combining the data sources results in a longer time span over which to analyze the short- and long-term periods of this star, thus increasing confidence in the resulting value.

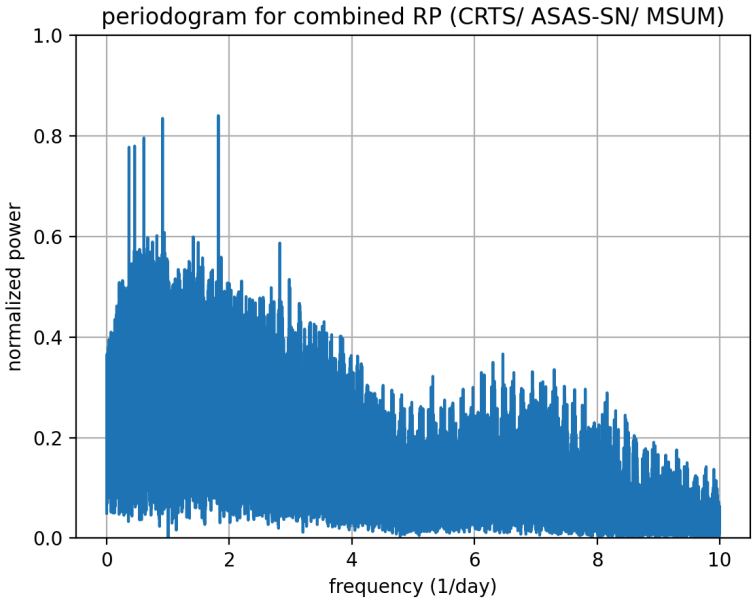

Figure 5. The periodogram of the combined CRTS, ASAS-SN, and Feder data.

Table 1. Table of the determined primary period for each data source using a Lomb-Scargle periodogram.

Data Source	Primary Period in days
CRTS	**0.549081 (13.177944 hours)**
ASAS-SN	**0.549060 (13.17744 hours)**
Feder	**0.549064 (13.177536 hours)**
TESS sectors 21 and 47	**0.549035 (13.17684 hours)**
Feder/ ASAS-SN/ CRTS joint	**0.5490739 (13.1777736 hours)**

Once the periodogram testing had been completed, the next step was to fold the TESS light curves on the given periods to see how accurately the period describes the data. It was chosen to fold the TESS light curves because of their very complete phase coverage.

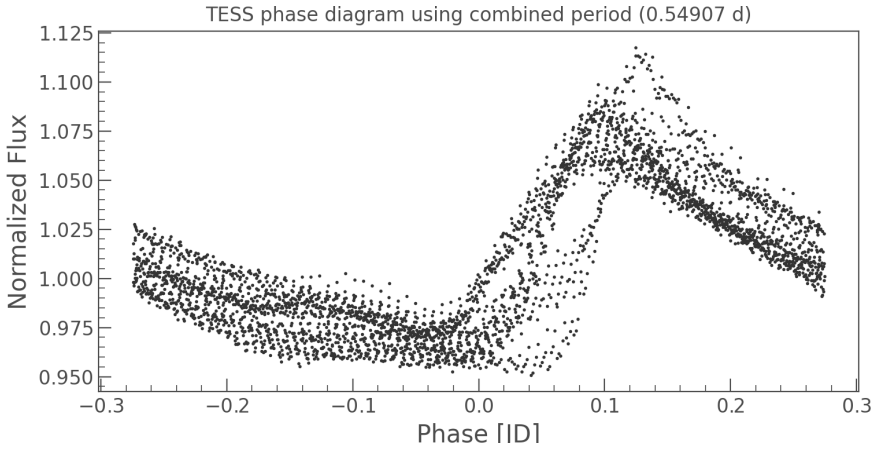

Figure 6. Folded TESS light curve using the period determined by simultaneously analyzing CRTS, ASAS-SN, and Feder data with a periodogram.

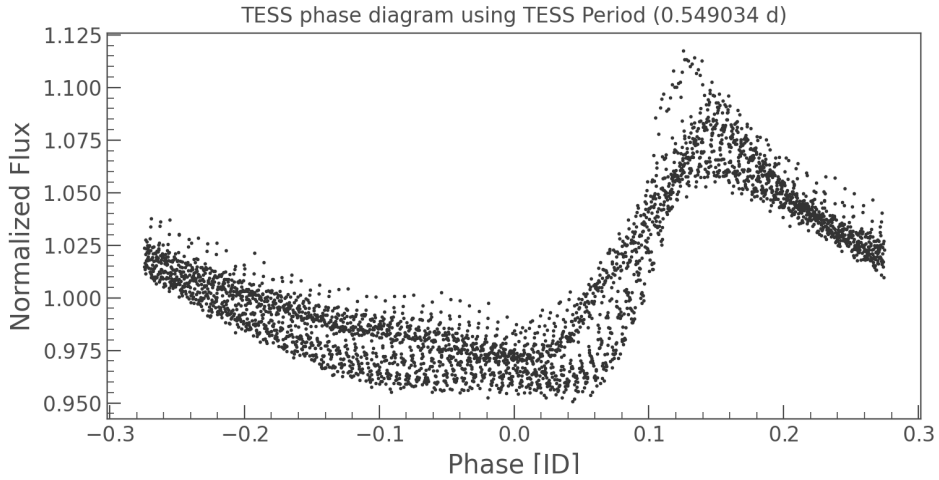

Figure 7. Folded TESS light curve using the period determined by analyzing both sectors of TESS data with a periodogram.

Looking at Figures 6 and 7, the given periods look close to correct, but it is likely the correct period is between the periods given in the above images. There is not a proper way to introduce error calculations into this form of data analysis at this time (VanderPlas 2017). In lieu of more formal error handling, for the scope of this project, the range of given periods from the varying data sources was used to estimate an error.

At this time, the primary period has been determined to be 0.54906 ± 0.000023 days, using the average of the first four rows in Table 1.

2.2.2 Blazhko Period

When it came to analyzing potential Blazhko periods for EY UMa, it was determined that the data from Feder and TESS was inconclusive. Feder data was inconclusive because there are very few observations at the time of maxima. The data from TESS was deemed inconclusive as there is not enough data to accurately measure the Blazhko period.

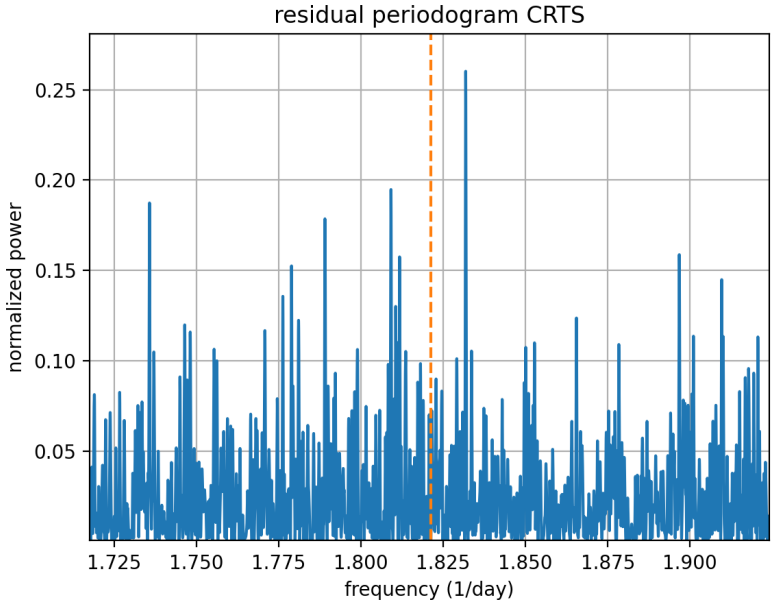

Figure 8. The residual periodogram for the CRTS data. The frequency difference between the primary peak and the tall side peak to its right corresponds to a period of 94.4 days, similar to the period from the ASAS-SN data in Figure 9.

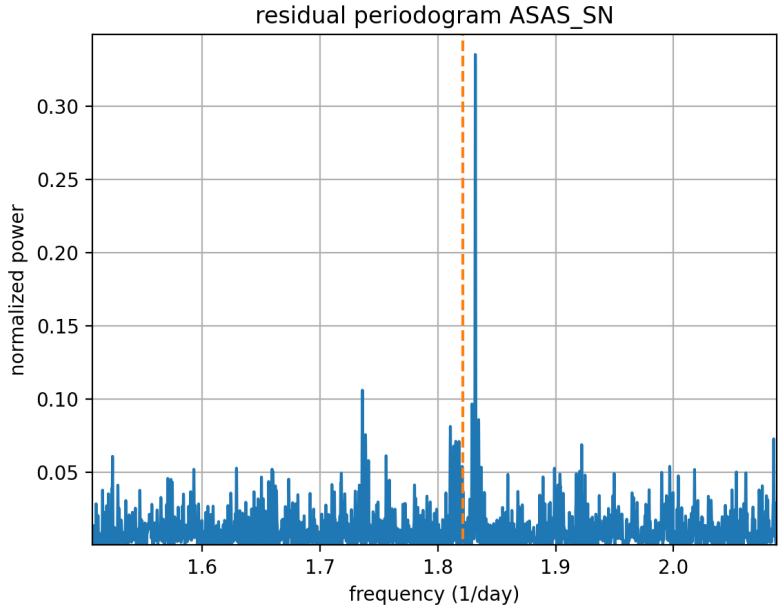

Figure 9. The residual periodogram for the ASAS-SN data. The frequency difference between the primary peak and the tall side peak to its right corresponds to a period of 94 days.

Table 2. The potential Blazhko periods for the modulation in amplitude of EY UMa.

Data Source	Blazhko Period in days
CRTS	**94.0 days**
ASAS-SN	**94.4 days**
Feder	**82.6 days**
Feder/ ASAS-SN/ CRTS	**93.5 days**

The Blazhko period from the CRTS and ASAS-SN data, around 94 days, is consistent with the Blazhko period reported from the first few years of Feder data from 2012-2015 (Heidt 2015). The result from the Feder data analyzed in this paper is likely incorrect because none of the observations included the maximum of the light curve. Though it is promising that the old and new data are consistent, to confirm this period a model would ideally be made to fit all of the current data on EY UMa. The current estimate for the Blazhko period is 94.2 days, calculated by taking the average of the first two rows in Table 2.

3. Conclusions

While the two potential Blazhko periods found above are quite similar, more analysis needs to be done to determine if this period is accurate. Next steps for this project include continuing to learn how to use multiband Lomb-Scargle to model all of the data sources together. With this, the primary and Blazhko periods should become more apparent. Then, data taken from surveys versus ground based observatories can be compared, determining their effectiveness with corroborating data found in sky surveys. There is modulation in the phase apparent in Figures 6 and 7 along with the amplitude modulation analyzed above. To analyze this, an O-C analysis is needed to measure the amplitude and period of the phase modulation.

Acknowledgements

Thank you to Dr. Matthew Craig for advising this project. Thank you to the Strong Summer Scholars Research Grant by the MSUM College of Science, Health & the Environment for funding research on this project in 2023.

This research made use of Lightkurve, a Python package for Kepler and TESS data analysis. This work made use of Astropy: a community-developed core Python package and an ecosystem of tools and resources for astronomy (Astropy Collaboration 2013, 2018, 2022). This paper includes data collected by the TESS mission. Funding for the TESS mission is provided by the NASA's Science Mission Directorate.

References

Bradley, L., Sipőcz, B., Robitaille, T., et al. 2023, astropy/photutils: 1.10.0 (1.10.0). Zenodo. https://doi.org/10.5281/zenodo.1035865

Craig, M., Crawford, S., Seifert, M., et al. 2023, astropy/ccdproc: 2.4.1 (2.4.1). Zenodo. https://doi.org/10.5281/zenodo.7986923

Drake, A.J. et al. First Results from the Catalina Real-time Transient Survey, 2009, ApJ, 696, 870

Heidt, N. Redetermining the Period of the Pulsating Variable Star EY UMa. 2015

Jester, S., Schneider, D. P., Richards, G. T. et al. 2005, AJ, 130, 3, pp. 873-895

LightKurve Collaboration (2018)

Lomb, N.R. 1976, Ap&SS, 39, pp. 447-462

Ricker et al., 2015, JATIS, 1

Scargle, J. D. 1982, ApJ, 263, 835

Shappee et al. 2014, ApJ, 788, 1, pp. 13

VanderPlas, J. T., 2017, ApJS, 236

Watson, E. et al., 2023, Proceedings of the AAVSO 112th Annual Meeting, ed. J. A. Guzik (Los Alamos, NM: LANL), 146-151

A Study of the High Amplitude Delta Scuti Star BP Peg

Amelia Abst, Dr. R.M. Blake, M. Guth, and H. Wildharber

University of North Alabama, Florence, AL

Abstract

As part of a program to monitor high-amplitude Delta Scuti stars, (HADS), we obtained times of maximum light for the HADS BP Peg over three observing seasons. Wong et al (2014) modeled BP Peg as a binary star with a period. Using data from the AAVSO archive and new observations obtained with the UNA observatory we measure new times of maximum light and use the binary ephemeris to determine if the O-C values match that of the model. We conclude that the binary model is able to account for the O-C values. We suggest that spectroscopic observations begin to allow an improved orbital determination.

The Power of Combining AAVSO Photometry and High Angular Resolution CHARA Imaging

Narsireddy Anugu, Douglas R. Gies, Rachael Roettenbacher, Gail Schaefer, and the CHARA Collaboration

CHARA Array (Owned by Georgia State University), Mount Wilson Observatory, Los Angeles, CA

Abstract

This study presents high-angular-resolution interferometric images of variable stars, captured using the CHARA Array. By combining these images with AAVSO photometric light curves, we investigate the underlying astrophysical phenomena driving stellar variability. Our analysis of RW Cep during its dimming and re-brightening phases suggests that the Great Dimming was caused by the formation of new dust, similar to the event observed in Betelgeuse. Additionally, we have imaged four red supergiants and one yellow hypergiant, detecting convection cells on their surfaces. These giant convection cells may have played a crucial role in driving the high mass-loss events, such as the Great Dimming observed in these evolved stars. Furthermore, we observed the rotation of these convection cells on the stellar surface of the yellow hypergiant, rho Cas. Overall, our findings demonstrate the power of combining CHARA imaging and AAVSO photometry to investigate a wide range of astrophysical phenomena associated with variable stars.

The Precision Frontier of Dark Matter: Constraints from Direct Acceleration Measurements

Dr. Sukanya Chakrabarti

Department of Physics and Astronomy, University of Alabama, Huntsville, AL

Abstract

For over a century, our understanding of dark matter has hinged on kinematic estimates derived from static snapshots of stellar positions and velocities. However, these methods are inaccurate for a time-dependent potential, and there are now many lines of observational evidence that show that our Galaxy has had a highly dynamic history. Recent technological advancements now empower us to carry out precision time-series measurements of the acceleration of stars that live within the gravitational potential of our Galaxy. I will discuss our comprehensive observational strategy to directly measure Galactic accelerations. Central to this discussion is our recent analysis of compiled pulsar timing data from which we were able to measure the Galactic acceleration for the first time and to derive fundamental Galactic parameters. Discernible differences in sub-structure exist among popular dark matter models on small scales, presenting testable nuances. I will discuss the potential for measuring dark matter sub-structure in the Milky Way by leveraging the diverse set of techniques we have developed, including pulsar timing, eclipse timing, and extreme-precision radial velocity observations. I will review initial results from our multi-pronged observing campaign, and end by discussing synergies between Galactic dark matter constraints and constraints on theories of gravity.

Using TESS Data to Discover New Exoplanets Around Binary Stars

Erika Dunning

Astronomy Department, San Diego State University, San Diego, CA

Abstract

About half of the star systems in the Milky Way contain two or more gravitationally bound stars. In spite of the large number of binary systems nearby the Sun, the vast majority of the ~5500 known exoplanets reside in single-star systems. The GAIA survey estimates there are 10 million binary systems closer than 250 pc to the sun. However, there are less than two dozen known exoplanets that orbit both stars in surveyed systems. These planets are known as circumbinary planets (CBPs). NASA's Transiting Exoplanet Survey Satellite (TESS) is conducting a comprehensive all-sky photometric survey to find planets via the transit method. The transit method applies to exoplanets with a nearly edge-on orbit around its host star (or host binary star) along the observed line of sight. When the planet transits in front of the star it will block part of the light from the star in every orbit. Our project seeks to find signatures of CBPs in the TESS survey by first cataloging systems as eclipsing binaries (EB) as part of team creating a comprehensive catalog of EB systems in TESS data. We selected systems with visually apparent eclipses with clear signal to noise and eclipse period longer than 6 days. So far, we have found one new circumbinary planetary candidate in over 11,000 surveyed systems. We will outline the methods we use and give a review of the results to date.

A Tool to Predict Binary Eclipses Observable from Your Location

Gabriel Grant and Dr. Matthew Craig

Physics Department, Minnesota State University, Moorhead, MN

Abstract

We had an initial, open-ended goal of observing eclipsing binary star systems. The AAVSO Target Tool was challenging to use for choosing targets. The target tool did not consider whether an eclipse was observable on a particular night or at our location; it simply lists stars that are visible.

We wrote an open-source program in Python to do this calculation and will also make this available as a web app. We generate predictions for the eclipsing binary stars listed in the Otero+ spreadsheet using period and eclipse duration looked up from VSX. The tool uses the observer location and observer-specified constraints on elevation and sky darkness to generate a list of upcoming full or partial transits observable from their location.

An observation of object V2480 Cyg was taken with the Paul P. Feder Observatory using the times that were calculated from the program. The observed time was roughly a couple hours off the prediction. This could be a result of either the period or the epoch reported in VSX being incorrect, or both. Fortunately, there was TESS data that we used to compare the period times. The periods between TESS and VSX agree only to the first three decimal places. We will present an updated ephemeris in our poster.

Improved Variability Data for the Brightest Solar-type Stars with TESS

Lauren Herrington and Sara Seager

Department of Earth, Atmospheric and Planetary Sciences, Massachusetts Institute of Technology, Cambridge, MA; laurenis@mit.edu

Abstract

Magnetic features rotating across the surface of a star cause low-amplitude photometric variations on timescales of days to weeks, enabling direct measurement of a star's rotation period. These variations typically measure much less than 0.1 magnitudes in amplitude, making them difficult to detect from the ground; but, with the improved precision offered by the Transiting Exoplanet Survey Satellite (TESS), rotational modulation can be observed in hundreds of bright stars. However, TESS's systematics interfere with automated methods of detecting variability, causing spurious detections and erroneous periods [1]. Therefore, we used direct visual examination to characterize the TESS light curves of 1,099 of the brightest G and K stars, searching for signs of rotation. The resulting catalog has a very low false-positive rate, and contains estimated periods, photometric amplitudes, and assorted variability data for over 350 stars. Most of the stars which we found to be variable are dominated by rotational variation, but a subset display other types of variability, such as binary ellipsoidal variation or flares. This data is being assessed for incorporation in VSX, and will be used to inform target selection for the Copernicus Constellation, a proposed satellite constellation designed to discover Earth-like exoplanets transiting nearby Sun-like stars. Copernicus' critical Phase 1 mission relies on targeting only the fastest-rotating stars, in order to resolve asteroseismic mode splits and identify stars with inclinations favorable to exoplanetary transits. The rotation periods obtained in this study will allow us to optimize Copernicus' asteroseismic search, extending the amount of mission time available for the Phase 2 transit search [2].

[1] Douglas, S. T., Agüeros, M. A., Covey, K. R., & Kraus, A. (2017). Poking the beehive from space: K2 rotation periods for Praesepe. The Astrophysical Journal, 842(2), 83.

[2] Herrington, L. & Seager, S. (2024). Rotation Rates of Bright Solar-type Stars with TESS. TESS Science Conference 3 (TSC3), Massachusetts Institute of Technology, Cambridge, MA, USA. Zenodo.

NASA's Imaging X-Ray Polarimetry Explorer (IXPE)

Dr. Philip Kaaret

NASA Marshall Space Flight Center, Huntsville, AL

Abstract

IXPE is NASA's first mission to study the polarization of X-rays from celestial objects. IXPE investigates some of the most extreme objects in the universe including black holes and their jets, supernova remnants, and neutron stars. I will describe the IXPE mission and some of the scientific advances it has made since launch in late 2021. I will highlight how some IXPE observations are enhanced by contemporaneous optical polarimetry and how AAVSO members could contribute.

Sunspottery: A Century of Supposed Solar Effects on Human Behavior in the Popular Imagination, 1878-1978

Dr. Kristine Larsen

Earth and Space Sciences, Central Connecticut State University, New Britain, CT

Abstract

In 1883, J.A.W. Oliver's Sunspottery critically evaluated myriad claims concerning the sun's influence on our planet. He recounts a public lecture in which an explanation of English economist (William) Stanley Jevons' 1878 paper "Commercial Crises and Sun-spots" was met with laughter by the audience. While Oliver, Richard Proctor and others debunked claimed connections between economics and sunspots in the 1880s, nearly a century later some economists continued to raise the specter of a possible correlation. Similarly, Russian scientist Alexander L. Tchijevsky aligned sunspot records with significant events in human history, including wars, revolutions, and riots, and claimed that the majority occurred near the time of solar maximum. His claims were brought to an American audience through a talk delivered in his stead at the 1926 annual meeting of the American Meteorological Society. Tchijevsky's work can be identified in several works of science fiction/horror. Newspaper reporter Mike Hamilton notes a disturbing pattern of suicides and violent murders in Clifford D. Simak's "Sunspot Purge" (1940). We also see echoes of Tchijevsky's claims in Robert Heinlein's The Year of the Jackpot (1952) and the 1975 Italian film Macchie Solari (Sunspots, dir. Armando Crispino). Given the current public interest in the solar cycle, fueled in part by the May 2024 auroral outbreaks as well as the persistence of erroneous fear-mongering surrounding the "Carrington Event", a close analysis of the connection between science, pseudoscience, and popular media in fueling persistent myths surrounding a solar activity/human behavior connection is timely.

References

Giegengack, R. 2015, Proc. Amer. Phil. Soc. 159, 421.
Jevons, W.S. 1878, Nature 19, 33.
Montgomery, P.M. 2003, Universal Economics Newsletter, 18 Jul., 1.
Oliver, J.A.W. 1883, Sunspottery: Or, What Do We Owe to the Sun?, Simpkin, Marshall and Co.
Proctor, R.A. 1880, Scribner's Monthly, 20.2, 170.
Tchijevsky, A.L. 1971, Cycles, 21.

Transient Stars in Cosmic Microwave Background Surveys

Dr. Tom Maccarone[1] and Dr. Gil Holder[2]

[1]Dept. of Physics and Astronomy, Texas Tech University, Lubbock, TX;
[2]University of Illinois, Urbana-Champaign, IL

Abstract

The cosmic microwave background is spatially extremely smooth and varies only on timescales of billions of years. However, in recent years, attempts to measure the small angular scale spatial variations of the microwave background have led to large numbers of repeated measurements of the same parts of the sky with reasonably good sensitivity and angular resolution. In the process of making these measurements, transient sources have been discovered, mostly from flares of red dwarf stars and tidally locked binary stars. In a few cases, TESS has fortuitously been looking at the locations of these objects, and, in some cases, they have shown optical flares of brightnesses easily achievable with telescopes under half a meter in size, while, in other cases, no flaring was seen. Some of these objects have shown relatively frequent flares, making them ideal targets for pointed observations that can provide more information and help produce unique data sets to understand the most extreme magnetically powered flares in stars. Because these flares are often faster than the cadences of sky surveys like ASAS-SN, often occur when TESS isn't looking, and are best observed in filters like U band and H-alpha, which are not part of current sky surveys, they represent an ideal niche for AAVSO members with access to the Southern Sky to participate in cutting edge science.

References

S. Guns et al. 2021, ApJ 916, 98
C. Tandoi et al. 2024, ApJ 972, 6

Candidate Exoplanet Observations

Jacob Mailhot, Hannah Crumby, and Dr. Matthew Craig

Department of Physics and Astronomy, Minnesota State University, Moorhead, MN;
jacob.mailhot@go.mnstate.edu; hannah.crumby@go.mnstate.edu; mcraig@mnstate.edu

Abstract

We report five observations of transits candidate exoplanets identified through the tool available to members of the TESS Follow-up Observers Program SG01. In three of the observations, we observed partial or full transits. In each case, we calculated relative flux of the exoplanet candidate using stellar plot and EXOTIC. Both were used to confirm that we had seen a transit and to check parameters of the transit for consistency. We reported one of the transits to the TESS project.

Astronomical Photometric Analysis with Cell Phone Cameras

Anusha Mehta and Lt. Col. Benjamin Roth

Department of Physics and Meteorology, United States Air Force Academy,
Colorado Springs, CO

Abstract

We present a hands-on approach to teaching basic photometry, one of the foundational aspects of observational astronomy, using only a smartphone camera and open-source software. By manipulating the basic magnitude equation, solving for the calibration constant, and using images to determine this constant, students gain an appreciation for working with astronomical data. The lab provides guidance on the use of SAOImageDS9 software, accessing and analyzing open star catalogs, plate solving an astronomical image captured by the student, and the application of aperture photometry. Students calculate the apparent magnitudes of stars, a measure of their brightness, achieving an uncertainty of less than ten percent. This methodology bridges the gap between theoretical concepts and practical applications, demonstrating the use of open-source and easily available technology in astronomical observations. We report this method as a more accessible and practical approach to learning astronomical photometry for those new to astronomy.

PA Number: USAFA-DF-2024-629

A More Precise Measurement of the Rate of Change of the Period of δ Scuti Variable DY Her

Abigale Moen and Dr. Matthew Craig

Department of Physics and Astronomy, Minnesota State University, Moorhead, MN;
abigale.moen.2@go.minnesota.edu; mcraig@mnstate.edu

Abstract

This study continues the period change observations of the high amplitude δ Scuti variable star, DY Her, from last year. DY Her has a period of 0.1486309 days and has been observed to have a slow overall period change from data gathered over several decades. Historical O-C data on DY Her has been obtained and analyzed alongside recent O-C observations using light curve data from the Paul P. Feder Observatory and observations of DY Her obtained from AAVSO from the past 21 years. This year, an additional year of AAVSO observations and one additional night of data from the Feder Observatory were added to the dataset, and the historical data were incorporated into our fits. Analysis of the O-C curve returned a period rate of change (1/P)*(dP/dt) of (–3.12 ± 0.09) x 10^{-8} yr^{-1}, which is consistent with, but more precise than, the recent values reported in the literature in Derekas et al. (2009), –2.9 x 10^{-8} yr^{-1}, and in Derekas et al. (2003), (–2.8±0.4) x 10^{-8} yr^{-1}.

T CrB: Brightest Nova in Generations

Dr. Bradley E. Shaefer

Dept. of Physics and Astronomy, Louisiana State University, Baton Rouge, LA

Abstract

T Coronae Borealis is a recurrent nova with observed eruptions in the years 1217, 1787, 1866, and 1946, plus a fifth eruption widely expected sometime in the year 2024. This peak will presumably get to V=1.7 (the same as the discovery by Mr. A. S. Kamenchuk in 1946), and be the brightest novae seen since 1946 (for T CrB itself). T CrB displays several unique and mysterious effects in its visual light curve, and it plays into the Grand Challenge Type Ia supernova progenitor problem. To solve these with the 2024 eruption, small telescope photometry and spectroscopy is the way to answer the big questions. For example, if T CrB displays bright [Ne III] lines three weeks after the peak, then the most-prominent single-degenerate models suffer a big failure. And the myriad of visual measures will define the orbital phase for measuring the apparently huge orbital period change across the nova event. Already, AAVSO spectroscopy has solved the case of the 'pre-eruption dip' (as discovered by L. Peltier), with this turning out to be a turning-off of the pre-eruption high state.

Evolution of RCB stars, and a General Law for the Shape of Isolated Dips

Dr. Bradley E. Shaefer

Dept. of Physics and Astronomy, Louisiana State University, Baton Rouge, LA

Abstract

Professional astronomers can never get the long runs of telescope time needed to produce running light curves of R CrB stars, whereas the small telescope amateurs around the world have wonderfully filled this need. I have used the vast number of visual and V magnitudes in the AAVSO International Database for 14 R CrB stars.

(1) Ordinary cool R CrB stars might show secular evolution on a century timescale, for example when the star enters or leaves the R CrB region on the HR diagram. With 323,464 magnitudes for ten ordinary cool R CrB stars, I extracted only magnitudes far away from any dip. These light curves show the stars at maximum light, and I sought linear trends or any type of significant variability. No variability was found, with typical uncertainties of ± 0.10 mag/century.

(2) I examined the at-maximum light curves for four 'Hot R CrB stars,' with these showing dust dips and a positioning to the left of the R CrB region on the HR diagram. All four stars are seen to be fading from ~1930 to present, at rates of 2.4, 1.2, 1.2, and 0.6 mag/century. Wow, we are seeing 'fast' evolution on individual stars in real-time. The secular declines are caused by the stars evolving to hotter temperature at constant luminosity, such that the bolometric correction to the optical band makes for an apparent dimming.

(3) I have used the AAVSO data to extract light curves of many individual isolated dips. These isolated dips all show a universal profile. I use ordinary theory of the dust formation and dispersal to derive this exact empirical profile, with the general equation $mobs = m0 + D[1 + (t - t0)/T0]^{-2}$, where m0 and T0 are constants for each R CrB star, while D and t0 are the magnitude-scale and time-shift parameters for each individual dip. Importantly, both theory and observation have the dip minima being flat-bottomed, and this demonstrates that the initial dust formation occurs in zero-velocity gas that is in the outer atmosphere of the RCB star.

Independent Discoveries by Two British Amateur Astronomers of the 1946 Eruption of T CrB

Jeremy Shears

British Astronomical Association Variable Star Section, Chester, United Kingdom;
bunburyobservatory@hotmail.com

Abstract

Amateur astronomers were the first to detect the last two eruptions of the recurrent nova, T CrB: John Birmingham, in Ireland, in 1866; A.S. Kamenchuk, in the Soviet Far East, and H.F. N. Knight, in England, in 1946. In the days following the 1946 eruption, reports appeared in the British press of a further independent discovery a few hours before Frank Knight's. The discoverer in this case was a 15-year-old schoolboy, Michael Woodman, observing in Wales. This talk examines the circumstances surrounding Knight's and Woodman's discoveries, based on correspondence between Knight and W.M. Lindley, then Director of the British Astronomical Association Variable Star Section, contemporary reports and the recollections of Michael Woodman.

Detecting Errors in Submitted Observations

Dr. Mark Spearman

Factory Physics Inc., TX; spearman@factoryphysics.com

Abstract

The integrity of AAVSO photometric data is of utmost importance in order to provide useful information to researchers. However, with the rise of automated systems, there appears to be an increase in the dissimilation of bad data. Moreover, the means of detecting erroneous data and either correcting them or removing them is not straightforward.

The purpose of this talk is to provide an indication of the magnitude of the problem and to offer means of automatically highlighting outliers that could be erroneous.

ROTUZ: Robotic Optical Telescope of University of Zielna Góra

Magdalena Szkudlarek and Michał Żejmo

Janusz Gil Institute of Astronomy, University of Zielona Góra, Poland;
mszkudlarek@uz.zgora.pl; mzejmo@uz.zgora.pl

Abstract

The ROTUZ (Robotic Optical Telescope of University of Zielona Góra) system is an innovative solution in the field of automated astronomical observations, located at an observatory in Chile. This project, conducted by the Institute of Astronomy at the University of Zielona Góra in Poland, utilizes two telescopes with diameters of 50 cm (CDK 20) and 28 cm (RASA 11), enabling observations across a wide range of optical wavelengths. Thanks to full automation and its location in one of the darkest places on Earth, ROTUZ plays an important role in asteroid and space debris monitoring, as well as in observing astrophysical phenomena such as exoplanet transits.

The ROTUZ system is operated remotely, allowing efficient operation without the need for a constant on-site presence of astronomers. The telescopes are used both for conducting research projects and for educational purposes, supporting students in learning observational methods and data analysis in astronomy. ROTUZ also serves as a platform for international collaboration, providing access to high-quality astronomical data for scientists worldwide.

The aim of the ROTUZ system is to continue research on dynamic processes in the Universe while promoting astronomy by engaging both the academic and outreach communities in astronomical observations.

The Continued Search for Variable Stars

Tanner Weyer and Dr. Matthew Craig

Department of Physics and Astronomy, Minnesota State University, Moorhead, MN;
tanner.weyer@go.mnstate.edu

Abstract

Over the course of 2022, 2023 and 2024 we utilized the Paul P. Feder observatory in conjunction with data from several other sources to search for variable stars in a field located in the Constellation Boötes. The field had no known variables but using data from the Feder Observatory, AAVSO member Geoff Stone, and NASA's TESS satellite, we have found several variable stars and have initial period estimates for them. During 2023 we selected eight promising stars based on data from our Feder Observatory, then during 2024 we obtained data from our observatory and NASA's TESS Quick Look Pipeline (QLP) to complement our ground-based observations. Of the eight stars initially selected from our data as potential variable, 3 of them are variable according to TESS's data. Utilizing a Lomb-Scargle periodogram we were able to estimate the period of these stars. All of the stars found thus far exhibit periods on the order of several days and magnitude changes of several millimagnitude. We are working to classify the stars.